İSTANBUL TECHNICAL UNIVERSITY ★ INSTITUTE OF SCIENCE AND TECHNOLOGY

ANALYSIS OF MICRO FLOWS USING A FINITE ELEMENT METHOD

Ph. D. Thesis by

Bayram ÇELİK, M.Sc.

Department : Space Sciences and Technology

Programme: Space Sciences and Technology

FEBRUARY 2006

İSTANBUL TECHNICAL UNIVERSITY ★ INSTITUTE OF SCIENCE AND TECHNOLOGY

ANALYSIS OF MICRO FLOWS USING A FINITE ELEMENT METHOD

Ph. D. Thesis by

Bayram ÇELİK, M.Sc.

(511972052)

Date of submission : 16 September 2005

Date of defence examination: 20 February 2006

Supervisor (Chairman): Assoc. Prof. Dr. Fırat Oğuz EDİS

Members of the Examining Committee Prof. Dr. Kadir KIRKKÖPRÜ (İTÜ)

Prof. Dr. M. Fevzi ÜNAL (İTÜ)

Prof. Dr. Ülgen GÜLÇAT (IÜ)

Assistant Prof. Dr. Ali ECDER (BÜ)

FEBRUARY 2006

İSTANBUL TEKNİK ÜNİVERSİTESİ ★ FEN BİLİMLERİ ENSTİTÜSÜ

MİKRO AKIŞLARIN SONLU ELEMANLAR YÖNTEMİYLE ANALİZİ

DOKTORA TEZİ

Y. Müh. Bayram ÇELİK

(511972052)

Tezin Enstitüye Verildiği Tarih: 16 Eylül 2005

Tezin Savunulduğu Tarih: 20 Şubat 2006

Tez Danışmanı: Doç. Dr. Fırat Oğuz EDİS

Diğer Jüri Üyeleri Prof. Dr. Kadir KIRKKÖPRÜ (İTÜ)

Prof. Dr. M. Fevzi ÜNAL (İTÜ)

Prof. Dr. Ülgen GÜLÇAT (IÜ)

Yrd. Doç. Dr. Ali ECDER (BÜ)

ŞUBAT 2006

ACKNOWLEDGMENTS

At the beginning of this study, a FEM solver that can be used for the solution of incompressible viscous fluid flow problem was the only tool in hand. Modifying this open source code and applying it to different fluid flow problems in literature was the path in mind to be followed. When recent studies of CFD in literature were scanned, to have an algorithm that can be applied both compressible and incompressible flow problems became the main goal of the further studies. For this aim a unified algorithm was constructed step by step over the solver in hand. At the end of any modification done, a problem was selected as a test case and the obtained results were compared to the other results in literature in terms of accuracy and computational costs. Finally, the capability of the unified FEM algorithm was extended as it can simulate to rarefied gas flow through the device in micro size.

I would like to express my gratitude to my supervisor Assoc. Prof. Dr. Fırat Oğuz Edis for his valuable guidance and suggestions, constructive critiques, helps and understanding during this study.

I would like to thank Prof. Dr. Ülgen Gülçat, Prof. Dr. M. Fevzi Ünal, Prof. Dr. A. Rüstem Aslan and Assoc. Prof. Dr. Aydın Mısırlıoğlu for sharing their experiences on CFD during my education at Istanbul Technical University.

I am grateful to my family for great childhood memories and their supports and loves through my long school years.

I would like to express my deep thanks to Didem Özgür Özden.

September 2005 Bayram Çelik

CONTENTS

ABBREVIATIONS

ALE	: Arbitrary-Lagrangian-Eulerian approach
CBS	: Characteristic Based Split procedure
CFD	: Computational Fluid Dynamics
DNS	: Direct Numerical Simulation
DSMC	: Direct Simulation Monte Carlo
FDM	: Finite Difference Method
FEM	: Finite Element Method
FVM	: Finite Volume Method
MD	: Modern Molecular Dynamics Computer Simulation
MEMS	: Micro-Electro-Mechanical-Systems
N-S	: Navier-Stokes
P1P1	: Linear Velocity/Pressure Elements
pP2P1	: pseudo-Quadratic Velocity/Linear Pressure Elements
SJA	: Synthetic Jet Actuator
SUPG	: Streamline-Upwind Petrov-Galerkin method
μSJA	: Micro Synthetic Jet Actuator

LIST OF TABLES

LIST OF FIGURES

LIST OF SYMBOLS

a	: Speed of sound
A	: Maximum deflection amplitude of synthetic jet diaphragm
A	: Physical constant for barotropic gas assumption
b	: General slip coefficient
c_p	: Specific heat at constant pressure
c_v	: Specific heat at constant volume
d	: Orifice width of synthetic jet
e	: Total energy per unit mass
Ec	: Eckert Number
f	. Frequency of oscillation diaphragm of synthetic jet
g_i	: Gravity acceleration
H	: Height of the synthetic jet cavity
h	: Orifice height of synthetic jet
k	: Boltzmann constant
k	: Thermal conductivity
Kn	: Knudsen Number
L	: Characteristic length of the flow
L_o	: Ejected fluid column length during the expulsion phase of SJA
M	: Mach Number
n	: Number of molecules per unit volume
N_E	: Energy shape function
n_i	: i' th component of the normal vector
N_p	: Pressure shape function
N_T	: Temperature shape function
N_u	: Momentum shape function
Pr	: Prandtl Number
R	: Gas constant
Re	: Reynolds Number
St	: Strouhal Number
T	: Temperature
T_g	: Guess temperature
U_i	: Mass flow fluxes
u_i	: Velocity component
u_i^g	: Grid velocity component
$\tilde{U}_i$	: Auxiliary momentum value
u_o	: Average expulsion velocity of SJA
W	: Weighting function
W	: Width of synthetic jet cavity
x_i	: Cartesian co-ordinate component
μ	: Dynamic viscosity
σ	: Gas molecule diameter
τ_{ij}	: Deviatoric stress component
Π	: Inlet to outlet pressure ratio

ρ : Density
Ω : Integration domain
Γ : Integration domain boundary
ν : Kinematic viscosity
δ_{ij} : Kronecker delta function
λ : Mean free path
$\bar{v}_m$: Mean molecular speed
ϕ : Scalar function
γ : Specific heat ratio
σ_v : Tangential-momentum-accommodation coefficient
σ_T : Thermal accommodation coefficient
$\bar{\alpha}$: Upwinding Coefficient of Petrov-Galerkin FEM algorithm
Δt : Time step size

ANALYSIS OF MICRO FLOWS USING A FINITE ELEMENT METHOD SUMMARY

The main objective of the thesis is to develop an algorithm and to apply it for the solution of compressible micro flow problems with moving or stationary boundaries. For this aim, Characteristic-Based-Split algorithm which can be used for the solution of both compressible and incompressible flow problems is constructed and its traditional no-slip/temperature-wall boundary conditions are modified to account for slip-velocity/temperature-jump conditions encountered in micro-sized geometries at standard conditions.

The set of the continuity, momentum and energy equations of compressible viscous fluid flow are known as Navier-Stokes equations (N-S). These equations can be written in Cartesian co-ordinates in conservative form as follows:

$$\frac{\partial \mathbf{V}}{\partial t}+\frac{\partial \mathbf{F_i}}{\partial x_i}+\frac{\partial \mathbf{G_i}}{\partial x_i}+\mathbf{Q}=0\,,\quad i=1,2,3 \tag{1}$$

$\mathbf{V}$, $\mathbf{F_i}$, $\mathbf{G_i}$ and $\mathbf{Q}$ shown in the Equation (1) are dependent variable, convection, diffusion and source vectors, respectively. These vectors can be written explicitly as follows:

$$\mathbf{V}=\begin{bmatrix}\rho\\ \rho u_1\\ \rho u_2\\ \rho u_3\\ \rho e\end{bmatrix},\mathbf{F_i}=\begin{bmatrix}\rho u_i\\ \rho u_1u_i+\delta_{1i}p\\ \rho u_2u_i+\delta_{2i}p\\ \rho u_3u_i+\delta_{3i}p\\ u_i(\rho e+p)\end{bmatrix},\mathbf{G_i}=\begin{bmatrix}0\\ -\tau_{1i}\\ -\tau_{2i}\\ -\tau_{3i}\\ -\left(k\,\partial T/\partial x_i\right)-\tau_{ij}u_j\end{bmatrix},\mathbf{Q}=\begin{bmatrix}0\\ \text{-}\rho g_1\\ \text{-}\rho g_2\\ \text{-}\rho g_3\\ -\rho\left(g_iu_i+r\right)\end{bmatrix} \tag{2}$$

Relationship between stress and rate of strain is defined by Stokes hypothesis and the stress components τ_{ij} are given with following equation:

$$\tau_{ij}=\mu\left[\left(\frac{\partial u_i}{\partial x_j}+\frac{\partial u_j}{\partial x_i}\right)-\delta_{ij}\frac{2}{3}\frac{\partial u_k}{\partial x_k}\right] \tag{3}$$

In the equations written above, u_i, p, ρ, T, x_i and t denote velocity component, pressure, density, temperature, Cartesian co-ordinate and time, respectively. k denotes the thermal diffusion coefficient. Viscosity is denoted with μ. It is a function of temperature and this relationship is defined with the Sutherland law. Source term and gravity force are denoted with r and g_i, respectively. δ_{ij} and τ_{ij} are the Kronecker delta function and viscous stress component. e is total energy per unit mass and it can be written explicitly as $e=c_vT+u_iu_i/2$ where c_v is the specific heat at constant volume. For compressible fluid flow, in addition to the equations given

above, pressure is related to temperature and density through the perfect gas equation given with $p = \rho RT$ where R is gas constant.

Fractional step method was proposed by Chorin for the solution of incompressible fluid flow problems in finite difference context. Zienkiewicz and Codina extended this method by the help of characteristic-Galerkin method, as it can be applied to both compressible and incompressible flow problems. Resulting method appeared in literature in 1999 as the Characteristic-Based-Split (CBS) algorithm.

With the exception of the pressure gradient term, the momentum equation of viscous compressible fluid flow and scalar convection-diffusion equation have similar structures. By using this similarity, the momentum equation can be discretized via the characteristic-Galerkin method, if the pressure gradient term appearing in this equation is considered as a source term. When the Chorin's fractional step method is applied to the resulting equations, totally self-adjoint equations are obtained for pressure. Similarly, when the energy equation is also discretized in time by applying characteristic-Galerkin method to it, auxiliary momentum, continuity, momentum correction and energy equations of CBS method are obtained. These equations are expressed explicitly as below:

$$\begin{aligned}\Delta\tilde{U}_i &= \tilde{U}_i - U_i^n \\ &= \Delta t\left[-\frac{\partial}{\partial x_j}\left(u_j U_i\right)^n + \frac{\partial \tau_{ij}^n}{\partial x_j} + \left(\rho g_i\right) + \frac{\Delta t}{2} u_k \frac{\partial}{\partial x_k}\left(\frac{\partial}{\partial x_j}\left(u_j U_i\right) - \rho g_i\right)\right]^n\end{aligned} \tag{4}$$

$$\Delta\rho = \left(\frac{1}{a^2}\right)^n \Delta p = -\Delta t\left[\frac{\partial U_i^n}{\partial x_i} + \theta_1 \frac{\partial \Delta\tilde{U}_i}{\partial x_i} - \Delta t\theta_1\left(\frac{\partial^2 p^n}{\partial x_i \partial x_i} + \theta_2 \frac{\partial^2 \Delta p}{\partial x_i \partial x_i}\right)\right] \tag{5}$$

$$\Delta U_i = U_i^{n+1} - U_i^n = \Delta\tilde{U}_i - \Delta t Q_i^{n+\theta_2} - \frac{\Delta t^2}{2} u_k \frac{\partial Q_i^n}{\partial x_k} \tag{6}$$

$$\begin{aligned}\Delta(\rho e) = &-\Delta t\left[\frac{\partial}{\partial x_i}\left(u_i \rho e\right) - \frac{\partial}{\partial x_i}\left(k\frac{\partial T}{\partial x_i}\right) + \frac{\partial}{\partial x_i}\left(u_i p\right) - \frac{\partial}{\partial x_i}\left(\tau_{ij} u_j\right)\right]^n \\ &+ \frac{\Delta t^2}{2}\left[u_k \frac{\partial^2}{\partial x_k \partial x_i}\left(u_i\left(\rho e + p\right)\right)\right]^n\end{aligned} \tag{7}$$

In the equation given above, $\tilde{U}_i$, U_i^n and Δt denote auxiliary momentum, momentum at time n and time step size, respectively. Q_i is the pressure gradient term which is considered as a source term. θ_1 and θ_2 parameters take the values in the range of 0 to 1 depending on the employed schemes such as implicit, explicit or semi-implicit. Since the equations given above are self-adjoint for pressure, they can be discretized in space using Galerkin approach. For different flow conditions (compressible, incompressible or barotropic flow) these equations are solved using different approaches. If the flow is incompressible, $\Delta\rho$ term appearing on the left hand side of the Equation (5) vanishes. Furthermore, the energy equation is solved independently at the beginning or end of the every time step, in order to obtain temperature values. If the flow is barotropic, pressure is related to density through $p = A\rho^\gamma$. If the flow is compressible, pressure and density are related to temperature

through the perfect gas equation ($p = \rho RT$) and required temperature values are obtained by solving the energy equation simultaneously with momentum and continuity equations.

If continuum approach is valid, the equations and solution procedures mentioned above can be used for solution of flow problems. It is very important to know under which conditions N-S equations are applicable and what kind of modifications carry on the validity of it. Thus, new definitions and parameters are needed. For gases, mean free path (λ) is the exact corresponding for these definitions. It is defined as the path traveled by a molecule between two consecutive collisions. Knudsen number is a measure of rarefaction and defined as the ratio of mean free path to the characteristic length of the flow (L):

$$Kn = \frac{\lambda}{L} \tag{8}$$

According to value on Knudsen number, following flow regimes are defined. The regime, where the Knudsen number is smaller than 0.001, is called continuum regime. In this regime, fluid flow problems can be simulated using the models based on continuum matter approach. The interval where the Kn is in the range of 0.001 to 0.1 is called slip regime. In this regime, continuum models such as N-S solver can be used for simulation of fluid flow, if slip-velocity/temperature-jump boundary conditions are employed instead of usual no-slip/no-jump (in temperature) boundary conditions on solid wall. In transition regime, Knudsen number is in the range of 0.1 to10. The fluid flow problems in this regime can be modeled using higher order continuum model such as Burnett equations or molecular based Direct Simulation Monte Carlo method (DSMC). In Free molecular flow regime where the Knudsen number is greater than 10, the interaction between the molecules is infrequent and rarefied gas flow is considered. Boltzmann equation can be used in this regime.

At standard conditions (T=288°K and p=1.01325x10^5 Pa), mean free path for air molecules is equal to 0.065 microns. Thus, for a device having characteristic length of 1 micron, Knudsen number is calculated as 0.065. This value indicates that the flow is in the slip regime. For the same device, if pressure decreases to ten percent while the temperature remains constant, the flow is in transition regime. For the same device again, Knudsen number is equal to 3x10^4 at altitude of 100 km and flow is in free molecular regime.

In recent years, extremely small sized devices have been manufactured due to the development in the production technologies. Some of these devices are used as sensor for pressure, temperature and mass flow or used as actuator for linear or angular movement. These devices are combinations of electrical and mechanical devices. Their sizes are in the range of 1 mm to 1 micron and they are called Micro-Electro-Mechanic-Systems (MEMS). Today, there is a wide range of applicability of MEMS in many fields such as industry and medical. Some of these applications are related directly or indirectly to fluid flow. Micro channels, micro synthetic jets are just two of this kind of MEMS devices. It is known that most of these micro sized devices work in slip regime under standard conditions. Thus, using appropriate numerical models would help to increase the productivity of them and to reach a better comprehension of their functions.

To simulate a fluid flow problem in slip regime with a model based on continuum approach (N-S solver), Beskok and Karniadakis proposed a second order slip-velocity (u_s^*) and temperature-jump (T_s^*) boundary conditions as given below:

$$u_s^* - u_{wall}^* = \frac{2-\sigma_v}{\sigma_v}\frac{Kn}{1-bKn}\left(\frac{\partial u^*}{\partial n^*}\right)_w + \frac{3}{2\pi}\frac{(\gamma-1)}{\gamma}\frac{Kn^2 Re}{Ec}\left(\frac{\partial T^*}{\partial s^*}\right)_w \tag{9}$$

$$T_s^* - T_{wall}^* = \frac{2-\sigma_T}{\sigma_T}\left[\frac{2\gamma}{(\gamma+1)}\right]\frac{Kn}{Pr}\left(\frac{\partial T^*}{\partial n^*}\right)_w \tag{10}$$

Slip-velocity/temperature-jump values given in the equations above are in non-dimensional form and *Re*, *Ec*, *Pr* denote the Reynolds, Eckert and Prandtl numbers, respectively. $\partial/\partial n$ and $\partial/\partial s$ represent the gradients normal and tangential to the wall. σ_v and σ_T are the tangential momentum accommodation and the energy accommodation coefficients. Using the Equation (9) and (10) instead of usual no-slip/no-jump boundary condition employed on solid wall in continuum regime, continuum models such as N-S can be used for the simulation of the flow in slip regime.

In this study, various fluid flow problems are simulated using CBS FEM solver. These problems are varying from incompressible to compressible flow, from laminar viscous flow through backward facing step flow to flow of micro sized synthetic jet which transfers momentum to main flow due to its oscillating diaphragm. In the solution of the problems mentioned above, the continuity equation given with Equation (5) is solved implicitly while the auxiliary momentum and momentum equations given with Equation (4) and (6) are solved explicitly. In order to reduce the size of implicit part of the algorithm, pseudo quadratic velocity/linear pressure type elements (pP2P1) are used within the computations. Thus, the solution can be considered to be obtained on two different grids, one for the velocity and other for pressure solution. pP2P1 type elements are obtained by inserting mid nodes to the linear pressure elements and interconnecting these to give 4 elements over which the velocity interpolated linearly

If one or more boundaries of computation domain are moving in time as seen in the synthetic jet problem, this movement should be modeled and coupled with solution procedure. If the position of nodes on the moving boundary is known or can be calculated in time *t*, the velocity of the nodes can also be calculated. It is obvious that, elements next to the boundary would be deformed according to the movement of the boundary. If amount of the maximum displacement of the boundary nodes is high enough compared to length of the element next to the boundary, this causes undesirable effect. Therefore, the mesh region surrounded by one or more moving boundaries is updated in time using desired interpolation formulas. Thus, the nodes in the updated region will have a grid velocity denoted with u_i^g. When the Arbitrary-Lagrangian-Eulerian (ALE) approach is used and grid velocity u_i^g is taken in to account, the auxiliary momentum equation given with Equation (4) takes the following form:

$$\Delta\tilde{U}_i = \tilde{U}_i - U_i^n$$
$$= \Delta t\left[-\frac{\partial}{\partial x_j}\left(u_j\left(U_i - U_i^g\right)\right)^n + \frac{\partial \tau_{ij}^n}{\partial x_j} + \left(\rho g_i\right)\right]^n \tag{11}$$
$$+ \Delta t\left[\frac{\Delta t}{2} u_k \frac{\partial}{\partial x_k}\left(\frac{\partial}{\partial x_j}\left(u_j\left(U_i - U_i^g\right)\right) - \rho g_i\right)\right]^n$$

In this study, second order slip-velocity/temperature-jump boundary conditions of Beskok and Karniadakis are used. Thus, the capability of CBS algorithm is extended to cover flow problems in slip regime. Moving deforming mesh concept is modeled using ALE approach and it is coupled with the modified algorithm. Using pP2P1 type elements within the CBS algorithm computations shows that there is a significant gain in terms of computational time and memory requirements.

In order to asses the performance of the proposed algorithm and to verify the implementations, various problems having different physical and numerical aspects are solved. Results of these analyses are compared with other solvers' and results from literatures in terms of accuracy and computational costs.

To verify the slip-velocity boundary condition implementation, straight micro channel is selected as a test case and obtained velocity and pressure distributions are compared with analytical and available numerical results. These comparisons show that the CBS algorithm yields accurate results for this test case.

Micro synthetic jet having a rectangular cavity is another micro flow problem numerically investigated in this study. Effect of geometrical parameters of the cavity on jet formation mechanism is numerically investigated. This analysis is one of the first comprehensive micro synthetic jet analysis performed using a compressible solver. For some of the numerically investigated cases, jet exit velocity reaches 140 m/s. It is obvious that compressibility effect cannot be neglected for these cases.

Another comprehensive analysis performed within the thesis is compressible fluid flow through micro backward facing step geometry in slip regime. In this analysis, results are obtained using CBS solver with both no-slip/no-jump and slip-velocity/temperature-jump boundary conditions. Then, obtained results are compared in terms of reattachment lengths, mass flow rate, inlet-outlet pressure difference.

The performed analyses, obtained results and comparisons show that the use of the proposed CBS algorithm with pP2P1 type elements is promising for fluid flow problems in both continuum and slip regime.

MİKRO AKIŞLARIN SONLU ELEMANLAR YÖNTEMİYLE ANALİZİ

ÖZET

Tez çalışmasının ana hedefi, bir algoritma geliştirerek hareketli veya durağan sınırlara sahip mikro akış problemlerinin çözümünde kullanmaktır. Bu amaçla, sıkıştırılabilir ve sıkıştırılamaz akış problemlerinin çözümünde kullanılabilen Karakteristik Tabanlı Ayırma algoritması oluşturulmuş ve bu algoritmaya ait alışılageldik kaymama/sıcaklıkta-sıçramama şartları, standart şartlarda mikro boyutlu geometrilerde meydana gelen kayma-hızı/sıcaklık-sıçraması şartlarını kapsayacak şekilde değiştirilmiştir.

Viskoz sıkıştırılabilir akışa ait süreklilik, momentum ve enerji denklemleri takımı, Navier-Stokes denklemleri (N-S) olarak adlandırılır. Bu denklemler kartezyen koordinatlarda, korunumlu halde aşağıdaki gibi yazılabilir:

$$\frac{\partial \mathbf{V}}{\partial t}+\frac{\partial \mathbf{F_i}}{\partial x_i}+\frac{\partial \mathbf{G_i}}{\partial x_i}+\mathbf{Q}=0\,,\quad i=1,2,3 \tag{1}$$

Denklem (1)'de yer alan $\mathbf{V}$, $\mathbf{F_i}$, $\mathbf{G_i}$ ve $\mathbf{Q}$ sırasıyla; bağımlı değişken, taşınım, iletim ve kaynak vektörleridir. Bu vektörler açık olarak aşağıdaki gibi yazılabilir:

$$\mathbf{V}=\begin{bmatrix}\rho\\ \rho u_1\\ \rho u_2\\ \rho u_3\\ \rho e\end{bmatrix},\mathbf{F_i}=\begin{bmatrix}\rho u_i\\ \rho u_1u_i+\delta_{1i}p\\ \rho u_2u_i+\delta_{2i}p\\ \rho u_3u_i+\delta_{3i}p\\ u_i(\rho e+p)\end{bmatrix},\mathbf{G_i}=\begin{bmatrix}0\\ -\tau_{1i}\\ -\tau_{2i}\\ -\tau_{3i}\\ -\left(k\,\partial T/\partial x_i\right)-\tau_{ij}u_j\end{bmatrix},\mathbf{Q}=\begin{bmatrix}0\\ -\rho g_1\\ -\rho g_2\\ -\rho g_3\\ -\rho\left(g_iu_i+r\right)\end{bmatrix} \tag{2}$$

Gerilme ile şekil değiştirme hızı arasındaki ilişki Stokes hipotezi ile tanımlanır ve τ_{ij} gerilme bileşenleri aşağıdaki denklemle verilir:

$$\tau_{ij}=\mu\left[\left(\frac{\partial u_i}{\partial x_j}+\frac{\partial u_j}{\partial x_i}\right)-\delta_{ij}\frac{2}{3}\frac{\partial u_k}{\partial x_k}\right] \tag{3}$$

Yukarıda verilen denklemlerde, u_i, p, ρ, T, x_i ve t, sırasıyla hız bileşeni, basınç, yoğunluk, sıcaklık, kartezyen koordinat ve zamanı temsil etmektedir. k ısıl iletim katsayısını, μ viskoziteyi göstermektedir. Viskozite sıcaklığın bir fonksiyonudur ve bu ilişki Sutherland yasası ile tanımlanmaktadır. Kaynak terimi ve yer çekimi kuvveti sırasıyla r ve g_i ile gösterilmiştir. δ_{ij} ve τ_{ij}, Kronecker delta fonksiyonu ve viskoz gerilmedir. e birim kütle başına toplam enerji olup, c_v sabit hacimdeki özgül ısıyı göstermek üzere, $e=c_vT+u_iu_i/2$ şeklinde yazılabilir. Sıkıştırılabilir akış için, yukarıda verilen denklemlere ek olarak; basınç, sıcaklık ve yoğunluk, $p=\rho RT$ şeklinde verilen ve gaz sabitinin R ile temsil edildiği mükemmel gaz denklemiyle ilişkilendirilmektedir.

Bölünmüş adımlar yöntemi, Chorin tarafından sıkıştırılamaz akış problemlerinin sonlu farklarla çözümü için önerilmiştir. Zienkiewicz ve Codina bu yöntemi, Karakteristik-Galerkin yöntemi yardımıyla, hem sıkıştırılabilir hem de sıkıştırılamaz akış problemlerine uygulanabilecek şekilde geliştirmişlerdir. Bu yöntem Karakteristik-Tabanlı-Ayırma (KTA) yöntemi olarak 1999 yılında literatürde yer almıştır.

Basınç gradyeni terimi dışında, sıkıştırılabilir viskoz bir akışa ait momentum denklemi ile skaler-taşınım-iletim denklemi aynı yapıdadır. Bu benzerlikten hareketle, momentum denkleminde yer alan basınç gradyeni terimi bir kaynak terimi gibi ele alınırsa, bu denklem karakteristik-Galerkin yöntemi kullanılarak ayrıklaştırılabilir. Bu ayrıklaştırma sonucunda elde edilen denklemlere Chorin'in bölünmüş adımlar yöntemi uygulandığında, basınç için tamamıyla kendine eş (self-adjoint) denklemler elde edilir. Benzer şekilde, enerji denklemi de karakteristik-Galerkin yaklaşımı uygulanarak zamanda ayrıklaştırıldığında, KTA yöntemine ait yardımcı momentum, süreklilik, tamamlayıcı momentum ve enerji denklemleri elde edilir. Bu denklemlerin açık ifadeleri aşağıda verildiği gibidir:

$$\begin{aligned}\Delta\tilde{U}_i &= \tilde{U}_i - U_i^n \\ &= \Delta t\left[-\frac{\partial}{\partial x_j}\left(u_j U_i\right)^n + \frac{\partial \tau_{ij}^n}{\partial x_j} + \left(\rho g_i\right) + \frac{\Delta t}{2} u_k \frac{\partial}{\partial x_k}\left(\frac{\partial}{\partial x_j}\left(u_j U_i\right) - \rho g_i\right)\right]^n\end{aligned} \tag{4}$$

$$\Delta\rho = \left(\frac{1}{a^2}\right)^n \Delta p = -\Delta t\left[\frac{\partial U_i^n}{\partial x_i} + \theta_1 \frac{\partial \Delta\tilde{U}_i}{\partial x_i} - \Delta t\theta_1\left(\frac{\partial^2 p^n}{\partial x_i \partial x_i} + \theta_2 \frac{\partial^2 \Delta p}{\partial x_i \partial x_i}\right)\right] \tag{5}$$

$$\Delta U_i = U_i^{n+1} - U_i^n = \Delta\tilde{U}_i - \Delta t Q_i^{n+\theta_2} - \frac{\Delta t^2}{2} u_k \frac{\partial Q_i^n}{\partial x_k} \tag{6}$$

$$\begin{aligned}\Delta(\rho e) = &-\Delta t\left[\frac{\partial}{\partial x_i}\left(u_i \rho e\right) - \frac{\partial}{\partial x_i}\left(k\frac{\partial T}{\partial x_i}\right) + \frac{\partial}{\partial x_i}\left(u_i p\right) - \frac{\partial}{\partial x_i}\left(\tau_{ij} u_j\right)\right]^n \\ &+ \frac{\Delta t^2}{2}\left[u_k \frac{\partial^2}{\partial x_k \partial x_i}\left(u_i\left(\rho e + p\right)\right)\right]^n\end{aligned} \tag{7}$$

Yukarıdaki denklemlerde yer alan $\tilde{U}_i$, U_i^n ve Δt sırasıyla, yardımcı momentum, n anındaki momentum ve zaman adımını temsil etmektedir. Q_i, kaynak terimi gibi düşünülen basınç gradyenidir. θ_1 ve θ_2 parametreleri, hesaplamada kullanılan şemanın açık, kapalı veya yarı kapalı olmasına bağlı olarak, sıfır ile bir aralığında değerler alırlar. Yukarıda verilen denklemler basınç için kendine eş olduğundan, Galerkin yaklaşımı uygulanarak uzayda ayrıklaştırılabilirler. Bu denklemler, farklı akış şartlarında (sıkıştırılabilir, sıkıştırılamaz veya barotropik) farklı yaklaşımlar uygulanarak çözüme kavuşturulur. Akış sıkıştırılamaz ise, (5) numaralı denklemin sol tarafında yer alan $\Delta\rho$ terimi sıfıra gider. Daha da önemlisi, enerji denklemi bağımsız olarak her zaman adımının başında veya sonunda sıcaklık değerlerini elde etmek için çözülür. Eğer akış barotropik ise, basınç ve yoğunluk, $p = A\rho^{\gamma}$ bağıntısında verildiği şekilde ilişkilidir. Sıkıştırılabilir bir akış söz konusuysa, basınç ve yoğunluk, mükemmel gaz denkleminde ($p = \rho RT$) verildiği şekilde sıcaklıkla

ilişkilidir ve enerji denklemi, momentum ve süreklilik denklemleri ile birlikte çözülerek gereken sıcaklık değerleri elde edilir.

Yukarıda sözü edilen denklem ve çözüm yöntemleri, sürekli ortam yaklaşımı geçerliyse, akış problemlerinin çözümünde kullanılabilirler. N-S denklemlerinin hangi şartlarda geçerli olduğu ve ne gibi iyileştirmelerle geçerliliğini koruduğunu bilmek oldukça önemlidir. Bu nedenle, yeni tanım ve parametrelere ihtiyaç duyulmaktadır. Gazlar için ortalama serbest uzaklık (λ), bu ihtiyaca cevap veren bir tanımdır. Ortalama serbest uzaklık, bir gaz molekülünün ardışık iki çarpışma arasında kat ettiği mesafe şeklinde tanımlanır. Knudsen sayısı seyrelmenin bir ölçüsüdür ve ortalama serbest uzaklığın karakteristik boya (L) oranı şeklinde tanımlanır:

$$Kn = \frac{\lambda}{L} \tag{8}$$

Knudsen sayısının aldığı değerlere bağlı olarak aşağıdaki akış rejimleri tanımlanmaktadır. Knudsen sayısının 0.001 den küçük olduğu bölge, sürekli rejim olarak isimlendirilmektedir. Bu rejimde yer alan akış problemleri, sürekli ortam yaklaşımına dayalı modeller kullanılarak temsil edilebilmektedir. Knudsen sayısının, 0.001-0.1 aralığında yer aldığı rejim, kayma rejimi olarak adlandırılır. Bu rejimde, N-S çözücüler gibi sürekli ortam yaklaşımına dayalı modeller, katı duvar üzerinde kullanılagelen kaymama/sıcaklıkta-sıçramama şartları yerine kayma-hızı/sıcaklık-sıçraması sınır şartları ile uygulanırsa, akışkan hareketinin temsilinde kullanılabilirler. Geçiş rejiminde, Knudsen sayısı, 0.1 ile 10 arasında değerler alır. Bu rejimde yer alan akış problemleri, Burnett denklemleri gibi yüksek mertebeli sürekli ortam modelleri veya moleküler yaklaşıma dayalı Direct Simulation Monte Carlo (DSMC) yöntemi kullanılarak modellenebilir. Serbest moleküler akış rejiminde, Knudsen sayısı 10'dan büyük olup, moleküller arası etkileşim düşüktür ve seyrelmiş gaz akışı söz konusudur. Boltzmann denklemi bu rejimde kullanılabilir.

Standard şartlarda (T=288°K ve p=1.01x10^5 Pa) hava molekülleri için ortalama serbest uzaklık 0.065 mikrondur. Dolayısıyla bu şartlarda, karakteristik boyu 1 mikron olan bir aygıt için Knudsen sayısı 0.065 olarak hesaplanır. Bu değer akışın kayma rejiminde olduğuna işaret eder. Aynı aygıt için, sıcaklık değişmezken basınç 10'da birine düşerse, akış artık geçiş rejimindedir. Yine aynı aygıt için, 100 km irtifada Knudsen sayısı 3x10^4 olup akış serbest moleküler akış rejimindedir.

Son yıllarda, üretim teknolojilerindeki gelişmelere bağlı olarak, çok küçük boyutlu aygıtlar üretilmiştir. Bu aygıtların bir kısmı, basınç, sıcaklık, kütle akışı vb. için algılayıcı, ya da doğrusal veya açısal hareket için eyleyici olarak kullanılmaktadır. Boyutları 1mm ile 1 mikron arasında değişen, elektrik ve mekanik aygıtların bir bileşimi olan bu aygıtlar, Mikro-Elektro-Mekanik-Sistemler (MEMS) olarak adlandırılırlar. Günümüzde, endüstri ve tıp gibi birçok sahada çok çeşitli MEMS uygulamaları vardır. Bu uygulamalardan bir kısmı, doğrudan ya da dolaylı olarak akışkan hareketi ile ilişkilidir. Mikro-kanal ve mikro-sentetik-jet, bu tip MEMS aygıtlarından sadece ikisidir. Bu mikro boyutlu aygıtların birçoğunun, standart şartlarda kayma rejiminde çalıştıkları bilinmektedir. Bu yüzden, uygun sayısal modellerin kullanılması, bu aygıtların çalışma verimlerinin arttırılması ve işlevlerinin daha iyi kavranmasına hizmet edecektir.

Beskok ve Karniadakis, kayma rejiminde yer alan bir akışın, sürekli ortam yaklaşımına dayalı bir modelle (N-S çözücüler gibi) temsil edilebilmesi için, aşağıda

açık ifadeleri verilmiş olan ikinci mertebeden kayma-hızı (u_s^*) ve sıcaklık-sıçraması (T_s^*) sınır şartlarını önermiştir.

$$u_s^* - u_{wall}^* = \frac{2-\sigma_v}{\sigma_v}\frac{Kn}{1-bKn}\left(\frac{\partial u^*}{\partial n^*}\right)_w + \frac{3}{2\pi}\frac{(\gamma-1)}{\gamma}\frac{Kn^2 Re}{Ec}\left(\frac{\partial T^*}{\partial s^*}\right)_w \tag{9}$$

$$T_s^* - T_{wall}^* = \frac{2-\sigma_T}{\sigma_T}\left[\frac{2\gamma}{(\gamma+1)}\right]\frac{Kn}{Pr}\left(\frac{\partial T^*}{\partial n^*}\right)_w \tag{10}$$

Yukarıdaki denklemlerde yer alan kayma-hızı ve sıcaklık-sıçraması değerleri boyutsuz olup, *Re, Ec* ve *Pr* sırasıyla Reynolds, Eckert ve Prandtl sayılarını göstermektedir. $\partial/\partial n$ ve $\partial/\partial s$, sırasıyla duvara dik ve duvar doğrultusundaki gradyenleri temsil etmektedir. σ_v ve σ_T, duvara paralel momentum ve enerji barındırma (accomodation) katsayılarıdır. N-S çözücüler gibi sürekli ortam modelleri (9) ve (10) numaralı denklemlerin, katı yüzeylerde uygulanan akışkanın sıcaklık ve hızının duvar değerlerine eşit olması şartı yerine kullanılmasıyla, kayma rejimindeki akışı temsil etmek için kullanılabilirler.

Bu çalışmada çeşitli akış problemleri, KTA SEY çözücüsü kullanılarak incelenmiştir. Bu problemler, sıkıştırılamaz akıştan sıkıştırılabilir akışa, ters basamak geometrisi içindeki laminer viskoz akıştan, hareketli diyaframı sayesinde ana akışa momentum transferi gerçekleştiren mikro boyuttaki sentetik jet akışına kadar çeşitlilik göstermektedir. Yukarıda sözü edilen problemlerin çözümünde, Denklem (5) ile verilen süreklilik denklemi kapalı, Denklem (4) ve (6) ile verilen yardımcı ve tamamlayıcı momentum denklemleri açık birer şema kullanılarak çözülmektedir. Algoritmanın kapalı kısmının boyutunu azaltmak için, sanki ikinci dereceden hız/doğrusal basınç (pP2P1) elemanları kullanılmıştır. Bu sayede, basınç ve hız alanları farklı ağlar üzerinde çözülüyormuşçasına sonuçlar elde edilmiştir. pP2P1 tipi elemanlar, doğrusal basınç elemanlarının ortalarına yeni düğüm noktaları yerleştirilmesi ve bu düğüm noktalarının, hızın doğrusal olarak interpole edildiği 4 eleman oluşacak şekilde birleştirilmesiyle elde edilir.

Sentetik jet probleminde olduğu gibi, hesaplamada kullanılan sayısal ağın sınırlarından bir veya birkaçı zamana bağlı bir hareket yapıyorsa, bu hareketin de modellenmesi ve çözüm yöntemiyle birleştirilmesi gerekir. Sınırda yer alan düğüm noktalarının herhangi bir *t* anındaki konumları biliniyor veya hesaplanabiliyorsa, bu düğüm noktalarının hızları da hesaplanabilir. Sınıra komşu olan elemanların, sınırdaki harekete bağlı olarak şekil değiştireceği açıktır. Sınırdaki en büyük yer değiştirme miktarı, sınıra komşu olan elemanın boyu ile kıyaslandığında yeterince büyük ise, bu istenmeyen sonuçlara yol açar. Bu yüzden bir veya daha fazla hareketli sınırla çevrelenmiş ağ bölgesi, her zaman adımında istenilen interpolasyon formülasyonu kullanılarak yenilenir. Böylece, her zaman adımında yenilenen ağ bölgesindeki düğüm noktaları, u_i^g ile gösterilen ağ hızına sahip olurlar. Keyfi-Lagrangian-Euleri (KLE) formülasyonu kullanılıp ağ hızı u_i^g de dikkate alındığında, (4) numaralı yardımcı momentum denklemi aşağıdaki formu alır:

$$\Delta\tilde{U}_i = \tilde{U}_i - U_i^n$$
$$= \Delta t\left[-\frac{\partial}{\partial x_j}\left(u_j\left(U_i - U_i^g\right)\right)^n + \frac{\partial \tau_{ij}^n}{\partial x_j} + \left(\rho g_i\right)\right]^n \tag{11}$$
$$+ \Delta t\left[\frac{\Delta t}{2} u_k \frac{\partial}{\partial x_k}\left(\frac{\partial}{\partial x_j}\left(u_j\left(U_i - U_i^g\right)\right) - \rho g_i\right)\right]^n$$

Bu çalışmada, Beskok ve Karniadakis'in ikinci mertebeden kayma-hızı/sıcaklık-sıçraması sınır şartları kullanılmıştır. Bu sayede, KTA algoritmasının kapasitesi, kayma rejimindeki akış problemlerini kapsayacak şekilde genişletilmiştir. Hareketli ve bozuntuya uğrayan ağ kavramı, KLE yaklaşımı kullanılarak modellenmiş ve geliştirilen algoritmayla birleştirilmiştir. pP2P1 tipi elemanların KTA algoritmasıyla yapılan hesaplamalarda kullanılması, hesaplama zamanı ve gereken hafıza açısından ciddi bir kazanç sağlandığını ortaya koymuştur.

Önerilen algoritmanın performansını ölçmek ve gerçekleştirilen uyarlamaları doğrulamak için, farklı fiziksel ve sayısal özelliklere sahip çeşitli problemler çözülmüştür. Bu analizlerden elde edilen sonuçlar, literatürdeki ve başka çözücüler kullanılarak elde edilenlerle, doğruluk ve hesaplama yükü açısından karşılaştırılmıştır.

Düz mikro kanal, kayma-hızı sınır şartı uyarlamasının doğruluğunu sınamak için test problemi olarak seçilmiş; elde edilen basınç ve hız dağılımları, analitik sonuç ve literatürde yer alan sayısal sonuçlarla karşılaştırılmıştır. Bu karşılaştırmalar, KTA algoritmasının bu problem için hassas sonuçlar verdiğini göstermiştir.

Dikdörtgen hazneli mikro sentetik jet, bu çalışmada sayısal olarak incelenen mikro akış problemlerinden biridir. Hazneye ait geometrik parametrelerin jet oluşum mekanizmasına etkisi sayısal olarak incelenmiştir. Yapılan bu analiz, literatürde yer alan ve sıkıştırılabilir çözücü kullanılarak gerçekleştirilen kapsamlı mikro sentetik jet analizlerinden biridir. Yapılan analizlerde incelenen bazı durumlar için, jet çıkış hızı 140 m/s ulaşmaktadır. Bu durumlar için sıkışabilirlik etkisinin ihmal edilemeyeceği açıktır.

Tez çalışması sırasında gerçekleştirilen bir başka kapsamlı analiz ise, ters basamak geometrisi içindeki sıkıştırılabilir mikro akış problemidir. Bu analizde sonuçlar, KTA algoritmasının hem kaymama/sıcaklıkta-sıçramama hem de kayma-hızı/sıcaklık-sıçraması sınır şartlarıyla kullanılması ile elde edilmiştir. Daha sonra elde edilen bu sonuçlar, tekrar duvara yapışma mesafesi, debi ve giriş çıkış basınç farkı açısından karşılaştırılmıştır.

Elde edilen sonuçlar, yapılan analiz ve karşılaştırmalar, önerilen KTA algoritmasının pP2P1 tipi elemanlarla kullanılmasının, hem kayma rejimi hem de sürekli rejimde yer alan akış problemleri için yararlı olacağını göstermektedir.

1. INTRODUCTION

1.1. Motivation

Characteristic Based Split algorithm has been introduced as a general (unified) algorithm for compressible and incompressible flows. In the second half of the 1990's, this Navier-Stokes solver was quite new and the preliminary research concerning it was published in following years. Using this new Finite Element algorithm for solution of different fluid flow problems, testing applicability and efficiency of the algorithm and comparison of it with the alternative ones were the subjects of many studies in those years. Even though wide varieties of fluid flow problems are included in these studies, no micro flow problem was solved using this algorithm.

Recent experiments show that fluid flow in or through a micro sized geometry differs from the one having larger size. Furthermore, the results of experiments with micro sized geometries could not be explained using a conventional model such as the Navier-Stokes equations. For example, micro channel experiments show that there is a significant increase in mass flow rate comparing with the results obtained via Navier-Stokes solvers. Now, it is well known that the inconsistency between the experimental and numerical results is due to the rarefaction effect which is encountered in flows in micro or smaller sized geometries.

To understand varying properties of fluid flow in a micro geometry, consider air flow in a long micro channel. At the channel inlet, pressure is atmospheric while the outlet is near vacuum. As air flows along the channel, the flow regime may change from incompressible to compressible and from continuum to rarefied. Therefore, a numerical model that can be applied to compressible, incompressible, rarefied and continuum flow problems at the same time is required for simulation of the micro channel flow mentioned above. It is known that a N-S solver can be used for the numerical simulation of slightly rarefied gas flow, if traditional no-slip/no-temperature-jump boundary condition applied at solid wall is modified appropriately. The reasons of this modification, its validity and details are given in following parts

of this thesis. It is also reported in the literature that N-S solver is the most efficient model among the alternatives when it is applicable. Motivation of this thesis is to investigate an efficient solver which is applicable to both compressible and incompressible micro flow problems.

1.2. FEM and Others

The pioneering studies on computational fluid dynamics (CFD) started with the first applications of digital computers. Starting from mid 1960's, with the introduction of panel method, computational techniques took an important role in aerodynamics design and analysis [1]. There has been a phenomenal progress in the development and application of the CFD algorithms for last two decades. This progress is advancing from 1-D to 3-D calculations, from steady to unsteady flows, from potential flow modeling to Reynolds averaged Navier-Stokes equations and Direct Numerical Simulation (DNS), from single block structured grids to unstructured and hybrid grids, and from pure CFD applications to a wide variety of multi disciplinary applications[2]. This progress is directly related to the increasing performance of computers during the last two decades.

Today, there are a number of software packages available that solve fluid flow problems, many courses offered at universities and many researchers are active in the field [3]. On the other hand, computational fluid dynamics is still in progress. This is mostly due to the complex mathematical structure of the Euler, Navier-Stokes and Burnett equations that are used to describe fluid motion.

The momentum equation of fluid flow is obtained by applying Newton's second law to a fluid particle under the body and surface forces. The stress and rate of strain relation is defined by Stokes hypothesis; the viscous forces are expressed explicitly in terms of appropriate flow variables. The resulting equations are called Navier-Stokes equations in honor of M. Navier and G. Stokes who independently obtained the equations in the first half of the nineteenth century [4]. Historically, only the momentum equations were called the Navier-Stokes equations; however, today the complete system of equations of viscous flow –the continuity, momentum and energy- is frequently referred to in the modern literature as the "complete Navier-Stokes equations"[4]. The Navier-Stokes equations (N-S) are second order partial differential equations of evolution type. Since the convection term in the N-S

equations is nonlinear, there do exist exact analytical solutions of N-S equations for a very few highly specialized flow problems [5].

The governing equations of fluid flow need to be discretized for performing a computational analysis. N-S equations can be discretized via finite difference (FDM), finite volume (FVM), boundary element (BEM) or finite element methods (FEM). The FDM, which requires the use of a Cartesian or a curvilinear mesh, directly approximates the differential operators appearing in the governing equations [1]. Therefore, FDM can not be used to analyze of flow for arbitrarily complex geometries. The FVM is evolved via the FDM in the early seventies [1]. In the FVM, the discretizations are accomplished by dividing the domain of the flow into a large number of small subdomains and applying the conservation laws in the integral volume. The mesh that creates the control volume can be structured or unstructured. In BEM, only the boundaries of computational domain are discretized by using isoperimetric elements, but it is not easy to implement to non-homogenous domain. FEM is one of the most popular tools for numerical solution of fluid flow problems. There are also some hybrid methods like FVM-FDM or FEM-FVM in literature. These methods aim to combine several methods according to the advantages of each one in different areas.

The FEM was first constructed as a procedure for structural analysis [6]. The method differs from FDM and FVM by inserting a local approximate solution into the exact equations. Although FEM and FVM produce equivalent or nearly equivalent results for many cases [7,8], the FEM considered to be more general and mathematically consistent approach which can provide alternative possibilities for accuracy/cost adjustment [6-9]. As mentioned before, the major difference between the finite volume and finite element method is that, the solution is assumed to be known in the FEM [7,8]. In FEM, solution domain is divided into finite numbers of elements for which the differential equations are approximated by appropriate interpolation functions [6,7]. Therefore, it can be used both on structured and unstructured grid [10].

In the FEM, variational principle (Rayleigh-Ritz Method) or approximation methods (weighted residual methods) can be used. Since it is not possible to find variational principles in some cases, weighted residuals methods come out to be essential. Collocation, Least Square, Subdomain and Galerkin are the four types of weighted

residuals methods [11]. In computational fluid dynamics problems, Galerkin's method is one of the commonly used weighted residuals method.

In this method, residuals are orthogonally projected onto a set of linearly independent complete functions, which are called weighting functions. It is not required that these functions are exact solution of the given equation. The only requirement is that the residuals must be identically equal to zero.

1.3. CBS History and Applications

Recently, various compressible, high speed flow problems are solved numerically via FEM. This is an expected result of the remarkable development of FEM procedures for the solution of high speed flow problem in last decades. One of these new procedures is the Taylor-Galerkin method [12,13]. This method is finite element equivalent of the Lax-Wendroff method which is developed in the finite difference context [14]. In Taylor-Galerkin process, temporal derivatives are written using Taylor's expansion, and then spatial discretization is done using standard Galerkin approach.

Characteristic-Galerkin method is another FEM which is also applicable to high speed compressible flow problems. The first study on this method was published in 1984 [15] and full description was published in the following years [10,16]. In this method, the convection–diffusion equation is discretized along the characteristics. Since, the resulting equation is self-adjoint in the moving coordinate, Galerkin spatial discretization is optimal. But difficulties of mesh updating due to moving coordinates are overcome using the approximate backward integration introduced by Löhner et al [15,17] (see also Appendix A). Different type of approximations can be used for average velocity along the characteristics, and they lead to different stabilizing term. It is proved that Galerkin spatial discretization is justified when the characteristic-Galerkin procedure is used [18,19]. Both of the FEM procedures mentioned above yield an identical approximation when a single variable and characteristic speed exist.

Fractional step algorithm was devised originally by Chorin [20,21] for the solution of incompressible flow problems in finite difference context and it was developed and has been used by many fluid dynamicist so far. In this method, a time steping process

is implemented for the momentum and continuity equation in which velocity and pressure are the essential variables. Sometimes this method is interpreted as a projection method since it starts obtaining an approximate (or auxiliary) velocity field. This approximate velocity field is obtained from the momentum equation in which the effect of pressure gradient is excluded. After the first step, unknown pressure values are obtained using approximate velocity field in continuity equation. Approximate velocity field is updated using computed pressure values in the final stage, called the correction step. This process is also known as velocity correction method.

In 1995, Zienkiewicz et al. introduced a unified algorithm designed to replace the Taylor-Galerkin (or Lax-Wendroff) methods that have been used by them so far in the solution of compressible flow problems [18]. Then, they have published several papers concerning the basis and applications of the new algorithm that can be applied to all fluid mechanics problems [22,23]. Finally they published a paper and the algorithm was named as Characteristic-Based-Split (CBS) algorithm [24]. Thus, fractional step process of Chorin is extended to solve the fluid dynamics equations of both compressible and incompressible forms.

The main aspect of the CBS procedure is to split the equations into two parts. The first part of the equations is a set of simple scalar convection-diffusion type equations. So, the characteristic-Galerkin procedure is applied to these equations and gives an optimal solution [18,19]. The second part of equations is self-adjoint. Therefore, the equations are discretized by the Galerkin approach.

It is known that the original Chorin's split could never be used in fully explicit code, whereas the CBS provides a fully explicit algorithm in the incompressible case for steady-state problems using artificial compressibility. The steady-state solution is not affected by this artificial compressibility. The algorithm is also applicable for fully compressible flows in both *explicit* and *semi-implicit* forms [19,22-23].

1.3.1. pP2P1 Type Elements

When semi-implicit form of the CBS algorithm is used, pressure field is obtained by solving the continuity equation implicitly. Therefore any reduction on the size of the continuity equation results in significant savings in the number of calculations and storage requirements. This is possible when pseudo-quadratic velocity/linear pressure

elements (pP2P1) are used instead of linear velocity-pressure elements (P1P1) [25,26]. These types of elements were first used for the solution of incompressible fluid flow using Streamline-Upwind Petrov-Galerkin method (SUPG)[25] and it was shown that using pP2P1 type element instead of P1P1 didn't degrade the accuracy of algorithm [26,27].

1.3.2. ALE Description

Arbitrary–Lagrangian-Eulerian (ALE) approach can be used for the solution of the fluid flow problems which have moving boundaries. Due to the movement of the boundary nodes, the elements next to the moving boundary are also deformed. If the amount of this deformation is not small compared to the length of the element, this deformation has to be diffused to surrounding elements in the computational grid using basic interpolation formulas to prevent forming of spurious elements in the domain. If the position of the moving boundary is known or can be computed at every time step, the velocity and location of other nodes are calculated and mesh is updated. Implementation of the CBS algorithm within ALE description is presented in Chapter 4.

1.4. MEMS

It is known that extremely small machines have been fabricated using modern manufacturing processes. These electrostatic, magnetic, electromagnetic, pneumatic and thermal actuators, motors, valves, gears, cantilevers, diaphragms and tweezers have characteristic lengths less than 0.1 mm. These machines have been used as sensors for pressure, temperature, mass flow, velocity, sound and chemical composition, as actuators for linear and angular motions, as simple components for complex systems, micro-heat-engines and micro-heat-pumps [28,29].

Micro-electro-mechanical systems (MEMS) which are fabricated using integrated circuit batch-processing technologies are combinations of electrical and mechanical components and they have characteristic lengths in the range of 1 mm to 1 micron [28,29]. To imagine the dimension of the MEMS, it can be said that a micro devices can have a characteristic length smaller than the diameter of a human hair. Surface and bulk silicon micromachining, lithography electrodeposition and plastic molding; and electrodischarge machining are current manufacturing techniques for MEMS

[29]. Increasing application areas of MEMS include variety of industrial and medical fields. Accelerometers for automobile airbags, keyless entry systems, dense arrays of micromirrors for high-definition optical displays, scanning electron microscope tips to image single atoms, micro-heat-exchangers for cooling of electronic circuits, reactors for separating biological cells, blood analyzers and pressure sensors for catheter tips are given in Reference [28] as a few of current usages examples of MEMS.

1.4.1. Micro Fluidic Devices

Some of the MEMS devices include fluid flow. Microducts, micronozzles, microturbines, and microvalves are a few examples of these type microfluidic devices. Some MEMS devices are indirectly related to the fluid flow. Microsensors and microactuators have potential to be used in flow control. In this study, some micro flow problems are numerically investigated.

1.4.2. Micro Synthetic Jet

One of the MEMS technology products is micro synthetic jet actuator (μSJA) and it is used for various applications including cooling of electronic packages, micro mixing and aerodynamic flow control [28-33]. In an effort to expand the understanding of flow fields generated by μSJA, a compherensive numerical study is included in the thesis [34]. An introduction to synthetic jet flow and jet formation mechanism is the subject of Chapter 6.

1.5. Fluid Modeling

Fluid flows can be modelled using molecular and continuum models. Continuum models assume that fluid is a continuous matter and macroscopic properties of the fluid such as pressure, density, velocity, and etc. can be defined at every point in space and time. A set of nonlinear partial differential equations form the continuum models. As seen in the Figure 1.1 adopted from Reference [28], Euler, N-S and Burnett are the continuum models.

Molecular models assume that fluid is a collection of gas molecules and as seen in the Figure 1.1, this type of models can be subdivided in to deterministic and probabilistic ones. Boltzmann and Direct Simulation Monte Carlo Method (DSMC)

are statistical models while the modern molecular dynamic computer simulation (MD) is deterministic. Details and validity of the models seen in the figure are given in following part of the thesis.

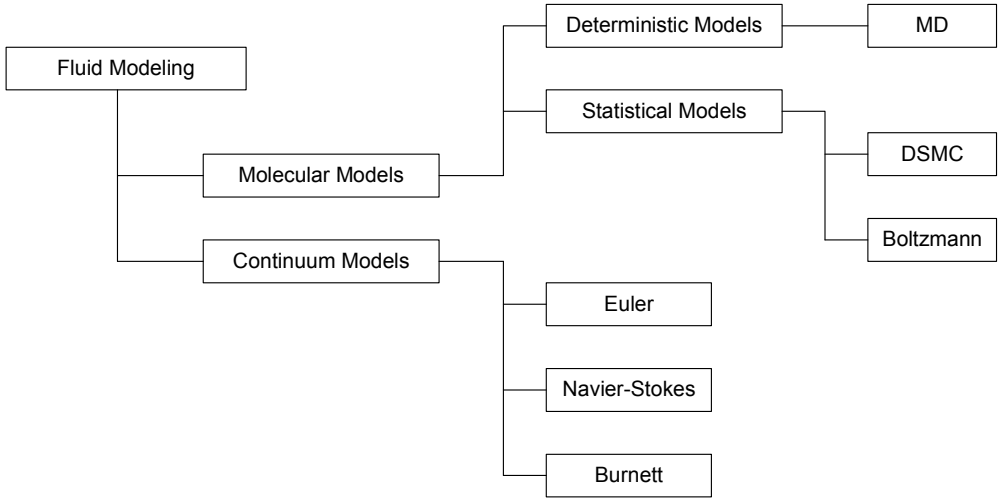

Figure 1.1 : Flow Models

1.5.1. Continuum Models

One of the continuum models is the N-S equations and it can be used for the solution of various problems of fluid mechanics. This continuum model ignores the molecular nature of the gases as Euler and Burnett do. However N-S equations can be derived from the Boltzmann equation which is a molecular model [28]. This is possible for dilute gas flows near equilibrium.

Governing equations of compressible viscous fluid flow are continuity, momentum and energy equations and are given in Chapter 2. In continuum models, local properties of fluid such as density, pressure, velocities and etc. can be defined as an average over a fluid element. If these element is large compared to the microscopic structure of the fluid and small enough compared to the scale of macroscopic phenomena, accurate prediction is obtained via continuum models. In addition to this, the use of continuum model is valid if the flow is not far from thermodynamic equilibrium.

As flow conditions deviate from thermodynamic equilibrium, first, traditional no-slip/no-jump conditions which are valid for viscous fluid flow on solid-fluid interface, break down. Then, the linear stress-strain rate and heat flux-temperature gradient relations given within the N-S equations (see Chapter 2) become invalid.

Higher order Burnett equations or molecular-based models are alternatives where linear relation given in the N-S equations breaks down for the fluid flow far from thermodynamic equilibrium. As expected, using alternative methods results in additional costs within the computation. For the cases in which no-slip/no-jump boundary conditions break down, alternative boundary conditions are discussed in this chapter and given in Chapter 5 with details.

1.5.2. Molecular Models

In molecular models, fluid is defined as a group of discrete particles. These particles are molecules, atoms, ions and electrons as expected. Determining position, velocity and state of all particles at any time is the main goal of the molecular models.

In deterministic molecular models, motion of the molecules is governed by the laws of the classical mechanics. As reported in Reference [28], Alder and Wainwrigth have done pioneering study of modern molecular dynamics computer simulation (MD) then, the method has been reviewed by many others so far. To simulate a reasonable flow field using MD simulation, huge computer resources are required. Therefore, MD can be used for the simulation of dense gases and liquids. For dilute gases in which the molecular interactions are frequent, the MD simulation is highly inefficient.

Statistical approaches are alternative to deterministic MD model mentioned above. The goal of these alternative methods is computing the probability of finding a molecule at a particular position and state. Molecular based Boltzmann equation is valid for all the flow cases mentioned here. But it is known that analytical solutions of this equation for arbitrary geometries are too difficult. This difficulty is due to the nonlinearity of the collision integral it has. Another statistical method is the direct simulation Monte Carlo (DSMC) method. This method was developed by Bird and details of the method can be found in Reference [35].

1.5.3. Continuum Models with Modified Boundary Condition for Micro Flow

Fluid flow through small devices such as MEMS differs from the larger ones. Fluid flow through that kind of devices has dominant surface effects. Surface to volume ratio for a machine which has characteristic length of 1 m is 1 m^{-1}, while this ratio for a MEMS device with characteristic length of 1 μm is 10^6 m^{-1}. The increase in the

surface-volume ratio due to the decreasing characteristic length affects transport of mass, momentum energy through the surfaces. Furthermore, flow deviates from the thermodynamic equilibrium and slip-flow, thermal creep, rarefaction, viscous dissipation, compressibility, intermolecular forces and other unconventional effects become important [28]. As mentioned before, first of all, the traditional no-slip/no-jump (for velocity and temperature at solid wall) boundary condition breaks down. In this case, continuum models such as N-S solvers can be used for the solution of fluid flow problems using slip-velocity/temperature-jump boundary conditions. There are the first and higher order slip-velocity/temperature-jump boundary conditions in the literature and their validity and details are given in Chapter 5.

1.6. Thesis Overview

In Chapter 2, governing equations of compressible viscous fluid flow are given in general and conservative form. Non-dimensional forms of the governing equations are also given at the end of this chapter. The well known no-slip/no-jump boundary conditions are also given for viscous fluid flow in this chapter.

In Chapter 3, implementation of the characteristic-Galerkin process to the continuity, momentum and energy equations of compressible, viscous fluid flow in conservative form are given with details. It is known that the characteristic-Galerkin process is applicable to scalar convection diffusion equations and the details of this process are given in Appendix A. Implementation of Chorin's fractional step method which is devised originally for the incompressible viscous flow problems is also given in this chapter with details. Hence, the temporal discretization of the governing equations using Characteristic-Based-Split procedure is defined and details are also given in this chapter.

In Chapter 4, spatial discretizations of the resulting equation obtained using characteristic-Galerkin process are given. Galerkin weak form of the algorithm and the matrix form of the equations are also given in this chapter. Modifications on the procedure due to the moving deforming grid concept and use of pseudo-quadratic velocity/linear-pressure elements are given in this chapter. Solution strategies and procedure of simplified equations due to the flow properties are other subtitles of this chapter.

The essential modifications on the boundary conditions due to the increasing effect of the rarefaction are given in Chapter 5. The fluid flow regimes which are also known as Knudsen regimes are defined and appropriate flow models in terms of computational cost and efficiency for these regimes are also given in this chapter. Use of continuum fluid models for a slightly rarefied gas flow with the second order slip-velocity and temperature-jump boundary conditions of Beskok and Karniadakis are given with details in this chapter.

One of comprehensive numerical studies done within this study is μSJA flow. Some useful information about synthetic jets and jet formation mechanism is given in Chapter 6 before giving the details of the numerical analysis done.

In Chapter 7, solutions of different fluid flow problems both in continuum and slip regimes solved via the CBS algorithm are given. The continuum fluid flow problems include incompressible, laminar internal flow to compressible external fluid flow around NACA0012 airfoil, while the micro flow includes micro synthetic jet flow to rarefied internal fluid flow through backward facing step geometry. Micro flow physics investigated numerically using CBS algorithm for the solution of different problems are given in this chapter. Finally, conclusion is given in Chapter 8.

2. GOVERNING EQUATIONS

For compressible viscous flow, full conservative form of Navier-Stokes equations can be written in Cartesian co-ordinate system (x_1, x_2, x_3) as follows:

$$\frac{\partial \mathbf{V}}{\partial t} + \frac{\partial \mathbf{F_i}}{\partial x_i} + \frac{\partial \mathbf{G_i}}{\partial x_i} + \mathbf{Q} = 0, \quad i = 1,2,3 \tag{2.1}$$

General form of the Navier-Stokes equation which is given above includes continuity, momentum and energy equations. In the equation; $\mathbf{V}$ is the dependent variable vector and it is in the following form:

$$\mathbf{V} = \begin{bmatrix} \rho \\ \rho u_1 \\ \rho u_2 \\ \rho u_3 \\ \rho e \end{bmatrix} \tag{2.2}$$

Convective flux vector in i th direction is denoted by $\mathbf{F_i}$ and it can be written explicitly as follows:

$$\mathbf{F_i} = \begin{bmatrix} \rho u_i \\ \rho u_1 u_i + \delta_{1i} p \\ \rho u_2 u_i + \delta_{2i} p \\ \rho u_3 u_i + \delta_{3i} p \\ u_i(\rho e + p) \end{bmatrix} \tag{2.3}$$

$\mathbf{G_i}$ denotes the diffusion terms.

$$\mathbf{G_i} = \begin{bmatrix} 0 \\ -\tau_{1i} \\ -\tau_{2i} \\ -\tau_{3i} \\ -\left(k\,\partial T/\partial x_i\right) - \tau_{ij} u_j \end{bmatrix} \tag{2.4}$$

The source terms due to gravity acceleration is given as below:

$$\mathbf{Q} = \begin{bmatrix} 0 \\ -\rho g_1 \\ -\rho g_2 \\ -\rho g_3 \\ -\rho\left(g_i u_i + r\right) \end{bmatrix} \tag{2.5}$$

In the Navier-Stokes equations written above, τ_{ij} are related to the velocity gradient linearly by the Stokes hypothesis as written below.

$$\tau_{ij} = \mu\left[\left(\frac{\partial u_i}{\partial x_j} + \frac{\partial u_j}{\partial x_i}\right) - \delta_{ij}\frac{2}{3}\frac{\partial u_k}{\partial x_k}\right] \tag{2.6}$$

In the equations given here, ρ is the density, u_i is the velocity component in x_i direction, p is the pressure, T is the temperature, g_i is the i th component of the gravity acceleration, r is a heat source, k is the thermal conductivity, μ is the viscosity and δ_{ij} is the Kronecker delta function ($\delta_{ij} = 1$ if $i = j$ and $\delta_{ij} = 0$ if $i \neq j$). The equations are completed by the perfect gas equation given below.

$$p = \rho RT \tag{2.7}$$

where R is gas constant. The total energy per unit mass is denoted with e (internal plus kinetic) and it is related to temperature and velocity through the following equation:

$$e = c_v T + u_i u_i / 2 \tag{2.8}$$

In the equation given above, c_v is the specific heat at constant volume.

In addition to governing equations given here, appropriate initial and boundary conditions are required for numerical simulation of a viscous flow problem. At a solid wall, Neumann or Drichlet type boundary conditions can be set for temperature to represent appropriate heat transfer conditions such as adiabatic wall (zero temperature gradient) or constant wall temperature. Velocity and temperature of the fluid particles adjacent to the solid wall are equal to the velocity and temperature of the wall. These relationships are formulated as follows.

$$\vec{u}_{fluid} = \vec{u}_{solid} \tag{2.9}$$

$$T_{fluid} = T_{solid} \tag{2.10}$$

Due to the rarefaction effect which is considered often in micro flow, fluid velocity and temperature near the solid wall may differ from the equations given above. Formulation and details of this behavior will be given in Chapter 5.

For a subsonic external flow, all quantities except density can be specified at the inlet, upper and lower sides of the computational domain. Using two basic types of boundary conditions given below, pressure and velocity are specified at the boundaries [19].

$$u_i = \bar{u}_i \ \ on \ \ \Gamma_u \tag{2.11}$$

$$t_i = \left(-p\delta_{ij} + \tau_{ij}\right)n_j = \bar{t}_i \ \ on \ \ \Gamma_t \tag{2.12}$$

In the equations given above, over bar values denote the prescribed values of velocity and traction on boundaries Γ_u and Γ_t. Implementation of these boundary conditions is given in Chapter 4..

2.1. Non-Dimensional Form of the Governing Equations

The governing equations of compressible viscous flow in conservative form given in this chapter can be written in non-dimensional form. Following expressions are generally used to non-dimensionalize the compressible viscous flow equations:

$$t^* = \frac{tu_\infty}{L}; \qquad x_i^* = \frac{x_i}{L}; \qquad \rho^* = \frac{\rho}{\rho_\infty}; \qquad p^* = \frac{p}{\rho_\infty u_\infty^2} \tag{2.13}$$

$$u_i^* = \frac{u_i}{u_\infty}; \qquad e^* = \frac{e}{u_\infty^2}; \qquad T^* = \frac{Tc_p}{u_\infty^2}; \qquad a^* = \frac{a}{u_\infty}$$

The symbol having subscript ∞ denotes the reference value. c_p and L are specific heat at constant pressure and reference length of the flow, respectively. The superscript $*$ denotes non-dimensional variable. Using the definition given in Equation (2.13), continuity, momentum, energy and gas state equations takes the following form.

$$\frac{\partial \rho^*}{\partial t^*} = \frac{1}{\left(a^*\right)^2}\frac{\partial p^*}{\partial t^*} = -\frac{\partial U_i^*}{\partial x_i^*} \tag{2.14}$$

$$\frac{\partial U_i^*}{\partial t^*} = -\frac{\partial}{\partial x_j^*}\left(u_j^* U_i^*\right) + \frac{1}{Re}\frac{\partial\left(\nu^* \tau_{ij}^*\right)}{\partial x_j^*} - \frac{\partial p^*}{\partial x_i^*} + \rho^* g_i^* \tag{2.15}$$

$$\begin{aligned}\frac{\partial\left(\rho^* e^*\right)}{\partial t^*} = &-\frac{\partial}{\partial x_j}\left(u_j^* \rho^* e^*\right) + \frac{1}{RePr}\frac{\partial}{\partial x_i^*}\left(k^* \frac{\partial T^*}{\partial x_i^*}\right) \\ &-\frac{\partial}{\partial x_j^*}\left(u_j^* p^*\right) + \frac{1}{Re}\frac{\partial}{\partial x_i^*}\left(\nu^* \tau_{ij}^* u_j^*\right)\end{aligned} \tag{2.16}$$

$$p^* = \frac{\rho^* R T^*}{c_p} = \rho^* R^* T^* = \rho^* \frac{(\gamma - 1)}{\gamma} T^* \tag{2.17}$$

In the equation written above *Re* and *Pr* denote non-dimensional numbers Reynolds and Prandtl. They are in the following form:

$$Re = \frac{\rho_\infty u_\infty L}{\mu_\infty} \tag{2.18}$$

$$Pr = \frac{\mu_\infty c_p}{k_\infty} \tag{2.19}$$

While *Re* number represents the ratio of inertia to viscous force, *Pr* represents the relative importance of momentum and energy transport by the diffusion process [36]. In addition to these two non-dimensional numbers, following non-dimensional variable definitions are used in the Equation (2.14)-(2.17).

$$g_i^* = \frac{g_i L}{u_\infty^2}, \quad \nu^* = \frac{\nu}{\nu_\infty}, \quad k^* = \frac{k}{k_\infty} \tag{2.20}$$

Using the expressions given above, following non-dimensional equations that are useful to relate energy, the speed of sound, pressure, temperature and etc. can be obtained:

$$e^* = \frac{T^*}{\gamma} + \frac{1}{2} u_i^* u_i^* \tag{2.21}$$

$$\left(a^*\right)^2 = (\gamma - 1) T^* \tag{2.22}$$

$$p^* = (\gamma - 1)\left(\rho^* e^* - \frac{1}{2}\frac{U_i^* U_i^*}{\rho^*}\right) \tag{2.23}$$

In the Equation given above, U_i^* denotes the nondimensional momentum value in *i* th direction and it can be written explicitly as $U_i^* = \rho^* u_i^*$. γ is the specific heat ratio. Even though, non-dimensional form of the governing equations is given in this chapter, discretization process and details are given in the following chapters using dimensional form of the equations for clarity.

3. CHARACTERISTIC BASED SPLIT ALGORITHM

3.1. Introduction

In this chapter, the governing equations of compressible viscous flow, given in the previous chapter are discretized along the characteristic using characteristic-Galerkin procedure as defined in Characteristic-Based-Split algorithm. This approach and discretization procedure in its full form was first introduced in 1995 by Zienkiewicz and Codina [18]. With the help of this new algorithm, the fractional step method, originally devised by Chorin for the solution of incompressible flow problems, is extended to compressible flow problems.

3.2. Discretization along the Characteristic and Split

In the previous chapter, governing equations of viscous fluid flow are given in general form which is applicable both to compressible and incompressible flow cases. Continuity, momentum and energy equations form the complete set of N-S equations. For compressible flow case, the energy equation is fully coupled with the momentum and continuity equation. For incompressible flow case, energy coupling disappears and the equations are simplified.

Writing these three equations separately instead of the fully conservative and standard form given in the previous chapter may help to see essential features of the all equations. If the mass fluxes are denoted with $U_i = \rho u_i$, continuity equation can alternatively be written as:

$$\frac{\partial \rho}{\partial t} = \frac{1}{a^2}\frac{\partial p}{\partial t} = -\frac{\partial U_i}{\partial x_i} \tag{3.1}$$

, where speed of sound is denoted with a and it depends on e, p and ρ. Assuming constant entropy, a relationship between these variables can be formulated as follows:

$$a^2 = \frac{\partial p}{\partial \rho} = \frac{\gamma p}{\rho} \tag{3.2}$$

In the equation above, γ is specific heat ratio. Momentum equation is in the following form:

$$\frac{\partial U_i}{\partial t} = -\frac{\partial}{\partial x_j}\left(u_j U_i\right) + \frac{\partial \tau_{ij}}{\partial x_j} - \frac{\partial p}{\partial x_i} + \rho g_i \tag{3.3}$$

And energy equation is as follows:

$$\frac{\partial(\rho e)}{\partial t} = -\frac{\partial}{\partial x_j}\left(u_j \rho e\right) + \frac{\partial}{\partial x_i}\left(k\frac{\partial T}{\partial x_i}\right) - \frac{\partial}{\partial x_j}\left(u_j p\right) + \frac{\partial}{\partial x_i}\left(\tau_{ij} u_j\right) \tag{3.4}$$

The similarity can be easily noticed between the momentum equation given with Equation (3.3) and scalar convection-diffusion type of equation written below.

$$\frac{\partial \phi}{\partial t} + \frac{\partial}{\partial x_i}\left(\phi u_i\right) - \frac{\partial}{\partial x_i}\left(k\frac{\partial \phi}{\partial x_i}\right) + Q = 0 \tag{3.5}$$

The scalar convection diffusion equation written above can be discretized in time using Characteristic-Galerkin procedure (see details in Appendix A). Except the pressure gradient term in the momentum equation (Equation (3.3)), these two equations are similar. So, if the pressure gradient term is assumed to be a known quantity such as source term Q appearing in the scalar convection diffusion equation, Equation (3.3) can be discretized via characteristic-Galerkin process. The momentum equation can also be written in the following form to which characteristic-Galerkin process can be applied.

$$\frac{\partial U_i}{\partial t} = -\frac{\partial}{\partial x_j}\left(u_j U_i\right) + \frac{\partial \tau_{ij}}{\partial x_j} + \rho g_i + Q_i \tag{3.6}$$

Following equation is obtained after discretization of the scalar convection-diffusion equation (Equation (3.5)) in time using characteristic-Galerkin process (see details in Appendix A) [18,19].

$$\phi^{n+1}-\phi^{n}=-\Delta t\left[\frac{\partial}{\partial x_j}\left(u_j\phi\right)-\frac{\partial}{\partial x_j}\left(k\frac{\partial\phi}{\partial x_j}\right)+Q\right]^{n}$$
$$+\frac{\Delta t^2}{2}u_i^{n}\frac{\partial}{\partial x_i}\left[\frac{\partial}{\partial x_j}\left(u_j\phi\right)-\frac{\partial}{\partial x_j}\left(k\frac{\partial\phi}{\partial x_j}\right)+Q\right]^{n} \tag{3.7}$$

In this process, the total derivatives in Equation (3.5) are discretized along the characteristics. After this discretization, standard Galerkin discretization in space is optimal but moving co-ordinate systems which leads to mesh updating becomes essential. This difficulty is overcome using some approximations (see Appendix A) [15-17]. Replacing ϕ with U_i in Equation (3.7), similar equation is obtained for momentum equation as given below:

$$U_i^{n+1}-U_i^{n}=\Delta t\left[-\frac{\partial}{\partial x_j}\left(u_jU_i\right)^{n}+\frac{\partial\tau_{ij}^{n}}{\partial x_j}+Q_i^{n+\theta_2}+\left(\rho g_i\right)^{n}\right]$$
$$+\frac{\Delta t^2}{2}u_k\frac{\partial}{\partial x_k}\left[\frac{\partial}{\partial x_j}\left(u_jU_i\right)-Q_i-\rho g_i\right]^{n} \tag{3.8}$$

, where $Q_i^{n+\theta_2}$ is assumed to be a known quantity evaluated at time $t=t^{n}+\theta_2\Delta t$ in a Δt time increment ($\theta_2\in[0,1]$). It can be written explicitly as following:

$$Q_i^{n+\theta_2}=-\frac{\partial p^{n+\theta_2}}{\partial x_i} \tag{3.9}$$

, with

$$\frac{\partial p^{n+\theta_2}}{\partial x_i}=\theta_2\frac{\partial p^{n+1}}{\partial x_i}+\left(1-\theta_2\right)\frac{\partial p^{n}}{\partial x_i} \tag{3.10}$$

To obtain momentum flux value at time *n+1* by using the Equation (3.8), it is necessary to obtain an approximation for *Q* which allows calculation to proceed before obtaining pressure values belonged time *n+1*. So split procedure becomes essential at this stage. The name of Characteristic-Based-Split (CBS) comes from this combination of characteristic-Galerkin and split procedure.

Defining an auxiliary variable for momentum flux and denoting it with $\tilde{U}$, the difference between momentum flux value at time *n* and auxiliary one can be written as follows:

$$\Delta\widetilde{U}_i = \widetilde{U}_i - U_i^n$$
$$= \Delta t\left[-\frac{\partial}{\partial x_j}\left(u_j U_i\right)^n + \frac{\partial \tau_{ij}^n}{\partial x_j} + \left(\rho g_i\right) + \frac{\Delta t}{2} u_k \frac{\partial}{\partial x_k}\left(\frac{\partial}{\partial x_j}\left(u_j U_i\right) - \rho g_i \right)\right]^n \tag{3.11}$$

Two different split procedures can be applied to the momentum equation in CBS procedure [19]. In the first, the pressure gradient term in the Equation (3.8) is retained. Removing the pressure gradient term completely from the auxiliary momentum equation (as given Equation (3.11)) is the second way. In this study, the second one is chosen.

By using the Equation (3.11), auxiliary momentum flux can be obtained explicitly. Correction step for the momentum flux is written as follows:

$$\Delta U_i = U_i^{n+1} - U_i^n = \Delta\widetilde{U}_i - \Delta t \frac{\partial p^{n+\theta_2}}{\partial x_i} + \frac{\Delta t^2}{2} u_k \frac{\partial^2 p^n}{\partial x_k \partial x_i} \tag{3.12}$$

It is known that, the second split procedures with second order pressure term in the equation above stabilizes the incompressible flow and allows the arbitrary interpolation while the first one does not [19]. The second type of split is also recommended for universally use of algorithm by Zienkiewicz and Codina.

To obtain new momentum values using momentum correction step given with Equation (3.12), the pressure field at time *n+1* have to be obtained before. The pressure values are obtained from the continuity equation. The continuity equation can be written in time interval *n* to *n+1* as follows:

$$\Delta\rho = \left(\frac{1}{a^2}\right)^n \Delta p = -\Delta t \frac{\partial U_i^{n+\theta_1}}{\partial x_i} = -\Delta t\left[\frac{\partial U_i^n}{\partial x_i} + \theta_1 \frac{\partial \Delta U_i}{\partial x_i} \right] \tag{3.13}$$

Using the auxiliary momentum flux value with Equation (3.11), the equation above can be written alternatively as:

$$\Delta\rho = \left(\frac{1}{a^2}\right)^n \Delta p = -\Delta t\left[\frac{\partial U_i^n}{\partial x_i} + \theta_1 \frac{\partial \Delta\widetilde{U}_i}{\partial x_i} - \Delta t\,\theta_1\left(\frac{\partial^2 p^n}{\partial x_i \partial x_i} + \theta_2 \frac{\partial^2 \Delta p}{\partial x_i \partial x_i} \right)\right] \tag{3.14}$$

In the equation above, the term $O\left(\Delta t^3\right)$ and higher order are neglected. Using characteristic-Galerkin process for time discretization of energy equation, following equation is obtained:

$$\Delta(\rho e) = -\Delta t\left[\frac{\partial}{\partial x_i}(u_i \rho e) - \frac{\partial}{\partial x_i}\left(k\frac{\partial T}{\partial x_i}\right) + \frac{\partial}{\partial x_i}(u_i p) - \frac{\partial}{\partial x_i}(\tau_{ij} u_j)\right]^n + \frac{\Delta t^2}{2}\left[u_k \frac{\partial^2}{\partial x_k \partial x_i}(u_i(\rho e + p))\right]^n \tag{3.15}$$

Spatial discretization of Equations (3.11), (3.12), (3,14) and (3.15) via Galerkin FEM approach is given in the following chapter. Solution procedures of resulting equations will also be explained in Chapter 4.

4. SPATIAL DISCRETIZATION AND SOLUTION PROCEDURE

In this chapter, the equations obtained after temporal discretization of continuity, momentum and energy equations in the previous chapter are spatially discretized using Gelerkin approach. The resulting FEM algorithm and its solution procedure for some flow cases with simplifications or assumptions are discussed in this chapter. Matrix form of the algorithm is also given in this chapter. Use of different type elements within the algorithm and the modification required to use a moving deforming grid is also presented in this chapter.

4.1. Galerkin Finite Element Formulation

Weighted residual integrals are obtained by multiplying Equations (3.11), (3.12), (3.14) and (3.15) with weighting function W and integrating them over the domain Ω. Weighted residual integrals for these equations are as follows:

$$\int_\Omega W\frac{\Delta\widetilde{U}_i}{\Delta t}d\Omega = -\int_\Omega W\left(\frac{\partial}{\partial x_j}\left(u_jU_i\right)-\rho g_i\right)^n d\Omega + \int_\Omega W\frac{\partial\tau_{ij}^n}{\partial x_j}d\Omega + \frac{\Delta t}{2}\int_\Omega\left(Wu_k^n\right)\frac{\partial}{\partial x_k}\left(\frac{\partial}{\partial x_j}\left(u_jU_i\right)-\rho g_i\right)^n d\Omega \tag{4.1}$$

$$\int_\Omega W\frac{\Delta\rho}{\Delta t}d\Omega = -\int_\Omega W\frac{\partial U_i^n}{\partial x_i}d\Omega - \theta_1\int_\Omega W\frac{\partial}{\partial x_i}\left(\Delta\widetilde{U}_i - \Delta t\frac{\partial p^{n+\theta_2}}{\partial x_i}\right)d\Omega \tag{4.2}$$

$$\int_\Omega W\frac{\Delta U_i}{\Delta t}d\Omega = \int_\Omega W\frac{\Delta\widetilde{U}_i}{\Delta t}d\Omega - \int_\Omega W\frac{\partial p^{n+\Theta_2}}{\partial x_i}d\Omega + \frac{\Delta t}{2}\int_\Omega Wu_k\frac{\partial}{\partial x_k}\frac{\partial p^{n+\Theta_2}}{\partial x_i}d\Omega \tag{4.3}$$

$$\int_\Omega W\frac{\Delta(\rho e)}{\Delta t}d\Omega = -\int_\Omega W\frac{\partial}{\partial x_i}\left[u_i(\rho e+p)\right]^n d\Omega + \int_\Omega W\frac{\partial}{\partial x_i}\left(k\frac{\partial T}{\partial x_i}+\tau_{ij}u_j\right)^n d\Omega + \frac{\Delta t}{2}\int_\Omega Wu_k^n\frac{\partial^2}{\partial x_k\partial x_i}\left[u_i(\rho e+p)\right]d\Omega \tag{4.4}$$

The equations written above are spatially discretized using standard Galerkin procedure since this discretization is fully justified for the characteristic-Galerkin

procedure. Galerkin weak forms of the equations are obtained by replacing W with appropriate shape functions in the weighted residuals integral given above [11].

4.1.1. Fractional Momentum Equation

Choosing velocity shape function N_u as a weighing function and applying Green's theorem (see Appendix B) to second order term appearing in Equation (4.1), following Galerkin weak form is obtained.

$$\begin{aligned}\int_{\Omega} N_u \Delta\widetilde{U}_i d\Omega = \Delta t\Bigg[&- \int_{\Omega} N_u \frac{\partial}{\partial x_j}\left(u_j U_i\right) d\Omega - \int_{\Omega} \frac{\partial N_u}{\partial x_j} \tau_{ij}^n d\Omega + \int_{\Omega} N_u \left(\rho g_i\right) d\Omega \Bigg]^n \\ &+ \frac{\Delta t^2}{2}\Bigg[\int_{\Omega} \frac{\partial}{\partial x_k}\left(u_k N_u\right)\left(- \frac{\partial}{\partial x_j}\left(u_j U_i\right) + \rho g_i \right) d\Omega \Bigg]^n \\ &+ \Delta t\Bigg[\int_{\Gamma} N_u \tau_{ij} n_j d\Gamma \Bigg]^n\end{aligned} \tag{4.5}$$

where n_j is the j th component of unit vector outward normal to boundary Γ. If no-slip or slip-velocity boundary condition is directly imposed during the calculation of auxiliary momentum value, there is no need to calculate boundary integral term given in the equation above on the solid wall.

4.1.2. Continuity Equation

Selecting pressure shape function N_p as test function and using the same procedure applied to the Equation (4.5) to the continuity equation gives following equation,

$$\begin{aligned}\int_{\Omega} N_p \frac{\Delta\rho}{\Delta t} d\Omega &= -\int_{\Omega} N_p \frac{\partial}{\partial x_i}\left(U_i^n + \theta_1 \Delta\widetilde{U}_i - \theta_1 \Delta t \frac{\partial p^{n+\theta_2}}{\partial x_i} \right) d\Omega \\ &= \int_{\Omega} \frac{\partial N_p}{\partial x_i}\left[U_i^n + \theta_1\left(\Delta\widetilde{U}_i - \Delta t \frac{\partial p^{n+\theta_2}}{\partial x_i} \right)\right] d\Omega \\ &\quad - \int_{\Gamma} N_p \left[U_i^n + \theta_1\left(\Delta\widetilde{U}_i - \Delta t \frac{\partial p^{n+\theta_2}}{\partial x_i} \right)\right] n_i d\Gamma\end{aligned} \tag{4.6}$$

Boundary integral term shown in the above equation is identically equal to zero at solid boundary since the normal component of the velocity is equal to zero.

4.1.3. Momentum Equation (Correction step)

Selecting same test function N_u with the fractional momentum equation, following equation is obtained.

$$\int_{\Omega} N_u \Delta U_i d\Omega = \int_{\Omega} N_u \Delta \tilde{U}_i d\Omega - \Delta t \int_{\Omega} N_u \left(\frac{\partial p^n}{\partial x_i} + \theta_2 \frac{\partial \Delta p}{\partial x_i} \right) d\Omega - \frac{\Delta t^2}{2} \int_{\Omega} \frac{\partial}{\partial x_j} \left(u_j N_u \right) \frac{\partial p^n}{\partial x_i} d\Omega \tag{4.7}$$

4.1.4. Energy Equation

Selecting energy shape function N_E as a weighing function, Equation (4.4) takes the following form:

$$\begin{aligned} &\int_{\Omega} N_E \Delta(\rho e) d\Omega \\ &= -\Delta t \left[\int_{\Omega} N_E \frac{\partial}{\partial x_i} \left[u_i (\rho e + p) \right] d\Omega + \int_{\Omega} \frac{\partial N_E}{\partial x_i} \left(k \frac{\partial T}{\partial x_i} + \tau_{ij} u_j \right) d\Omega \right]^n \\ &+ \frac{\Delta t^2}{2} \left[\int_{\Omega} \frac{\partial (u_k N_E)}{\partial x_k} \left[\frac{\partial}{\partial x_i} \left(u_i (\rho e + p) \right) \right] d\Omega \right]^n \\ &+ \Delta t \left[\int_{\Gamma} N_E \left(k \frac{\partial T}{\partial x_i} + \tau_{ij} u_j \right) n_i d\Gamma \right]^n \end{aligned} \tag{4.8}$$

4.2. Pseudo Second Order Velocity Interpolation Elements

Pseudo-quadratic velocity/linear pressure interpolation elements are constructed by dividing the pressure element, over which the pressure is interpolated linearly or bi-linearly, into sub-elements, over which the velocity is also interpolated linearly or bi-linearly. Combination of these first order velocity interpolations can be considered as pseudo second order velocity interpolation over the original pressure elements. Overall, the solution can also be considered to be obtained on two different grids, one for the velocity and the other for the pressure solution. In this thesis, only pseudo-quadratic velocity/linear pressure interpolation elements (pP2P1) are considered. Such an element is obtained by inserting mid nodes to the parent pressure element and interconnecting them to give 4 sub-elements over which the velocity is interpolated linearly. These elements, node numbering and other details are given in Appendix C.

The number of pressure elements for which the stiffness matrix for the FEM is constructed is four times smaller compared to that of the constructed using the P1P1 element pair with the same number of velocity elements.

4.3. Matrix Form of the CBS Algorithm

Auxiliary momentum equation given with Equation (4.5) can be written in matrix form as follows:

$$\Delta\widetilde{\overline{\mathbf{U}}} = -\mathbf{M}_u^{-1}\Delta t\left[\left(\overline{\mathbf{C}}_u\overline{\mathbf{U}} + \mathbf{K}_\tau\overline{\mathbf{u}} - \mathbf{f}\right) - \Delta t\left(\mathbf{K}_u\overline{\mathbf{U}} - \mathbf{f}_s\right)\right]^n \tag{4.9}$$

, where the over bar quantities indicate the nodal values. The matrices seen in the equation given above are denoted with bold letters, and they are in explicit form as follows:

$$\mathbf{M}_u = \int_\Omega \mathbf{N}_u^{\mathrm{T}}\mathbf{N}_u d\Omega \tag{4.10}$$

$$\mathbf{C}_u = \int_\Omega \mathbf{N}_u^{\mathrm{T}}\left(\nabla\left(\mathbf{u}\mathbf{N}_u\right)\right)d\Omega \tag{4.11}$$

$$\mathbf{K}_\tau = \int_\Omega \mathbf{B}^{\mathrm{T}}\mu\left(\mathbf{I_0} - \frac{2}{3}\mathbf{m}\mathbf{m}^{\mathbf{T}}\right)\mathbf{B}d\Omega \tag{4.12}$$

$$\mathbf{f} = \int_\Omega \mathbf{N}_u^{\mathrm{T}}\rho\mathbf{g}d\Omega + \int_\Gamma \mathbf{N}_u^{\mathrm{T}}\mathbf{t}^d d\Gamma \tag{4.13}$$

where $\mathbf{g} = \begin{bmatrix} g_1 & g_2 & g_3 \end{bmatrix}^{\mathrm{T}}$ and $\mathbf{t}^d$ is the traction corresponding to the deviatoric stress components seen in the Equation (4.5). The matrices seen in the explicit form of the $\mathbf{K}_\tau$ are as follows (for details see Reference [9]):

$$\mathbf{S}=\begin{bmatrix} \dfrac{\partial}{\partial x_1} & 0 & 0 \\ 0 & \dfrac{\partial}{\partial x_2} & 0 \\ 0 & 0 & \dfrac{\partial}{\partial x_3} \\ \dfrac{\partial}{\partial x_2} & \dfrac{\partial}{\partial x_1} & 0 \\ 0 & \dfrac{\partial}{\partial x_3} & \dfrac{\partial}{\partial x_2} \\ \dfrac{\partial}{\partial x_3} & 0 & \dfrac{\partial}{\partial x_1} \end{bmatrix} \tag{4.14}$$

$$\mathbf{B}=\mathbf{S}\mathbf{N}_u \tag{4.15}$$

$$\mathbf{I}_0=\begin{bmatrix} 2 & & & & & \\ & 2 & & & & \\ & & 2 & & & \\ & & & 1 & & \\ & & & & 1 & \\ & & & & & 1 \end{bmatrix} \tag{4.16}$$

$$\mathbf{m}=\begin{bmatrix} 1 & 1 & 1 & 0 & 0 & 0 \end{bmatrix}^{\mathrm{T}} \tag{4.17}$$

The terms coming from the discretization along the characteristics are as follows:

$$\mathbf{K}_u=-\frac{1}{2}\int_{\Omega}\left(\nabla^{\mathrm{T}}\left(\mathbf{u}\mathbf{N}_u\right)\right)^{\mathrm{T}}\left(\nabla^{\mathrm{T}}\left(\mathbf{u}\mathbf{N}_u\right)\right)d\Omega \tag{4.18}$$

$$\mathbf{f}_s=-\frac{1}{2}\int_{\Omega}\left(\nabla^{\mathrm{T}}\left(\mathbf{u}\mathbf{N}_u\right)\right)^{\mathrm{T}}\rho\mathbf{g}d\Omega \tag{4.19}$$

, where $\mathbf{u}=\begin{bmatrix} u_1 & u_2 & u_3 \end{bmatrix}^{\mathrm{T}}$. The continuity equation which is given in the weak form within the Equation (4.6) can be written in matrix form as follows:

$$\left(\mathbf{M}_p+\Delta t^2\theta_1\theta_2\mathbf{H}\right)\Delta\overline{\mathbf{p}}=\Delta t\left[\mathbf{G}\overline{\mathbf{U}}^n+\theta_1\mathbf{G}\Delta\widetilde{\overline{\mathbf{U}}}-\Delta t\theta_1\mathbf{H}\overline{\mathbf{p}}^n-\mathbf{f}_p\right] \tag{4.20}$$

Pressure field at time *n+1* is obtained by solving the equation given above. The matrices seen in the equation can be written explicitly as follows:

$$\mathbf{H}=\int_{\Omega}\left(\nabla\mathbf{N}_p\right)^{\mathrm{T}}\nabla\mathbf{N}_p d\Omega \tag{4.21}$$

$$\mathbf{M}_p = \int_{\Omega} \mathbf{N}_p^{\mathrm{T}} \left(\frac{1}{a^2} \right) \mathbf{N}_p d\Omega \tag{4.22}$$

$$\mathbf{G} = \int_{\Omega} \left(\nabla \mathbf{N}_p \right)^{\mathrm{T}} \mathbf{N}_u d\Omega \tag{4.23}$$

$$\mathbf{f}_p = \Delta t \int_{\Gamma} \mathbf{N}_p^{\mathrm{T}} \mathbf{n}^{\mathrm{T}} \left[\overline{\mathbf{U}}^n + \theta_1 \left(\Delta \widetilde{\overline{\mathbf{U}}} - \Delta t \nabla p^{n+\theta_2} \right) \right] d\Gamma \tag{4.24}$$

The last matrix given above contains boundary conditions. And finally correction step for the momentum equation is as follows:

$$\Delta \overline{\mathbf{U}} = \Delta \widetilde{\overline{\mathbf{U}}} - \mathbf{M}_u^{-1} \Delta t \left[\mathbf{G}^{\mathrm{T}} \left(\overline{\mathbf{p}}^n + \theta_2 \Delta \overline{\mathbf{p}} \right) + \frac{\Delta t}{2} \mathbf{P} \overline{\mathbf{p}}^n \right] \tag{4.25}$$

The velocity field is obtained by using the pressure field obtained from Equation (4.20) in the equation given above. In the matrix form of the correction step of the momentum equation, $\mathbf{P}$ matrix can be written explicitly as follows:

$$\mathbf{P} = \int_{\Omega} \left(\nabla \left(\mathbf{u} \mathbf{N}_u \right) \right)^{\mathrm{T}} \nabla \mathbf{N}_p d\Omega \tag{4.26}$$

In similar manner, matrix form of the energy equation and matrices seen in this equation can be written explicitly as follows:

$$\Delta \overline{\mathbf{E}} = -\mathbf{M}_E^{-1} \Delta t \left[\mathbf{C}_E \overline{\mathbf{E}} + \mathbf{C}_p \overline{\mathbf{p}} + \mathbf{K}_T \overline{\mathbf{T}} + \mathbf{K}_{\tau E} \overline{\mathbf{u}} + \mathbf{f}_e - \Delta t \left(\mathbf{K}_{uE} \overline{\mathbf{E}} + \mathbf{K}_{up} \overline{\mathbf{p}} + \mathbf{f}_{es} \right) \right]^n \tag{4.27}$$

$$\mathbf{M}_E = \int_{\Omega} \mathbf{N}_E^{\mathrm{T}} \mathbf{N}_E d\Omega \tag{4.28}$$

$$\mathbf{C}_E = \int_{\Omega} \mathbf{N}_E^{\mathrm{T}} \nabla^{\mathrm{T}} \left(\mathbf{u} \mathbf{N}_E \right) d\Omega \tag{4.29}$$

$$\mathbf{C}_p = \int_{\Omega} \mathbf{N}_E^{\mathrm{T}} \nabla^{\mathrm{T}} \left(\mathbf{u} \mathbf{N}_p \right) d\Omega \tag{4.30}$$

$$\mathbf{K}_T = \int_{\Omega} \left(\nabla \mathbf{N}_E \right)^{\mathrm{T}} k \nabla \mathbf{N}_T d\Omega \tag{4.31}$$

$$\mathbf{K}_{\tau E} = \int_{\Omega} \mathbf{B}^{\mathrm{T}} \mu \left(\mathbf{I_0} - \frac{2}{3} \mathbf{m} \mathbf{m}^{\mathbf{T}} \right) \mathbf{B} d\Omega \tag{4.32}$$

$$\mathbf{K}_{uE} = -\frac{1}{2} \int_{\Omega} \left(\nabla^{\mathrm{T}} \left(\mathbf{u} \mathbf{N}_E \right) \right)^{\mathrm{T}} \left(\nabla \mathbf{N}_E \right) d\Omega \tag{4.33}$$

$$\mathbf{f}_e = \int_{\Omega} \mathbf{N}_E^{\mathrm{T}} \mathbf{n}^{\mathrm{T}} \left(\mathbf{t}^d \mathbf{u} + k \nabla T \right) d\Omega \tag{4.34}$$

$$\mathbf{K}_{up} = -\frac{1}{2} \int_{\Omega} \left(\nabla^{\mathrm{T}} \left(\mathbf{u} \mathbf{N}_E \right) \right)^{\mathrm{T}} \left(\nabla \mathbf{N}_p \right) d\Omega \tag{4.35}$$

4.4. Solution Procedure and Strategies

To obtain velocity and pressure values at time *n+1*, Equation (4.5), (4.6), (4.7) and (4.8) need to be solved. Either pressure or density can be chosen as dependent variable during the solution procedure of the equations. The solution procedure also differs from one to another when the fluid flow changed from incompressible to compressible flow case. The density can be used as dependent variable for the barotropic and perfect gas flow cases which are expressed with details in following parts. Since the solver is in more general form, pressure is chosen as dependent variable in this thesis.

The scheme is referred as being *fully explicit* or *semi-implicit* depending on the value of the parameter θ_2 used in the continuity equation. In *fully explicit* form, $1/2 \le \theta_1 \le 1$ and $\theta_2 = 0$. Choosing θ_2 being equal to zero means solving Equation (3.21) explicitly. This is possible only for compressible flow case for which $a \neq \infty$. The time step limitations given for the convection-diffusion equations are applicable for fully explicit form of the CBS algorithm and it is as follows:

$$\Delta t \le \frac{h}{a + |u|} \tag{4.36}$$

In the equation above viscosity effects are neglected. Many complex problems of compressible flow are solved using this explicit form (see Reference [19]). In the semi implicit form of the algorithm, θ_1 and θ_2 are in the range of $1/2$ to 1. Maximum time step size can be taken as to be equal to the critical time step size of characteristic-Galerkin process due to the solution of the first step of the CBS algorithm. This stability limit is given with the two equations as follows [19]:

$$\Delta t \le \Delta t_{\sigma} = \frac{h}{|u|} \tag{4.37}$$

$$\Delta t \le \Delta t_{v} = \frac{h^2}{2v} \tag{4.38}$$

In the equation above, ν is kinematic viscosity. These two time step criteria can be written in one equation as follows:

$$\Delta t \le \frac{\Delta t_\sigma \Delta t_\nu}{\Delta t_\sigma + \Delta t_\nu} \tag{4.39}$$

To avoid severe time step restriction, besides the continuity equations, diffusion terms (viscosity, thermal conductivity, etc.) can be treated implicitly. In other words, the implicit form connecting the viscous terms with auxiliary momentum are solved at each time step. For high viscosity and low Mach number flows, solving the equations simultaneously at each time step implicitly have great advantages. This solution approach is referred as quasi-(nearly) implicit scheme. In this scheme, $\Delta t \le h/|u|$ is the time step limitation and is very reasonable. The implicit equations appearing in the *semi-implicit* and *quasi-(nearly) implicit* form are solved generally using conjugate gradient method.

Different solution procedures can be followed due to the physical properties of fluid flow which result in some simplification in equations waiting to be solved. Therefore, the fluid flows are categorized due to the pressure-density relationship which is required to solve continuity equation. These flow cases and details of solution procedure are given as follows [23]:

4.4.1. Incompressible and Slightly Compressible Flow

For these two types of flows, the relationship between pressure and density variable is given as follows:

$$\Delta\rho = \alpha \Delta p \tag{4.40}$$

where $\alpha = 0$ for fully incompressible flows. $\alpha = 1/a^2$ (a is a positive constant) for slightly compressible flows. So the continuity equation in weak form with pressure as a variable is as follows:

$$\begin{aligned}\int_\Omega N_p \alpha \Delta p d\Omega = \Delta t \int_\Omega \frac{\partial N_p}{\partial x_i}\left[U_i^n + \theta_1\left(\Delta \widetilde{U}_i - \Delta t \frac{\partial p^{n+\theta_2}}{\partial x_i}\right)\right] d\Omega \\ - \int_\Gamma N_p \left[U_i^n + \theta_1\left(\Delta \widetilde{U}_i - \Delta t \frac{\partial p^{n+\theta_2}}{\partial x_i}\right)\right] n_i d\Gamma\end{aligned} \tag{4.41}$$

4.4.2. Barotropic Flow

Barotropic fluids assumption is valid if there is an equation of state that involves only the pressure and density but not temperature. In general, the equation can be written in the form as $p = p(\rho)$. Using adiabatic exponent γ and physical constant A, this relationship can be written explicitly as follows:

$$p = A\rho^{\gamma} \tag{4.42}$$

For this flow case, pressure and density can be related using $\alpha = \rho^n / (\gamma p^n)$ within the Equation (4.40).The solution procedure of the algorithm for the barotropic flow case is as follows:

1. Solve the fractional momentum equation (Equation (4.5))
2. Solve the continuity equation for p^{n+1} (Equation (4.6))
3. Obtain ρ^{n+1} from the equation of state (Equation (4.42))
4. Solve the end-of-step momentum equation (Equation (4.7))

In this flow case, the energy equation is uncoupled from the others. So, this equation can be solved at the beginning or end of the time step.

4.4.3. Perfect Gases

In this case, the equation of state involves pressure, density and temperature. The equation is

$p = \rho RT$; where R is the gas constant. The appearance of the temperature in this equation complicates the continuity equation. For this case, the equation of state is in the form as follows,

$$\rho^{n+1} = \frac{p^{n+1}}{RT^{n+1}} \tag{4.43}$$

To uncouple the energy and the resulting continuity equation, there is need to guess the value of T^{n+1} by T_g. Then, the equation of state can be written as

$$\Delta\rho = \frac{\Delta p}{RT_g} + \left(\frac{p^n}{RT_g} - \frac{p^n}{RT^n} \right) \tag{4.44}$$

For this case, the iterative scheme is as follows,

1. Solve the energy equation (Equation (4.8))
2. Solve the fractional momentum equation (Equation (4.5))
3. Guess a temperature T_g
4. Solve the continuity equation for p^{n+1} (Equation (4.6))
5. Obtain ρ^{n+1} from the equation of state (Equation 4.43))
6. Solve for the end-of-step momentum (Equation 4.7))
7. Correct T_g using T^{n+1}
8. Check convergence. If not satisfactory, go to step 4

4.5. Moving Deforming Grid

Using the CBS algorithm with barotropic fluid assumption and modifying the equation for moving deforming mesh concept ALE [37-39], the convection term in the fractional momentum equation (Equation (4.5)) of standard CBS algorithm is modified using grid velocity u_i^g , and it takes the following form;

$$\begin{aligned}\int_\Omega N_u \Delta\tilde{U}_i d\Omega = \Delta t\Bigg[&-\int_\Omega N_u \frac{\partial}{\partial x_j}\left(u_j\left(U_i - U_i^g\right)\right)d\Omega - \int_\Omega \frac{\partial N_u}{\partial x_j}\tau_{ij}^n d\Omega + \int_\Omega N_u\left(\rho g_i\right)d\Omega\Bigg]^n \\ &+\frac{\Delta t^2}{2}\left[\int_\Omega \frac{\partial}{\partial x_k}\left(u_k N_u\right)\left(-\frac{\partial}{\partial x_j}\left(u_j\left(U_i - U_i^g\right)\right)+\rho g_i\right)d\Omega\right]^n \\ &+\Delta t\left[\int_\Gamma N_u \tau_{ij} n_j d\Gamma\right]^n\end{aligned} \tag{4.45}$$

At the beginning of the new time step, computational mesh is updated and grid velocities at nodal points are calculated.

5. MICRO FLOW ANALYSIS USING A CONTINUUM MODEL

Fluid flows around or through micro devices such as MEMS differ from larger devices. It is obvious that the difference encountered in MEMS or smaller sized geometry is a result of increasing surface volume ratio. In other words surface effects dominate in that kind of small devices. So it is required to define the amount of this effect encountered in diminished scale and modify the traditional continuum solver to capture it. Following subtitles are introduced for this aim.

5.1. Knudsen Number and Regimes

For gases, the mean free path is defined as the distance traveled by molecules between collisions and it is denoted with λ. The mean free path is related to temperature and pressure of gas. This relationship can be formulized for an ideal gas which has molecules modeled as a rigid sphere with diameter of σ as follows:

$$\lambda = \frac{1}{\sqrt{2}\pi \, \mathrm{n} \, \sigma^2} = \frac{\mathrm{k}\, T}{\sqrt{2}\pi p \sigma^2} \tag{5.1}$$

, where n is the number of molecules per unit volume which is also known as number density and k is the Boltzmann constant ($1.38 \cdot 10^{-23}$ J·K^{-1}·molecule^{-1}). It is known that continuum model approach is valid when the characteristic length of the flow is much greater than mean free path. If it is not, linear relation between stress and rate of strain and no-slip velocity condition are invalid. Similarly, linear relation between the heat flux and temperature gradient and no-jump in temperature condition at a solid-fluid interface are not valid. Therefore, the ratio of the mean free path to the characteristic length of the flow is used as a key parameter which characterizes the breakdown of the continuum assumption. This parameter is called Knudsen number and defined as follows:

$$Kn = \frac{\lambda}{L} \tag{5.2}$$

From the kinetic theory of gases, following equation can be written for viscosity.

$$\mu = \frac{1}{2}\rho\lambda\bar{\upsilon}_m \tag{5.3}$$

In the equation above $\bar{\upsilon}_m$ is the mean molecular speed and it is function of the speed of sound a as follows:

$$\bar{\upsilon}_m = \sqrt{\frac{8}{\pi\gamma}}a \tag{5.4}$$

Using the Equation (5.3) and (5.4), dimensionless number *Kn* can be written in terms of well known dimensionless numbers of fluid mechanics Mach and Reynolds as follows [28]:

$$Kn = \sqrt{\frac{\pi\gamma}{2}}\frac{M}{Re} \tag{5.5}$$

Ma and *Re* can be written explicitly using velocity u as follows:

$$M = \frac{u}{a} \tag{5.6}$$

$$Re = \frac{\rho u L}{\mu} \tag{5.7}$$

During the gas flow in small geometries such as MEMS devices at standard temperature and pressure or around standard geometries such as flight vehicles at very high altitude which means low pressure environment, rarefied gas flow is encountered. It is known that as the *Kn* increases, rarefaction effects become important and the continuum approach completely breaks down. Degree of rarefaction and validity of continuum model can be determined by the local value of the Knudsen number. In Reference [28] different flow regimes are defined due to the changing values of Knudsen number as follows:

Continuum regime: if the Knudsen number is smaller than 10^{-3} for a fluid flow, continuum models can be used for simulation of the flow. It is known that continuum models ignore the molecular nature of gases and liquids. So, the flow is described using temporal and spatial variations of density, velocity, pressure, temperature and other macroscopic flow quantities.

Slip regime: If the Knudsen number is in the range of 10^{-3} to 10^{-1}, the flow is slightly rarefied and this interval is called the slip regime. In this regime, fluid flow can also

be simulated using continuum models such as Navier-Stokes equations, if proper modifications are done on the boundary conditions using Equation (2.9) and (2.10). These modifications are essential since there are discontinuities in velocity and temperature field near the wall due to the insufficient collision between fluid particles and the surface. So, no-slip/no-jump boundary conditions are not valid in this regime. There are finite discontinuities in velocity and temperature values at the solid wall in this regime. While the slip-velocity is linearly changed in *Kn* around the lower limit of this region, as the *Kn* reaches upper limit of this region (Kn=10^{-1}) the change of slip-velocity in *Kn* becomes nonlinear.

Transition Regime: For the values of *Kn* in the range of $10^{-1}$and 10, the flow is moderately rarefied and microscopic nature of gases can not be ignored and the flow can not be simulated using continuum based model anymore. This is a result of breaking down of the linear relationship between stress and rate of strain, heat flux and temperature gradient. Hence alternative continuum (e.g. Burnett or higher order equations) or molecular-based models have to be used for analysis at this regime. Direct Simulation Monte Carlo (DSMC) method is a good alternative in this regime [35].

Free molecular flow: For the values of *Kn* grater than 10, Boltzmann Equation is very simplified due to the negligibility of the nonlinear collision integral. So, Boltzmann equation can be used in this regime. For free molecular flow through or in simple geometries, obtained analytical solutions show that the numerical integration of Boltzmann equation gives accurate surface reflection characteristics [40].

5.2. Slip-Velocity and Temperature-Jump Formulation

In Chapter 2, the equation of motion is given in conservative form for viscous compressible fluid flow in continuum regime. Boundary conditions at solid-fluid interface are also given in this chapter. It is well known that the highest spatial derivative of velocity for inviscid equation of fluid motion is first of order. Therefore only normal component of the velocity is specified at the solid wall. It means that a fluid particle path can not go through impermeable wall. In fact, real fluids are viscous and the equations of motion consists second order derivatives in space as given in Chapter 2. So, additional boundary condition on tangential component of velocity due to the second order derivatives is the no-slip boundary condition.

Similar relationship can be seen between the no-jump (in temperature) boundary condition and energy equation.

No-slip/no-jump condition means that there can not be finite discontinuities in velocity and temperature field at solid wall. In other words, if the fluid flow adjacent to the surface is in thermodynamic equilibrium, the fluid velocity and temperature can not differ from the wall velocity and temperature. Existence of this thermodynamic equilibrium is closely related to the frequency of collisions between the fluid and solid surface. It is also known that the continuum models (no-slip/no-jump boundary condition) give accurate results in continuum regime where *Kn* is smaller than 0.001 [28,29]. However, for the values of *Kn* in slip regime, since collision frequency is not high enough, certain degree of tangential velocity-slip and temperature-jump have to be allowed within the continuum models.

Simplest kinetic model states that when a gas molecule hits a solid wall surface, energy and momentum of the molecule exchange with the surface. Amount of these two exchanges are related to surface and gas properties as expected and they are characterized with two different coefficients. Tangential momentum accommodation coefficient characterizes the exchange of momentum between the wall and fluid and it is denoted with σ_v. Similarly energy accommodation coefficient is denoted with σ_T and it characterizes the energy exchange of molecules and surface [41].

For an isothermal wall, slip velocity derived by Maxwell [28] is as follows:

$$u_{gas} - u_{wall} = \frac{2-\sigma_v}{\sigma_v} \lambda \left. \frac{\partial u}{\partial n} \right|_w \tag{5.8}$$

, where $\left. \partial u / \partial n \right|_w$ denotes the velocity gradient at the wall through the normal direction. It can be seen that as the λ increases (as a result of decreasing collision frequency), Maxwell's first order slip velocity written above also increases.

Similarly temperature jump condition (first order) was obtained by von Smoluchowski [28]. For an ideal gas flow in slip regime, if there are temperature gradients along the wall and normal to the wall, complete first order temperature-jump and slip-velocity boundary conditions are written as follows [29]:

$$u_{gas} - u_{wall} = \frac{2-\sigma_v}{\sigma_v} \lambda \left(\frac{\partial u}{\partial n} \right)_w + \frac{3}{4} \frac{\mu}{\rho T_{gas}} \left(\frac{\partial T}{\partial s} \right)_w \tag{5.9}$$

$$T_{gas} - T_{wall} = \frac{2-\sigma_T}{\sigma_T}\left[\frac{2\gamma}{(\gamma+1)}\right]\frac{\lambda}{Pr}\left(\frac{\partial T}{\partial n}\right)_w \tag{5.10}$$

In the Equation (5.9), given above, the temperature gradient tangential to the wall is denoted with $(\partial T/\partial s)$. *Pr* denotes the Prandtl number, which is ratio of viscous diffusion rate to thermal diffusion rate, is given as follows:

$$Pr = \frac{\mu c_p}{k} \tag{5.11}$$

The second term on the right hand side of Equation (5.9) is thermal creep term. As the mean free path λ increases due to the decreasing density (see Equation (5.3)), this term becomes effective and produces extra slip (see Equation 5.3). In other words, creep phenomenon is potentially significant at large values of mean free path (or *Kn*) since it is second order.

Beskok derived a higher order slip-velocity boundary condition for isothermal walls [42]. But implementation of this higher order boundary condition to the numerical model is too difficult since the second and higher order derivatives of velocity can not be computed accurately near the wall. Then Beskok [43] and Beskok and Karnidiakis [44,45] proposed alternative higher order boundary conditions based on asymptotic analysis. These new boundary conditions also include thermal creep term and they can be written in dimensionless form as follows:

$$u^*_{gas} - u^*_{wall} = \frac{2-\sigma_v}{\sigma_v}\frac{Kn}{1-bKn}\left(\frac{\partial u^*}{\partial n^*}\right)_w + \frac{3}{2\pi}\frac{(\gamma-1)}{\gamma}\frac{Kn^2 Re}{Ec}\left(\frac{\partial T^*}{\partial s^*}\right)_w \tag{5.12}$$

$$T^*_{gas} - T^*_{wall} = \frac{2-\sigma_T}{\sigma_T}\left[\frac{2\gamma}{(\gamma+1)}\right]\frac{Kn}{Pr}\left(\frac{\partial T^*}{\partial n^*}\right)_w \tag{5.13}$$

b appeared in the Equation (5.12) is the high-order slip coefficient. Its value can be determined analytically for the rarefied gas flow for simple geometry in slip or early transition regime. For gas flow in complex geometry, its value is determined using no-slip solution obtained numerically ($b = u''_w / u'_w$). *Ec* appeared in Equation (5.12) denotes the nondimensional number Eckert and it can be written explicitly as follows:

$$Ec = \frac{u^2}{c_p \Delta T} \tag{5.14}$$

In the equation given above, ΔT is the reference temperature difference between the wall surface and fluid. *Ec* is the ratio of dynamic temperature due to the fluid motion to reference temperature difference. If it is small, the viscous energy generation effects due to the motion of the fluid can be neglected since the temperature difference involved in the heat transfer process is dominant. As the *Ec* decreases, thermal creep term appeared in the slip-velocity formulation (see Equation (5.12)) becomes effective for same Knudsen and Reynolds numbers.

To perform rarefied gas flow analysis using continuum based N-S FEM solver CBS, Equation (5.12) and (5.13) proposed by Beskok and Karniadakis are used as slip-velocity/temperature-jump boundary conditions within this study.

6. SYNTHETIC JET ACTUATOR AND JET FORMATION MECHANISM

One of the interesting problems analyzed during the study is the micro synthetic jet actuator flows. Even though computational details and results of this problem are given in Chapter 7, some introductory information about synthetic jet actuator and jet formation mechanism are given in this chapter.

6.1. Micro Synthetic Jet Actuator

Generally, a synthetic jet actuator (SJA) consists of a cavity which has one or more orifice that is opening to the free stream. The orifice can be circular, creating an axisymmetric jet, or rectangular with a high aspect ratio, creating a 2-D jet. It is known that this type of SJA has been built with both square and rectangular cavities. The SJA can excite the main flow without net mass addition. Since total mass flow into and out of the cavity is equal to zero, it is also known as zero mass jet actuator. However, net momentum transferred to the main flow is not zero. Even though numbers of different geometries have been proposed for the synthetic jet design, most popular synthetic jet geometries have an enclosed cavity which has a small orifice on one face.

In Figure 6.1, a SJA with a rectangular cavity is shown. Oscillating diaphragm of the SJA is placed at the bottom of the cavity as a wall. Oscillations of the diaphragm cause a pressure gradient through the orifice placed on upper wall of the cavity. Hence, a flow is created in accordance with the position and direction of the diaphragm. The diaphragm can be actuated with one of the various methods including piezoelectric, electrostatic, acoustic or magnetic methods and it is reported that piezoelectrically driven synthetic jet diaphragm frequency varies 0.5 to 20 kHz. In the figure, cavity height and width are denoted with H and W. Width and height of the orifice are denoted with h and d while the maximum deflection amplitude of the diaphragm is denoted with A.

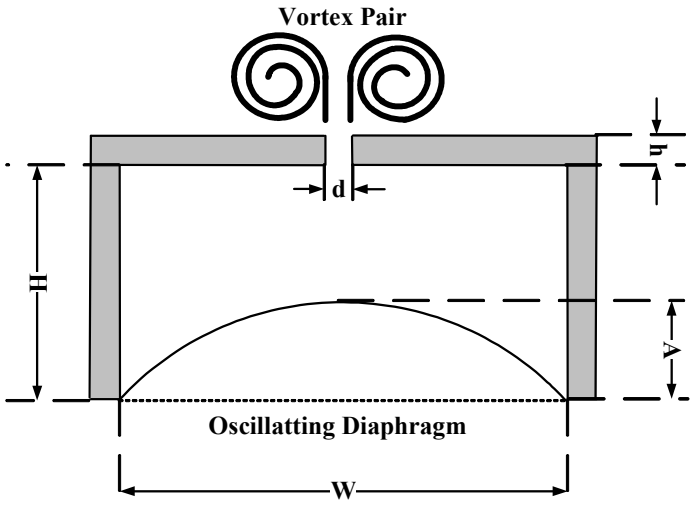

Figure 6.1 : Schematics of synthetic jet with rectangular cavity.

Four diaphragm stages in a cycle of the SJA with rectangular cavity are shown in Figure 6.2. At the maximum expulsion stage, the diaphragm is at level position and has the maximum vertical velocity towards to orifice. The highest position of the diaphragm is called minimum volume since the cavity region has the minimum area. Following case is called the maximum ingestion and the membrane has maximum vertical velocity opposite direction to the orifice. Finally, the lowest level position of the diaphragm is called the maximum volume stage. At the maximum and minimum volume stage the diaphragm velocity is equal to zero.

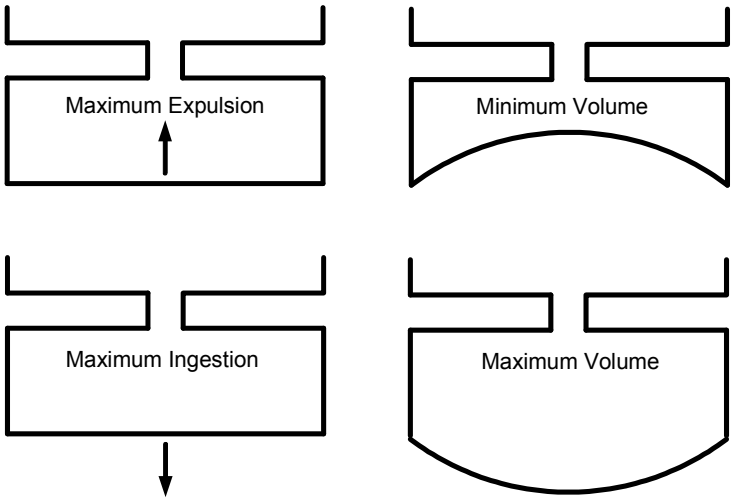

Figure 6.2 : Movement of the piezoelectric-driven-diaphragm in time

Separation control, thrust vectoring and aeroshaping are a few potential applications proposed for SJA [30-32,46]. Augmentation of heat transfer and combustion by micromixing constitute other promising application areas [47]. Micro synthetic jet

actuator (μSJA) is one of the MEMS technology products and it has similar potential application with SJA. μSJAs offer many advantages compared to the larger SJA due to their smaller size, lower production costs and energy consumption. These properties of μSJA result in using them in clustered configurations and applicability on other micro devices such as micro aerial vehicles and biomedical devices [29]. Potential μSJA's with different cavity geometries given in Reference [30] are shown in the Figure 6.3.

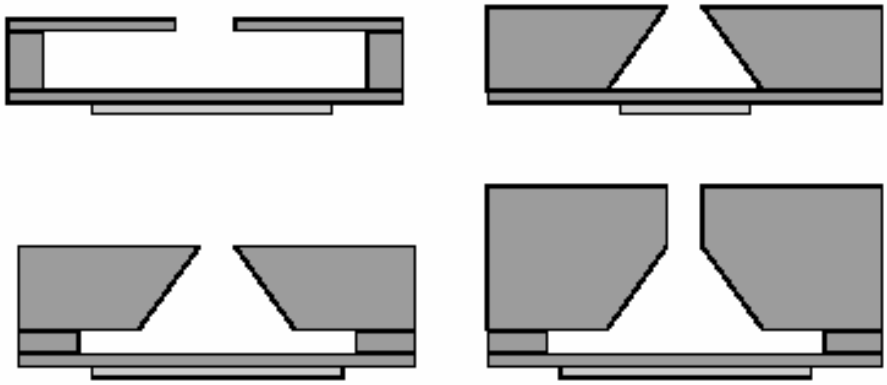

Figure 6.3 : Potential μSJ geometries [30]

6.2. Jet Formation Mechanism

Recently, production of SJA having smaller characteristic lengths and its numerical simulations are reported [48,49]. In Reference [33], many experimental and numerical studies for SJA are given. Jet formation mechanism, evolution of the near and far field of the synthetic jet and its interactions with cross-flow are the subjects of this publication and they are expressed with details in it. Since most of these studies mentioned here consider relatively large SJA at standard conditions, these flows are in continuum regime and these studies use continuum approach with assumption of incompressibility. It can be expected that the flow cases in slip regime can be encountered with smaller devices at higher altitudes and different gases. In that case, it is required to use continuum model with slip-velocity/temperature-jump boundary condition as mentioned in previous chapter.

During the expulsion portion of oscillating diaphragm cycle for 2-D or axisymetric jets, a pair of vortices or a vortex ring is formed at the orifice as seen in Figure 6.1. Shedding of this vortex ring is highly related to the value of dimensionless

number Re_d. This non-dimensional number can be calculated using following equations:

$$Re_d = \frac{u_0 \, \mathrm{d}}{\nu} \tag{6.1}$$

In the equation above, u_0 is the average expulsion velocity, d is the orifice width or diameter and ν is the kinematic viscosity. Another important non-dimensional parameter for jet formation mechanism is stroke length. It is defined as L_0 / d, where L_0 can be considered as the length of the fluid column ejected from the orifice during the expulsion phase. If stroke length is large enough, then the vortices are shed from the orifice and, travel far enough such they are not pulled back into the cavity during the subsequent suction portion of the cycle. Formation of a train of such vortices eventually leads to their interaction and thus to the formation of a, usually turbulent, jet, downstream of the orifice.

The mechanism given above with details, yields following two distinct criteria for jet formation:

i) For vortex shedding, Re_d has to be large enough

ii) L_0/d has to be large enough to carry away these vortices.

In a recent study [50], separate threshold values are proposed for 2-D and axisymetric SJA's using last criteria given above. These values are based on an order-of-magnitude analysis and review of available computational and experimental results. For a SJA, the practical values of cavity/orifice dimensions, oscillation amplitudes and frequencies result in high Re_d numbers. So, former criterion has not been considered for SJA's yet. However, for a μSJA, Re_d is not guaranteed to be high enough to create vortex shedding.

Rectangular cavity geometry is one of the wide variety of geometries proposed and built for synthetic jet design. In this study, μSJA with a rectangular cavity is selected as test geometry (see Figure 6.1). The movement of the diaphragm in time can be formulized using the following equation:

$$y(x,t) = A \sin\left(\left(\frac{x + W/2}{W}\right)\pi\right)\sin(\omega t) \tag{6.2}$$

Based on the given cavity and membrane geometry, conservation of mass for incompressible case yields following equation:

$$\begin{aligned} \mathrm{d}\cdot u_0(t) &= \int_{-\mathrm{d}/2}^{\mathrm{d}/2} u(x,t)dx = \int_{-\mathrm{W}/2}^{\mathrm{W}/2} \frac{\partial y(x,t)}{\partial t}dx \\ &= \int_{-\mathrm{W}/2}^{\mathrm{W}/2} \mathrm{A}\,2\pi f\cdot\cos(2\pi ft)\sin\left\{\pi\left(\frac{x}{\mathrm{W}}+\frac{1}{2}\right)\right\}dx \end{aligned} \tag{6.3}$$

In the equation above, f denotes the diaphragm frequency. $u_0(t)$ denotes the spatially averaged expulsion velocity and it can be written explicitly as follows:

$$u_0(t) = \frac{4\,\mathrm{A}\,f\,\mathrm{W}}{\mathrm{d}}\cos(2\pi ft) \tag{6.4}$$

Thus, the average velocity for the expulsion phase and the stroke length L_0 can be obtained from the following equations:

$$u_0 = 2fL_0 = 2f\int_{-T/4}^{T/4} u_0(t)dt = \frac{8\,\mathrm{A}\,f\,\mathrm{W}}{\pi\,\mathrm{d}} \tag{6.5}$$

The Strouhal number is function of stroke length and it can be calculated in terms of cavity dimensions as

$$St = \frac{\omega\,\mathrm{d}}{u_0} = \frac{\pi\,\mathrm{d}}{L_0} = \frac{\pi^2\,\mathrm{d}^2}{4\,\mathrm{AW}} \tag{6.6}$$

The Reynolds number can be written in terms of diaphragm frequency as follows:

$$Re_{\mathrm{d}} = \frac{8\,\mathrm{A}\,f\,\mathrm{W}}{\pi\nu} \tag{6.7}$$

As seen from these equations, Re_{d} is calculated from Equation (6.7), whereas L_0/d or St is independent from the oscillation frequency of the cavity. One has to change the cavity or membrane geometry in order to increase the stroke length.

7. RESULTS AND DISCUSSIONS

7.1. Introduction

During the code implementation of CBS algorithm, different benchmark problems of CFD are solved as test cases. The first benchmark problem is laminar flow past a backward facing step. For the solution of this problem semi-implicit version of the algorithm is used. For two different Reynolds numbers, solver is tested and results are compared to available results in literature. pP2P1 type elements are used within the computation in addition to P1P1 type elements.

The second problem is compressible external fluid flow around a NACA0012 airfoil with M_{in}=0.5. Using barotropic gas assumption and the solution procedure given in the Chapter 4, this problem is simplified and solved. pP2P1 type elements are also used for the solution of this problem.

Micro channel flow is a rarefied gas problem which is numerically solved within this study. This problem is used as a verification case. Beskok's second order slip-velocity is implemented within the CBS algorithm for the solution of this problem.

To simulate micro synthetic jet flow, ALE approach is coupled with the CBS algorithm. Thus, oscillating diaphragm of the μSJA is numerically modeled. A comprehensive analysis is done for micro synthetic jet flow in terms of jet formation mechanism in addition to verification of ALE implementation using available results in literature.

Flow in a micro backward facing step is numerically simulated using general solution procedure of the CBS algorithm. Beskok and Karniadakis's second-order slip-velocity and temperature-jump boundary conditions are implemented on the solid wall. Obtained results are compared with available results in literature for verification. A comprehensive analysis is performed to investigate the effect of rarefaction on macroscopic flow properties.

7.2. Laminar Flow past Backward Facing Step

Incompressible fluid flow past a backward facing step of *Re*=191 and *Re*=229 are benchmark problems. These internal flow cases are numerically investigated in this study, since experimental and numerical results are available [51,52]. The geometry and the boundary conditions for these problems are as given below in Figure 7.1.

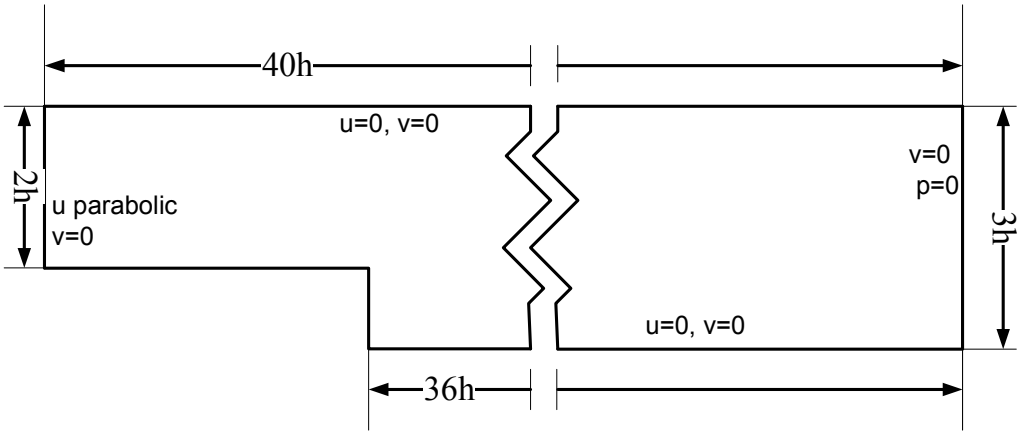

Figure 7.1 : Geometry and boundary conditions for laminar flow past a backward facing step geometry

The grid generated for this problem consists of 2176 triangular elements with 1161 nodes. The details of grid can be seen below in Figure 7.2.

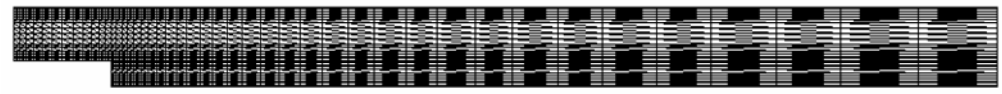

Figure 7.2 : Grid for laminar flow a past backward step, 1161 nodes, and 2176 elements.

In addition to CBS algorithm, two fractional step FEM algorithms which are Galerkin and Petrov-Galerkin FEM fractional step are used for numerical computations of the fluid flow with both *Re*. The results obtained using these methods are compared with each other in addition to the comparison with the experimental data.

Solution procedures of CBS algorithm for incompressible fluid flow are as explained in Chapter 4. Using semi implicit form of the CBS algorithm (with $\theta_1 = \theta_2 = 1$), Equation (3.11), (3.12) and (3.14) need to be solved. Except the term coming from discretization along the characteristics appearing in the auxiliary momentum

equation, CBS and standard Galerkin FEM equations are identical. The auxiliary momentum equation of Petrov-Galerkin FEM algorithm has an upwind term while the Galerkin FEM has not [26]. The upwind term of P-G FEM algorithm is similar to the extra term coming from the discretization along the characteristics of CBS algorithm. If there is no gravity acceleration, the only difference between these two terms is that P-G FEM has a variable multiplier in it while the CBS has constant. These two terms can be written explicitly as follows:

$$\frac{\Delta t}{2} u_k \frac{\partial}{\partial x_k}\left(u_j \frac{\partial u_i}{\partial x_j} \right) \tag{7.1}$$

$$\overline{\alpha} u_k \frac{\partial}{\partial x_k}\left(u_j \frac{\partial u_i}{\partial x_j} \right) \tag{7.2}$$

The auxiliary momentum equation given with Equation (3.11) is simplified for incompressible flow case. Hence, the term coming from the discretization along the characteristics takes the form given with Equation (7.1). The multiplier denoted with $\overline{\alpha}$ in Equation (7.2) is a suitable variable based on element lengths and velocity [25].

In all of the computations done using these three FEM algorithms, *Re* is based on the average velocity at the inlet and step height. For all two cases and schemes, pP2P1 and P1P1 type elements are used in computations.

Obtained results are presented in Figure 7.3 and 7.4 as pressure contours. The velocity field presents a recirculation region behind the step. The length of this recirculation region, denoted as the reattachment length, is an important quantity for comparison of different solutions. Reattachment lengths obtained using the CBS and Petrov-Galerkin algorithms are given in the Table 7.1 in comparison with the data [51] and CBS predictions of [52].

Table 7.1: Comparison of reattachment lengths obtained by various methods

Re	CBS-present	Petrov-Galerkin	CBS [52]	Exp. [51]
191	10.2	10.5	9.2	8.6
229	11.9	11.9	10.9	10.0

Since Galerkin FEM algorithm fails to yield physical results for both *Re* numbers, reattachment length is not included in the table for this FEM fractional step algorithm (see Figure 7.3 and 7.4). This behavior of Galerkin FEM algorithm is related to the improper approximation of the convection term for high element Peclet numbers on

the computational grid used. It is observed that pressure fields obtained using Petrov-Galerkin upwind and CBS formulations are very similar.

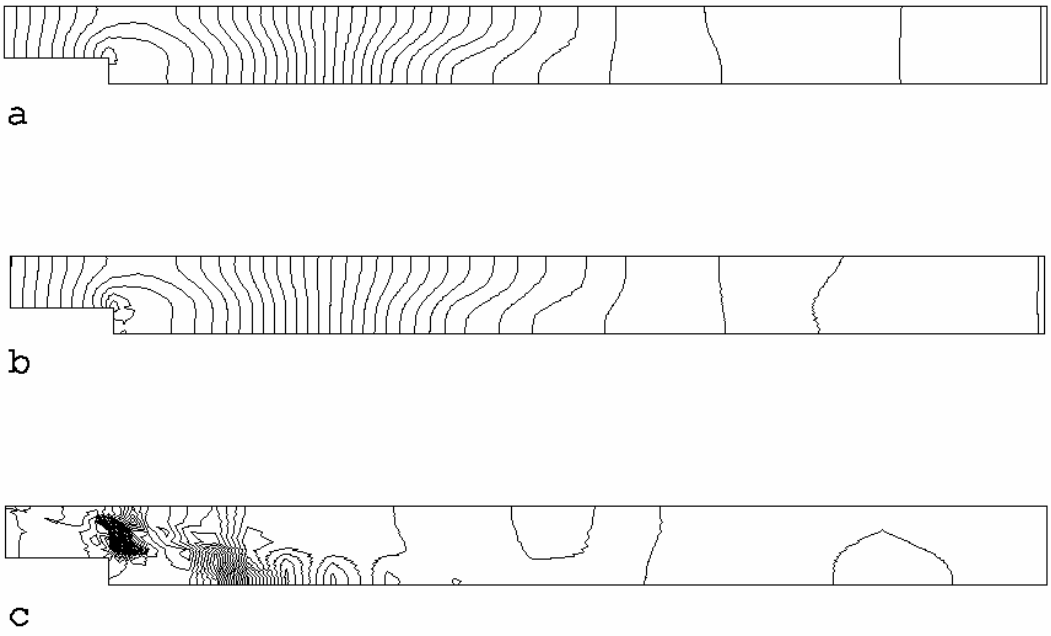

Figure 7.3 : Pressure contours for laminar flow past a backward facing step (*Re*=229) a) CBS formulation b)Petrov-Galerkin c) Galerkin

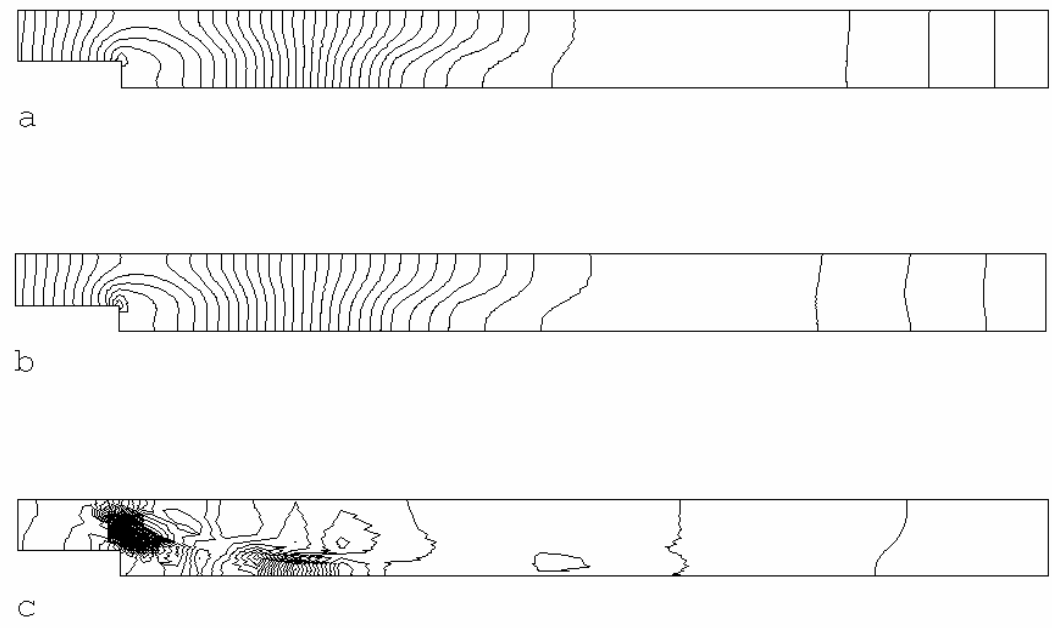

Figure 7.4 : Pressure contours for laminar flow past a backward facing step (*Re*=191) a) CBS formulation b)Petrov-Galerkin c) Galerkin

For Re=191, the streamwise *u* velocity obtained using P-G and CBS algorithms with two type of elements are plotted at four downstream stations behind the step in Figure 7.5 in comparison with data [51]. In this study, parabolic velocity profile (developed channel flow) is prescribed at the channel inlet for all computations as an initial condition. However obtained results differ from the results given in Reference [51,52]. This difference shows that the inlet velocity profiles of experimental and numerical data given in References is slightly different than the one used in this study. This difference affects the obtained reattachment lengths (see Table 7.1) in addition to downstream velocity profiles given in Figure 7.5.

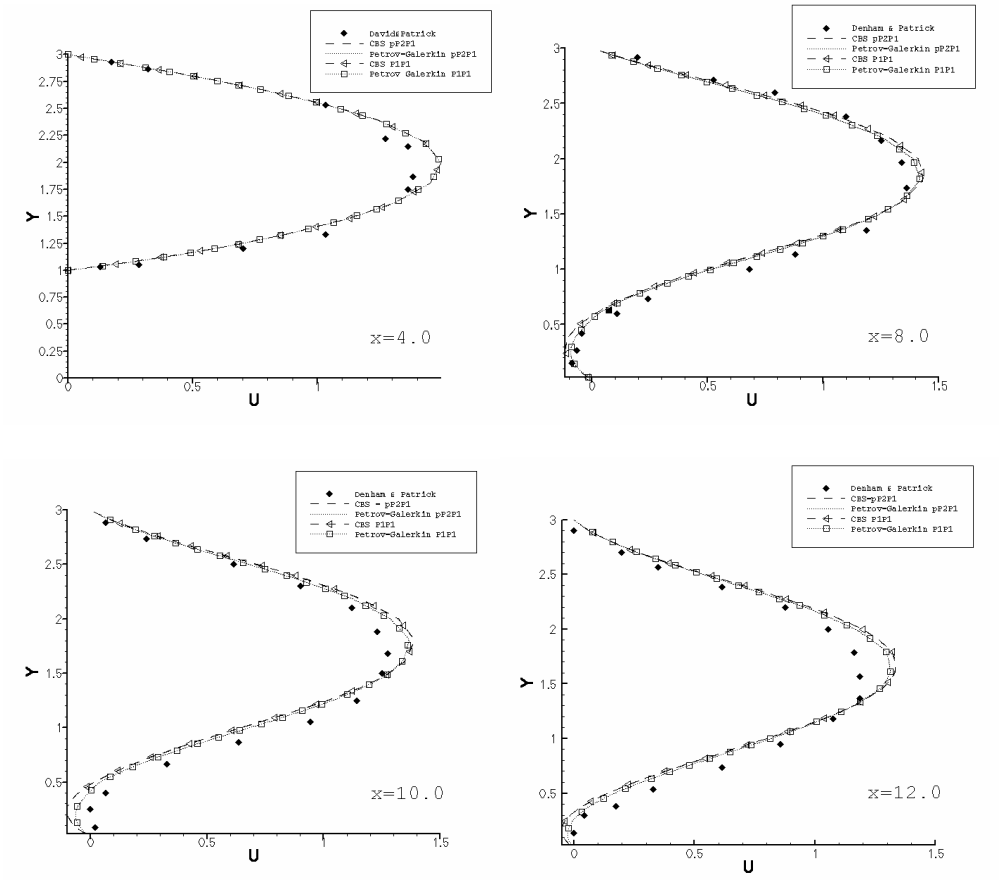

Figure 7.5 : Velocity profiles obtained using P1P1 and pP2P1 elements downstream of the step in comparison with data [51], *Re*=191

For Re=229, downstream *u* velocity obtained using two schemes with pP2P1 type elements are plotted in Figure 7.6. Except little difference in the recirculation both algorithms yield nearly identical result.

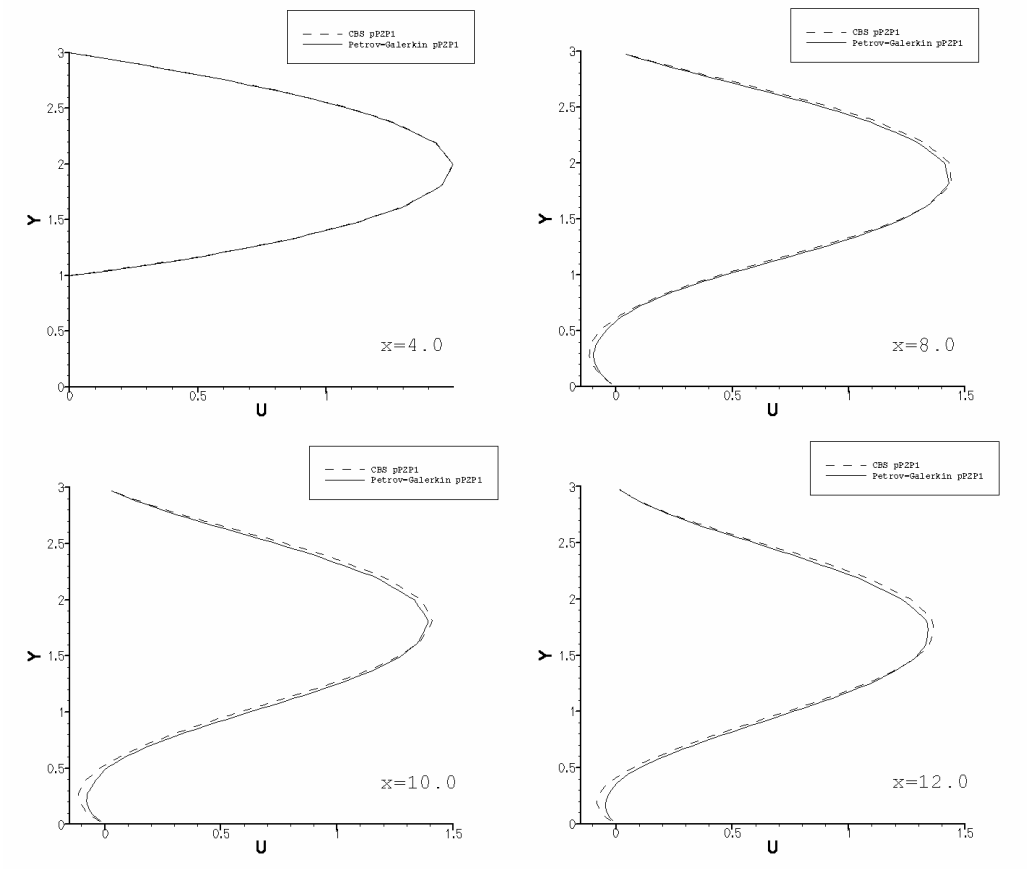

Figure 7.6 : Velocity profiles obtained using pP2P1 elements downstream of the step, *Re*=229

Table7.2: Efficiency of pP2P1 elements compared to P1P1 (*Re*=191)

Method	CPU time with P1P1 elements, s	CPU time with pP2P1 elements, s	% Saving
Galerkin	403	220	45
Petrov-Galerkin	228	100	56
CBS	248	103	59

Efficiency of pP2P1 type elements with respect to the use of P1P1 elements are shown for all the algorithms considered in the Table 7.2. It can be seen that computational costs are reduced up to %59, if the pP2P1 elements are used instead of P1P1 elements [26]. Since the main goal of this preliminary numerical computation is to compare the CBS algorithm with alternatives such as P-G methods, and evaluating it in terms of accuracy and computational costs, a difference with other data [51] is considered acceptable.

7.3. Laminar Viscous Flow over NACA0012 Airfoil

Laminar viscous flow past NACA0012 airfoil at Mach number 0.5 and angle of attack 0° was selected as the test case. *Re* is equal to 5000 for this test case. Semi implicit version of the CBS algorithm with barotropic gas assumption is used within this computation.

To generate an unstructured mesh around the airfoil, the commercial code named Gambit is used. Since it is not so practical to generate P1P1 type of triangular elements using Gambit for boundary layer, rectangular types of elements are generated for this region. Then these elements were divided into two triangular elements using a Fortran code. And finally, all the P1P1 types of elements in the computational domain are converted to pP2P1 type of elements using another Fortran code. The generated mesh in which the far field boundary was situated at a distance of 20 chords from the airfoil surface can be seen in Figure 7.7. The grid details around the airfoil also can be seen in Figure 7.8. The mesh seen in these two figures were used for the velocity calculation and it consists of 20472 elements and 10340 nodes.

The wall (airfoil surface) is adiabatic and Prandtl number is equal to 0.72. The velocity is prescribed at the inflow as 1.0 in the x-direction and 0.0 in the y-direction. The temperature is also prescribed at the inflow as 1.0. The density ρ_{∞} at the outflow is fixed as 1.0. No-slip boundary condition is imposed on the airfoil. The adiabatic exponent γ and constant A for the barotropic gas assumption are equal to 1.4 and 2.857136, respectively.

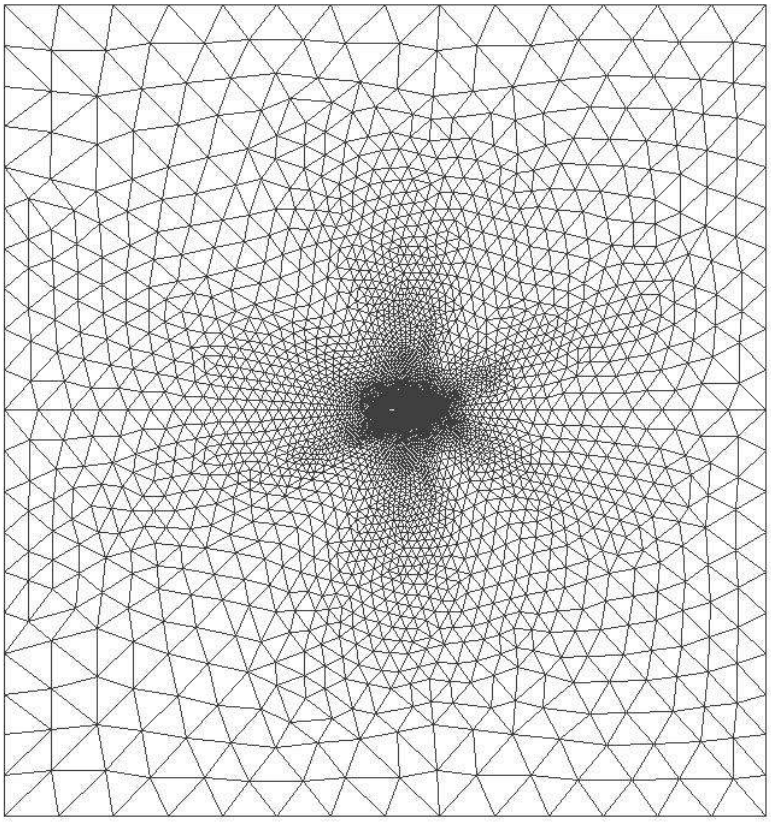

Figure 7.7 : Flow over NACA0012 airfoil

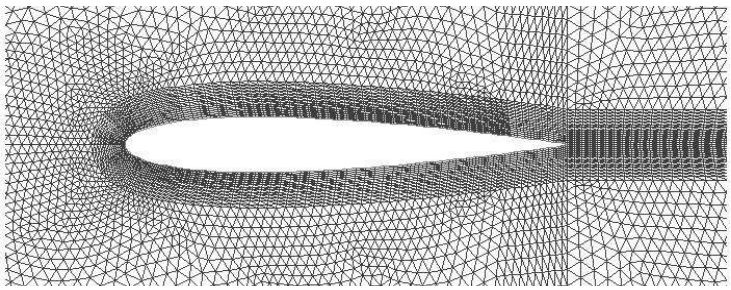

Figure 7.8 : Detail of the mesh; airfoil close- up

For the test case, the velocity field is obtained by using barotropic gas assumption. When barotropic gas assumption is used instead of the ideal gas assumption, the energy equation is uncoupled from the other equations (see details of the procedure in Chapter 4). Pressure contours and its details near the stagnation point are given in Figure 7.9 and Figure 7.10. Details of velocity vectors around the leading edge are given in Figure 7.11.

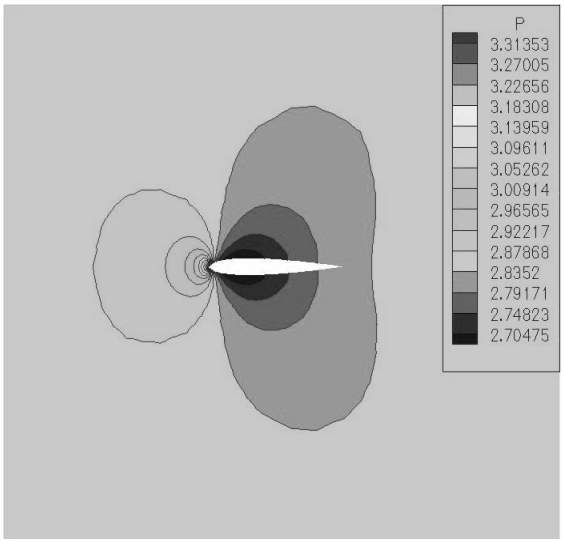

Figure 7.9 : Pressure contours obtained using barotropic gas assumption

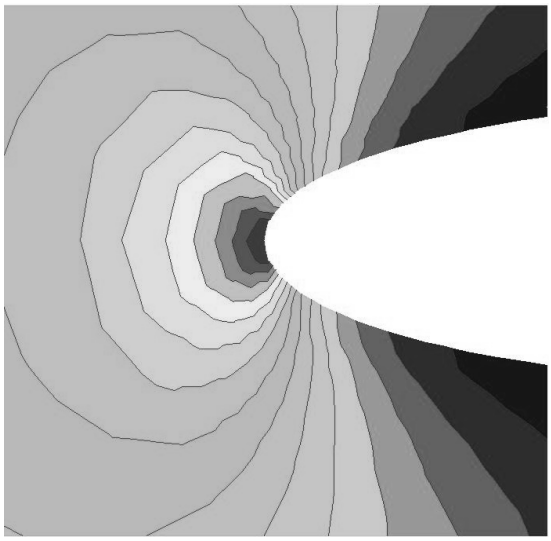

Figure 7.10 : Detail of Pressure contour near the stagnation point (barotropic case)

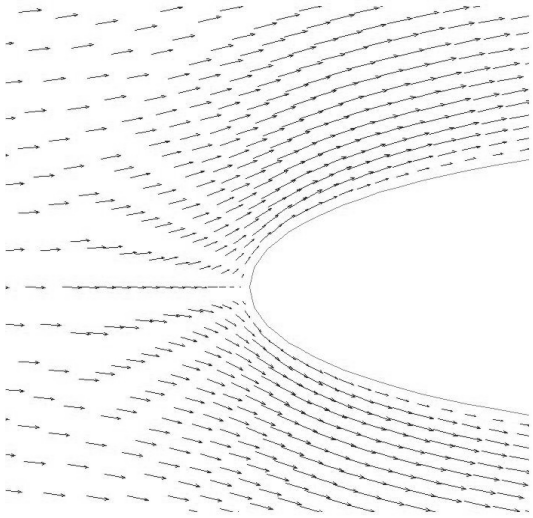

Figure 7.11 : Detail of velocity field near the stagnation point

The Mach contours obtained using barotropic gas assumption within the CBS algorithm is plotted and given in Figure 7.12. The Mach contours obtained in Reference [53] are also given in Figure 7.13 for comparison. Even though pP2P1 type elements are used in the computations and results are obtained without solving energy equation (it is possible if barotropic assumption is done), Mach contours are very similar with Reference [53].

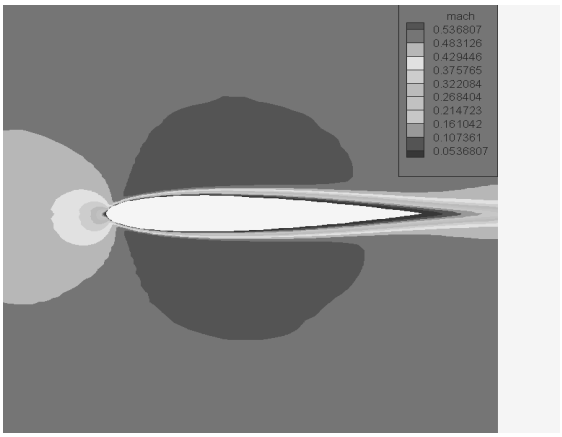

Figure 7.12 : Mach contour (barotropic case)

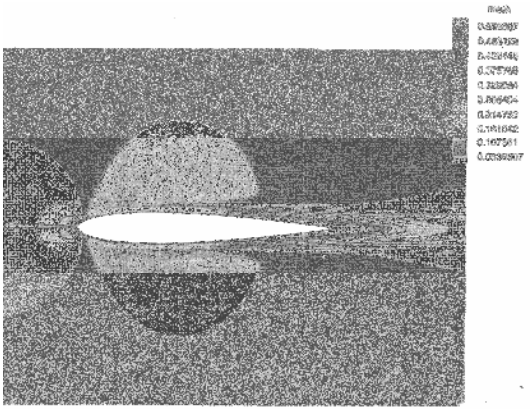

Figure 7.13 : Mach contour (Reference [53])

7.4. Flow in a Micro Channel

Another flow problem solved during the study is the pressure driven flow through a straight micro channel in slip regime. This problem has been studied before by Beskok using DSMC and μFlow (spectral-element-based continuum CFD solver) [54]. A N-S and Burnett equations solver have been used by Agarwall&Yun [40] for the same geometry. Baysal&Aslan [55] have solved the same problem using first order slip velocity of Maxwell and Beskok's second order slip velocity within the Finite Volume N-S solver. Since there are various computational and analytical results for this problem in literature, it is a good choice to test the implementation of Beskok's second order slip velocity within the present CBS implementation.

Inlet to outlet pressure ratio of the micro channel is equal to 2.28 and it is denoted with Π within this study. The flow is assumed to be isothermal and reference temperature is taken as 273°K. Knudsen number is equal to 0.2 at the outlet of the channel. The ratio of channel length to the height (L/h) is equal to 20. All the values given in this paragraph are same with the References [55].

For the reason mentioned in the previous problem pP2P1 type elements were used again within the computation. The velocity mesh consists 53 and 21 grid points in horizontal and vertical direction. Details of the grid can be seen in the Figure 7.14. Total number of triangular elements used for the velocity calculation is 2080.

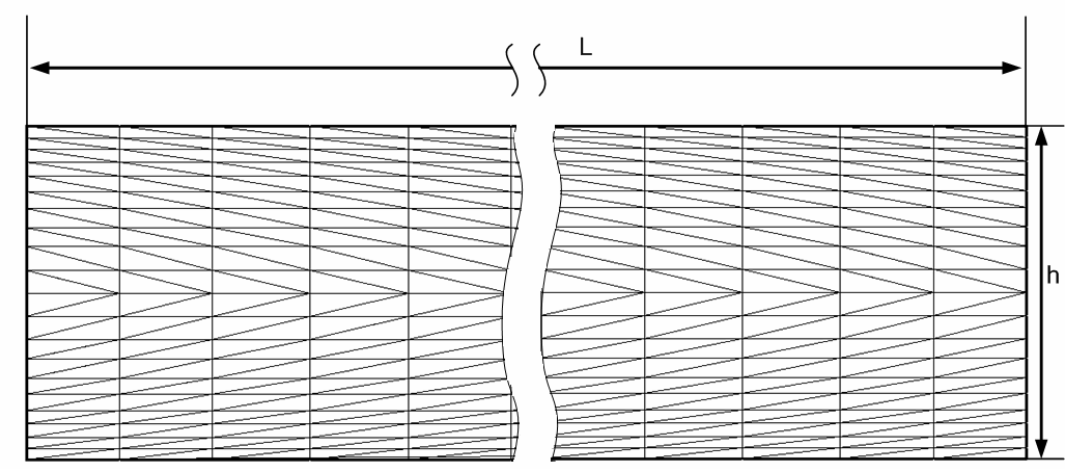

Figure 7.14 : Velocity mesh of straight micro channel

To simulate rarefied fluid flow through this channel, semi implicit version of the CBS algorithm needs to be modified to accommodate for slip-velocity. Thus, Beskok's second order slip velocity formulation (WS) was used instead of general no slip boundary (NS) condition. The pressure values which satisfy the inlet to outlet pressure ratio and outlet Knudsen number were prescribed at the inlet and outlet of the channel. The velocity vectors obtained using no-slip and slip-velocity boundary conditions are plotted for comparison in Figure 7.15. The increase in the slip-velocity along the channel walls towards the exit can also be seen in the figure.

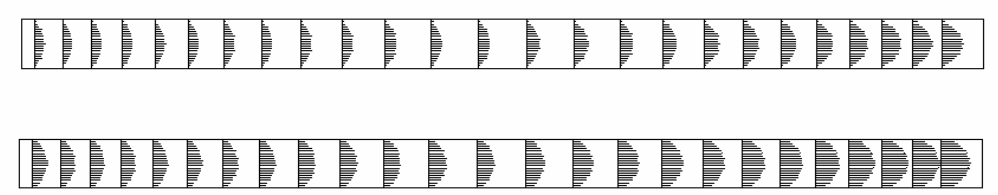

Figure 7.15 : Velocity distribution along the straight micro channel with slip-velocity (lower) and no-slip boundary conditions (upper)

The pressure variation obtained along the centerline of the channel both with slip-velocity and no-slip boundary conditions are given in Figure 7.16. It can be observed from the figure that the pressure distribution computed via the CBS scheme are in excellent agreement with the results presented in References [54,55] and analytical result [56]. Nonlinearity in pressure distribution is due to the compressibility. For the results obtained using slip-velocity (WS) boundary condition, the pressure distribution is slightly lower in magnitude compared to the results with no-slip-velocity (NS) boundary condition.

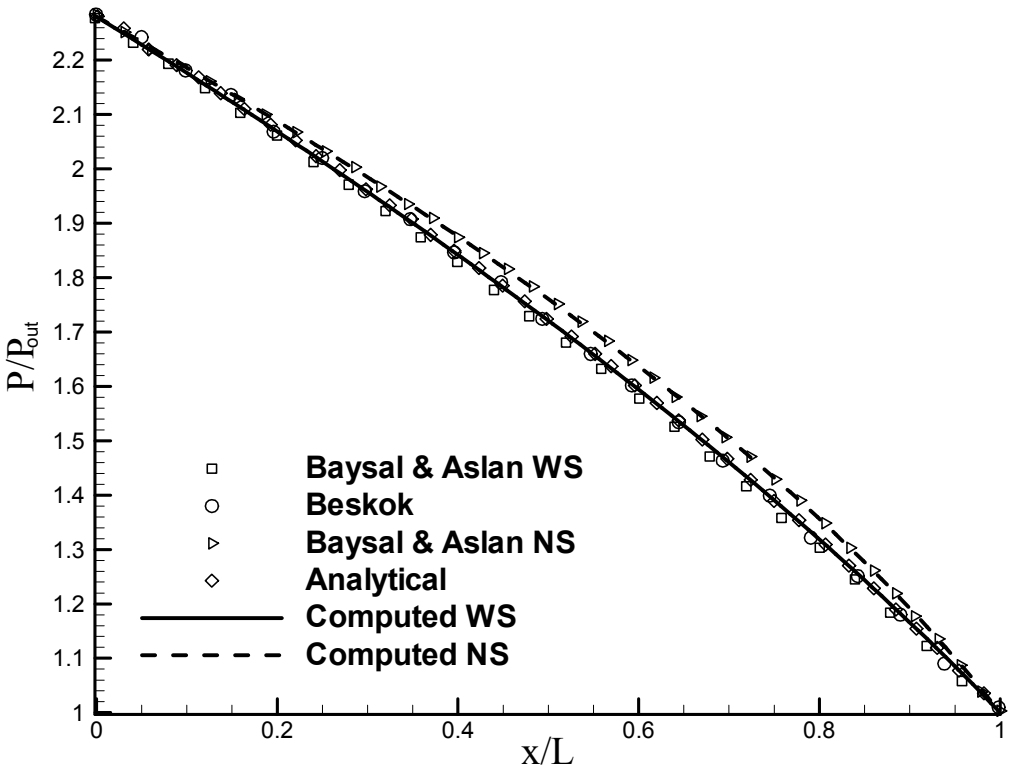

Figure 7.16 : Pressure distribution along the straight micro channel centerline, Kn_{out}=0.2, Π=2.28

Decreasing density values result in increasing velocity values through the channel (see Figure 7.15 and 7.17). The slip-velocity variation along the channel wall obtained using the CBS algorithm with second order slip-velocity boundary condition (BC) is normalized using the centerline velocity value at the channel inlet and given in Figure 7.18. The available results in literature are also used for comparison for this flow problem. The results denoted with Baysal&Aslan in the figure are based on numerical solution of N-S equation using FVM with first and second order slip-velocity BC [55]. Agarwal&Yun's results are based on Burnett equation solution [40]. Since the Analytical results [56] given in the figure are based on first order approximation, it matches the first order results of the Baysal&Aslan. DSMC results of Beskok are slightly different from the other results in the first half of the channel. Towards the exit of the channel, its results also match the other results. Among all the results given in Figure 7.18, computed results are in good agreement with the Reference [40] and [55] as expected. Maximum difference in magnitude between the computed slip-velocity and the Reference [55] is less than %1.

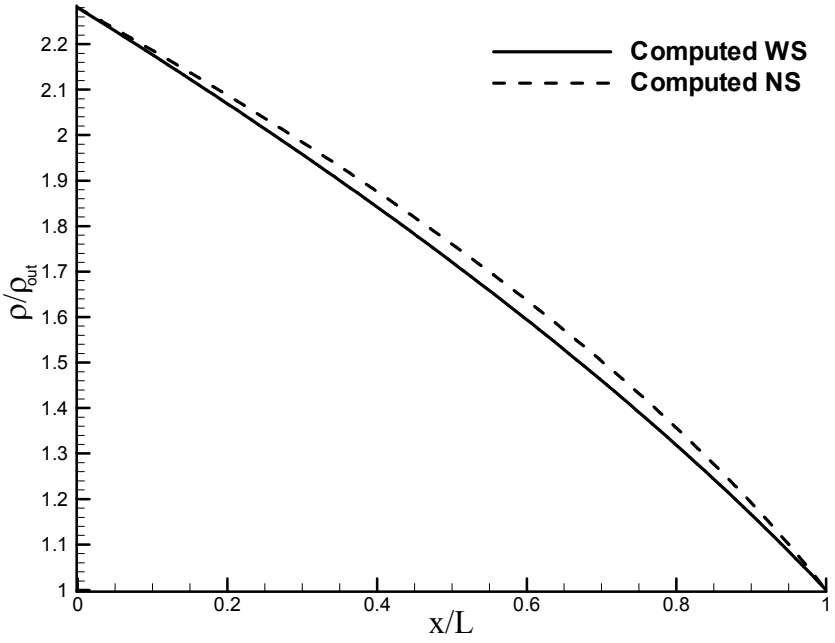

Figure 7.17 : Density distribution along the straight micro channel centerline, Kn_{out}=0.2, Π=2.28

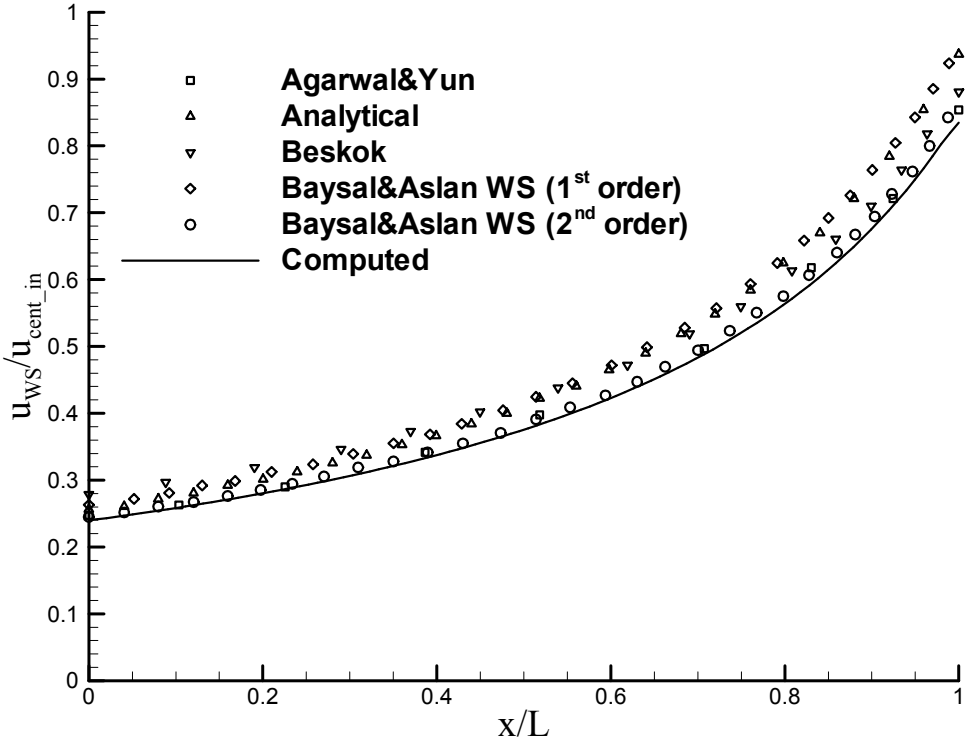

Figure 7.18 : Slip-velocity variation along straight micro channel wall, Kn_{out}=0.2, Π=2.28

7.5. Micro Synthetic Jet

Fluid flow generated by a micro synthetic jet actuator with rectangular cavity was simulated using CBS algorithm. Since compressible flow analysis is required for an accurate prediction of the flow field inside the cavity of micro synthetic jet, semi implicit version of the CBS algorithm with barotropic gas assumption is used within the simulation. pP2P1 type elements are employed in order to reduce implicit part of the algorithm as done before. To account for slip effect at the solid wall of the micro synthetic jet, general no slip boundary condition of CBS scheme is modified using Beskok's second order slip-velocity boundary condition. The Arbitrary-Lagrangian-Eulerian (ALE) approach [37] was used and coupled with CBS scheme to model the deforming grid due to movement of the of actuator diaphragm [34,57].

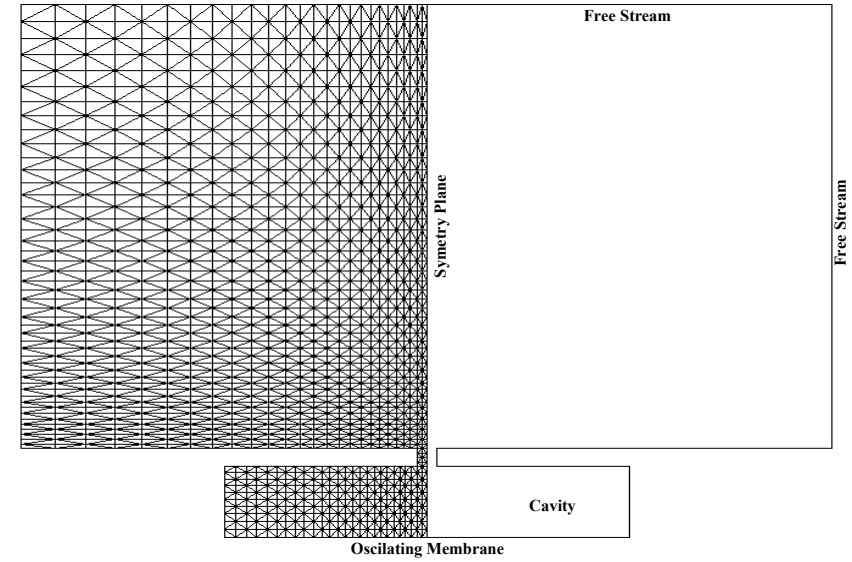

Figure 7.19 : Computation domain and the pressure mesh for the SJA with rectangular cavity geometry.

Computational domain consists of three different grid blocks. These are the cavity, orifice and outside regions. For the quiescent external flow condition, the flow field can be assumed symmetric. Thus, only half of the domain is considered for numerical computation (see Figure 7.19). The external flow domain has 20*d* in length and 25*d* in width. Orifice width is denoted with *d* (see Figure 6.1). Number of nodes within the generated mesh for cavity, orifice and outside regions are 209x81, 17x33 and 209x369 (in horizontal x vertical direction). Since the bottom wall of the cavity represents the oscillating diaphragm, it is required to define the movement of

this wall in time. For this problem, it is assumed that the movement of the diaphragm is only in vertical direction. So, deformation and movement of the diaphragm is given with following equation:

$$y(x,t) = A\sin\left(\left(\frac{x+W/2}{W}\right)\pi\right)\sin(\omega t) \tag{7.3}$$

where ω is the the diaphragm frequency, t is time and W is cavity width. A denotes the maximum deflection amplitude. Shape and velocity of the diaphragm is calculated from the equation written above and updated at every time step. Internal node coordinates and velocities are interpolated linearly from surrounding boundaries of cavity region and they are also updated at every time step.

In order to verify the implementation of the ALE technique to the CBS solver, a SJA flow from literature [31] was analyzed and results are compared in Figure 7.20. In the figure, at four different position of the diaphragm, orifice exit velocity was normalized with $u_{\max}^{avg} = u_0(0)$, was plotted for comparison with reference results. The results are in good agreement with the Reference [31] for all stages except little difference near the wall due to the reduced number of nodes of the computational grid near this region (see Figure 7.21). In Figure 7.22, pressure and velocity meshes generated for the whole domain can be seen.

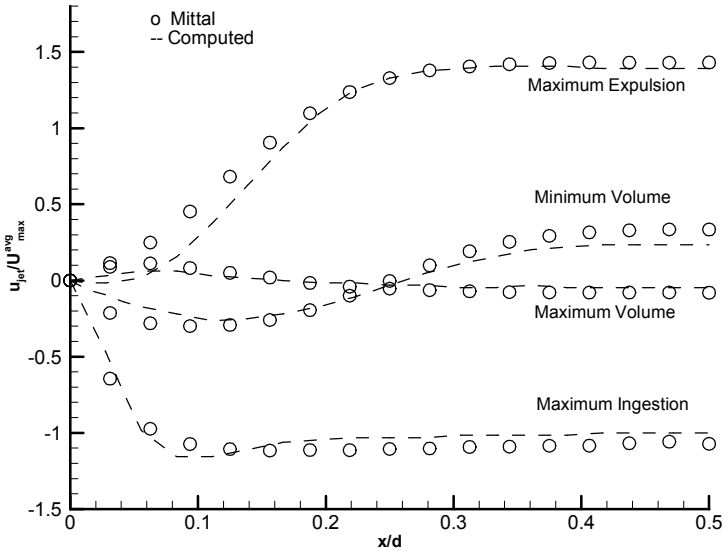

Figure 7.20 : Comparison of the normalized velocity profile at the orifice exit with [31]

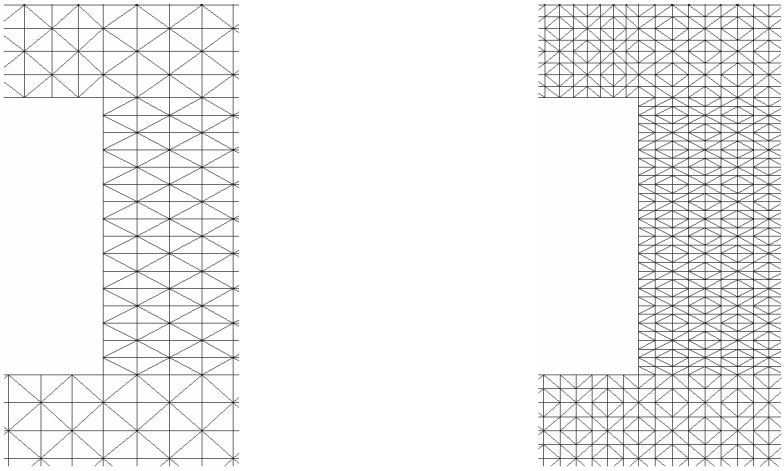

Figure 7.21 : Details of the meshes for the pressure and velocity field near the orifice

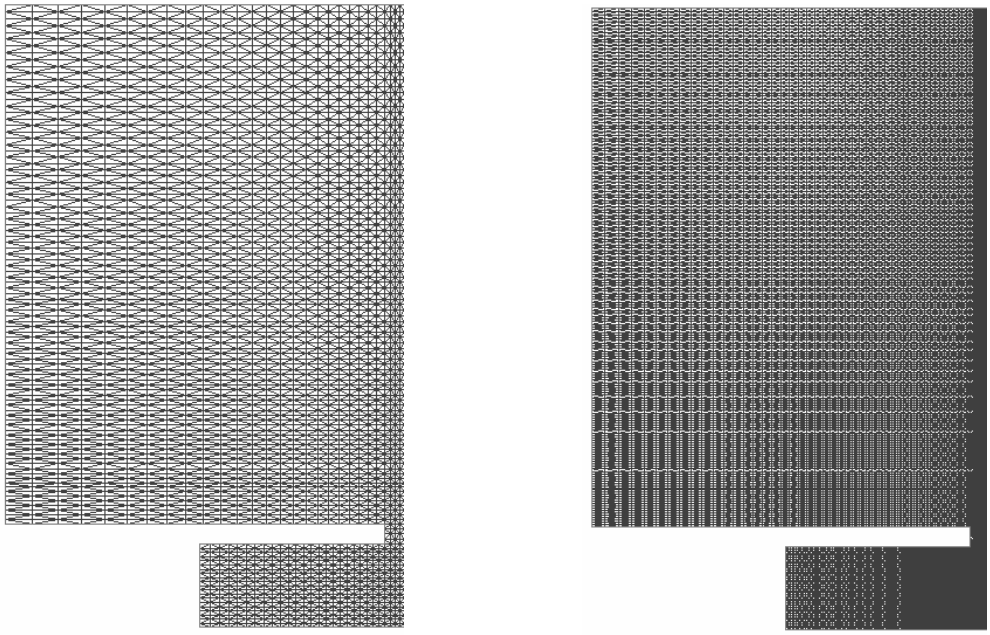

Figure 7.22 : Numerical grids used for pressure and velocity field of the μSJA configuration

The vorticity plots are given in Figure 7.23 at four different positions of the oscillating membrane which are maximum expulsion, minimum volume, maximum ingestion and maximum volume. It was observed that the flow field reaches a periodic behavior after four cycles. All the results presented here correspond to 6^{th} cycle for this case. Velocity distributions and vorticity contours given in the Figure 7.20 and Figure 7.23 reasonably agree with the results presented in Reference [31], where an incompressible solver is used.

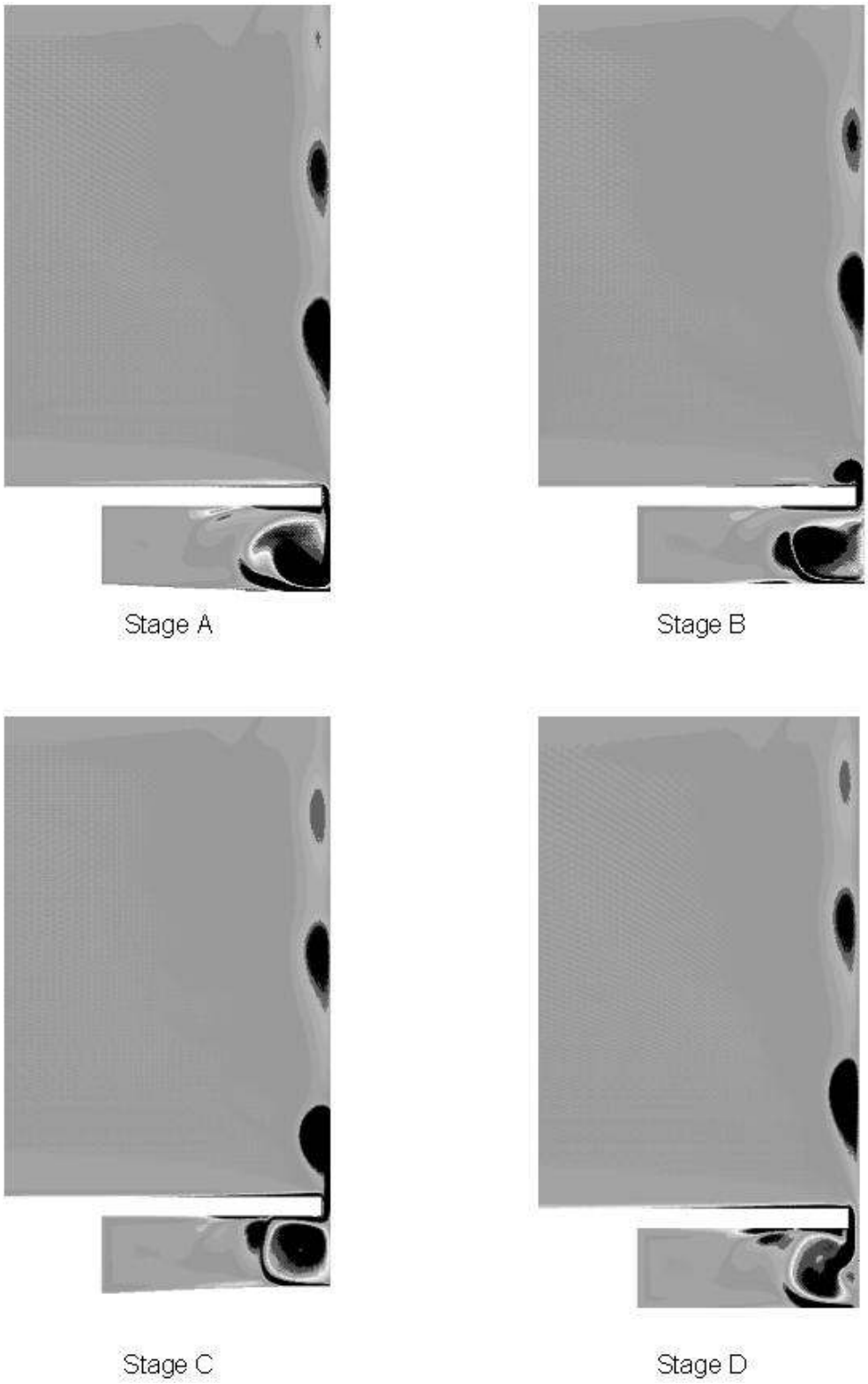

Figure 7.23 : Vorticity contours at the four stages of the diaphragm oscillation cycle

To investigate the effect of geometrical parameters of μSJ with rectangular cavity, various flow cases were set by selecting different cavity width, height and deflection amplitudes of the oscillatory diaphragm. For cases listed in the Table 7.3, orifice width, height, oscillation frequency and kinematic viscosity were kept constant as $d=h=12.5\ \mu m$, f=80000 Hz , $\nu=1.46x10^{-5}\ m^2/s$). Characteristic non-dimensional parameters Re_d and St which are defined in Chapter 6 are also listed for each case in the table.

Table 7.3: Computed cases for the analysis of μSJA in quiescent environment

Case	W/d	H/d	(A/d) x10	Re_d	1/St	Vortex Shedding	Vortex Train
1	10	4	4	8.7	1.62	No	No
2	20	4	4	17.4	3.24	Yes	No
3	30	4	4	26.2	4.86	Yes	Yes
4	10	4	2	4.4	0.81	No	No
5	20	4	2	8.7	1.62	No	No
6	30	4	2	13.1	2.43	Yes	No
7	10	4	8	17.4	3.24	Yes	No
8	20	4	8	34.9	6.48	Yes	Yes
9	30	4	8	52.3	9.73	Yes	Yes
10	10	6	4	8.7	1.62	No	No
11	20	6	4	17.4	3.24	Yes	No
12	30	6	4	26.2	4.86	Yes	Yes
13	10	8	4	8.7	1.62	No	No
14	20	8	4	17.4	3.24	Yes	No
15	30	8	4	26.2	4.86	Yes	Yes

The 'Vortex Shedding' column is filled based on the flow field at the maximum volume stage which is named Stage A in Figure 7.23. If a strong vortex core remains outside of the cavity at this stage, it is convected downstream without diffusing during the expulsion phase as expected. For all the values of Re_d smaller than 13.1, there are no vortices observed outside the cavity at Stage A. For the values of Re_d in the range of 13.1-26.2, a vortex is observed above the orifice in the flow field but this vortex diffuses before being convected away from the orifice during the following expulsion phase since it is not strong enough. Therefore, no vortex train is formed. For the values of Re_d greater than or equal to 26.2, strong vortices are observed in the flow field and these vortices are convected away from the orifice before diffusing. Thus they form a vortex train. As seen in the table, vortex train is formed for all the cases in which $1/St$ are greater than 3.24. This threshold value is higher

than the value of 2 given for 2-D jets in Reference [50]. Additional cases, run using Case 9 as a baseline and changing Re and St values revealed that if 1/St = 0.97 and Re_d=52.3 no vortex train is formed, confirming the presence of a threshold value for Strouhal number for jet formation.

The effect of cavity width to the orifice velocity magnitude and profile is also investigated. To do this, 3 cavities having different widths are analyzed and the results are presented in Figure 7.24. It is observed that cavity width affects the orifice velocity magnitude strongly at all four position of the diaphragm.

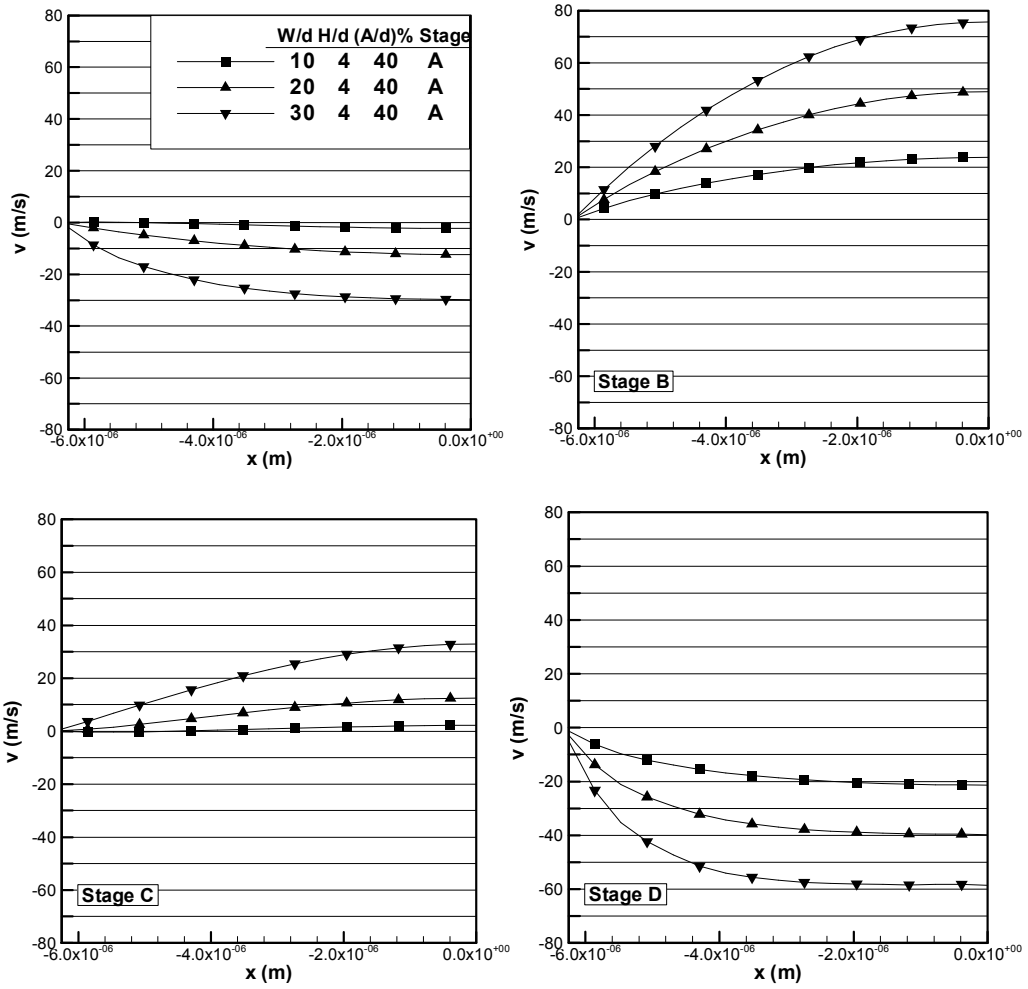

Figure 7.24 : Effect of cavity width on orifice velocity distribution.

In similar manner, the effects of cavity height and deflection amplitude are also investigated and velocity profiles for both cases are plotted at four different stages in Figure 7.25 and Figure 7.26. It can be seen in the figure that an increase in cavity height is not as effective as an increase in cavity width. Especially, at maximum ingestion and expulsion stages, this effect can not be noticed easily. On the other hand, an increase in the deflection amplitude directly affects the exit jet velocity magnitude at every stage of the cycle.

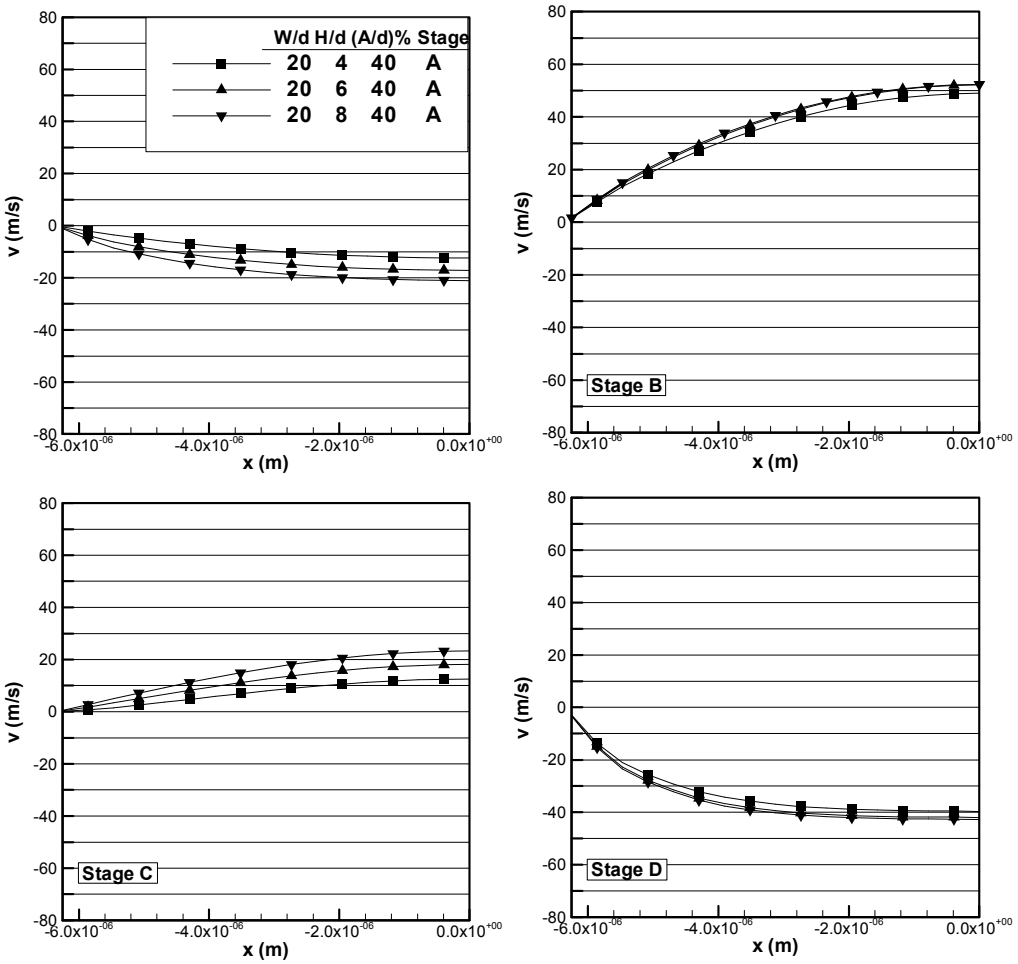

Figure 7.25 : Effect of cavity height on orifice velocity distribution.

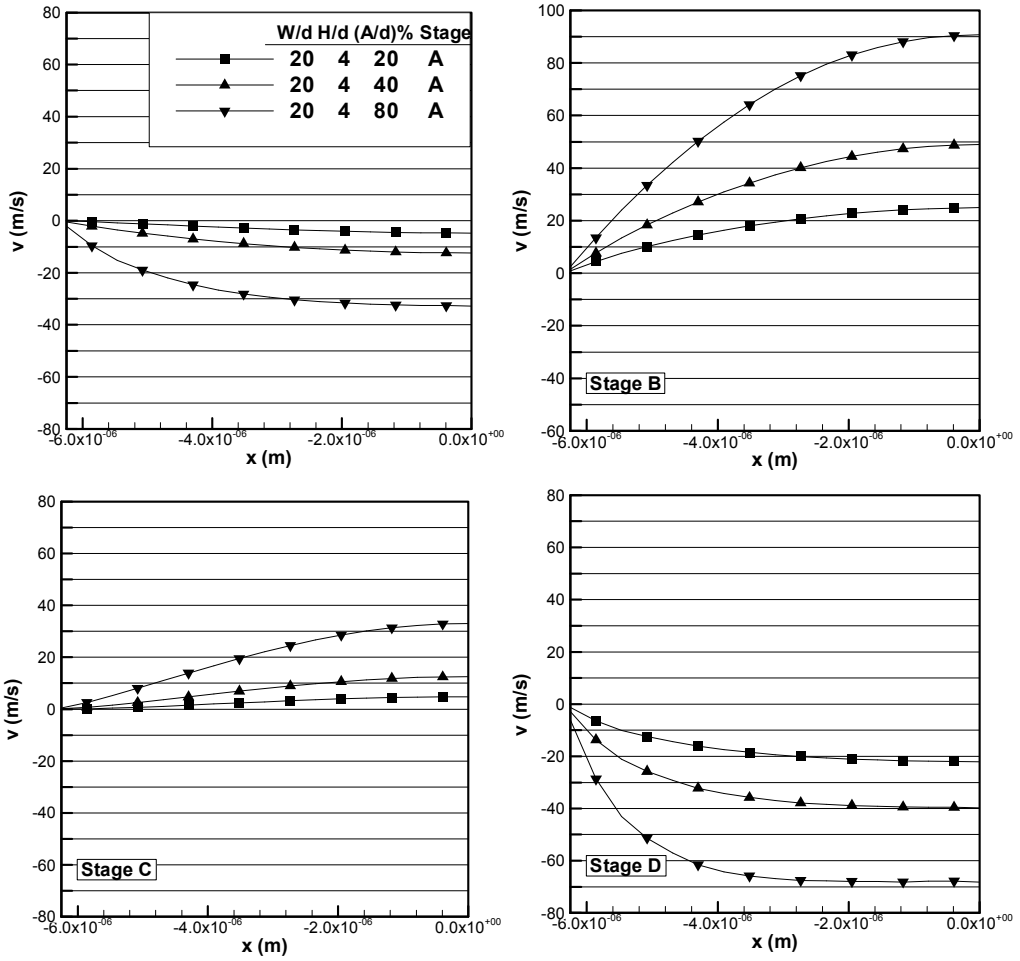

Figure 7.26 : Effect of diaphragm oscillation amplitude on orifice velocity distribution.

In Figure 7.27-a, variations of normalized values of maximum expulsion velocity at the orifice center are plotted against cavity width for two different cavity heights. The velocity values are normalized using the maximum value of space averaged expulsion velocity. In this figure, there is a decrease in maximum velocity while the cavity width is in increase and height has constant value of 8. This behavior can be interpreted as a result of the compressibility.

For two different cavity widths, normalized maximum expulsion velocity at orifice center is plotted against to oscillation amplitude in Figure 7.27-b. It can be said that for an increased cavity width such as W/d=30, increased deflection amplitude results in a more uniform orifice velocity distribution. Similarly, as shown in Figure 7.27-c, for cases where cavity width is high, the maximum velocity is lower for higher cavity

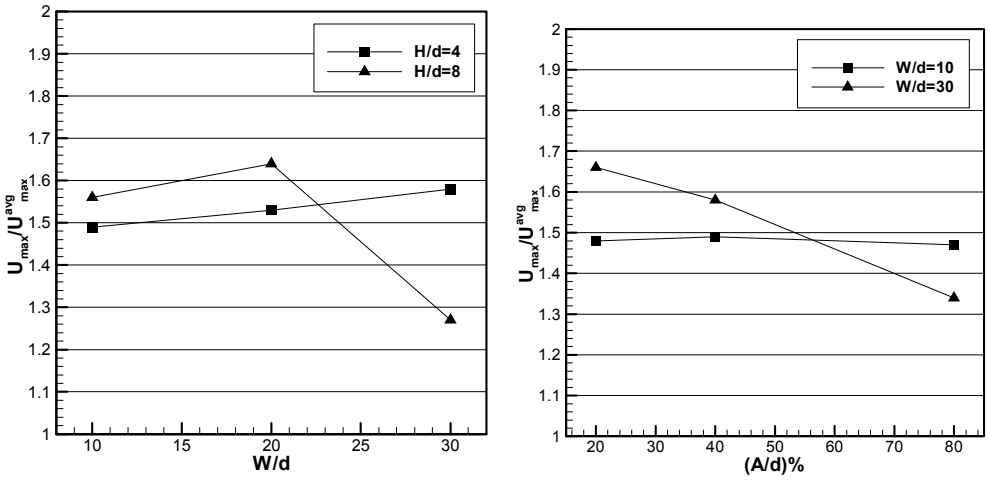

a b

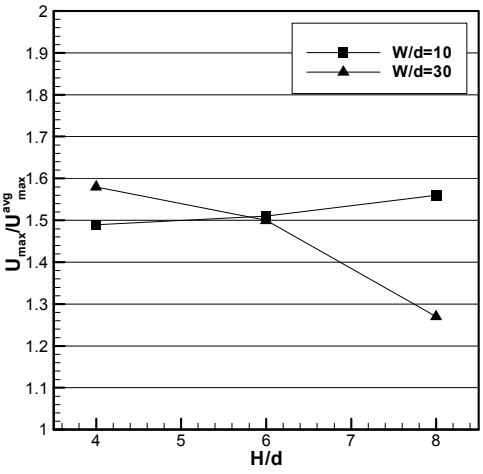

c

Figure 7.27 : Effects of various geometrical parameters on normalized maximum orifice velocity.

Some of the cases listed in Table 7.3 resulted in orifice velocities up to 140 m/s, justifying the use of a compressible flow solver. Slip-velocities on the other hand, remained within 3-4 percent of the maximum velocity for the cases analyzed.

The results, obtained for cases with various cavity dimensions, are compared in terms of exit jet velocity magnitude and vortex dynamics in both the cavity and external region. It is shown that, the orifice Reynolds number and Strouhal numbers are important parameters determining the formation of a jet [34,57]. Furthermore,

compressibility is an important factor affecting the flow for μSJA. The threshold values of *Re* and *St* for jet formation depend on upon the orifice velocity profile. Changes in geometrical properties of the cavity affect the shape of the velocity profile, as well as the *Re* and *St*, thus affecting the jet formation.

The obtained velocity distribution and comparisons show that, the implementation of second-order slip-velocity boundary condition and ALE approach to the CBS algorithm yields accurate results for this test case.

7.6. Separated Flow in Micro Backward Facing Step

Fluid flow through micro backward facing step geometry is an excellent test case to verify the boundary condition modification done within the CBS solver for the simulation of micro fluid flow. It is known that, there are sharp gradients in flow field for this case. These sharp gradients cause significant variation of the mean free path of the gas and wall shear stress. It is also known that these two variations are highly related to the slip-velocity and temperature-jump boundary condition. The rarefaction effect is two-dimensional due to significant cross flow variation in this test case. Thus the effect of second order slip-velocity and temperature-jump boundary conditions on an internal micro-flow with separation can be investigated by modeling the fluid flow through this geometry.

Dimensions of the micro backward facing step geometry can be summarized as follows. The ratio of the channel length (L) to the exit height (h) is equal to 5.6. The entry to the channel is also simulated and it is located at x/h=0.86. Ratio of step height (S) to the height of the channel h is 0.467. (see Figure 7.28).

pP2P1 type of elements are used for computations. 11776 velocity elements and 2944 pressure elements are used within the mesh (see Figure 7.28). Since this flow case is not isothermal as the other cases presented in this chapter, it is essential to use CBS algorithm with ideal gas assumption. So, for this case, semi implicit version of the CBS algorithm was used within the computations with ideal gas assumption.

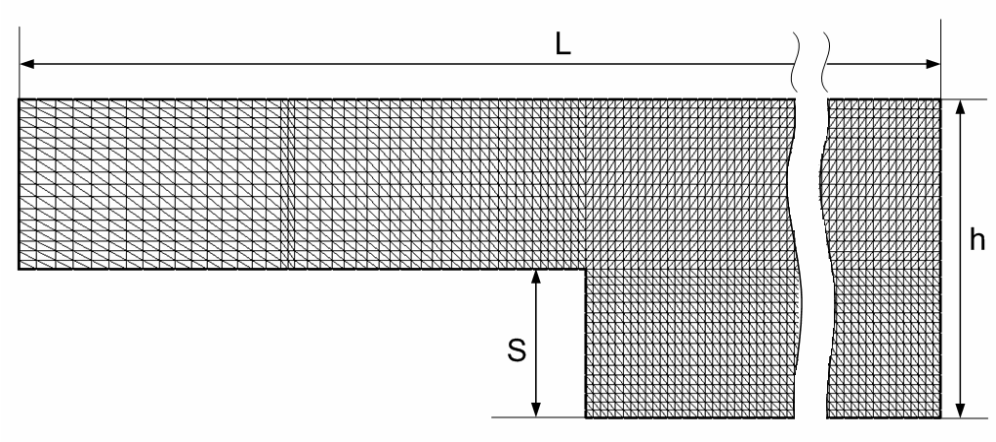

Figure 7.28 : Velocity mesh of Micro step duct

Baysal&Aslan[55] and Beskok[54] studied same geometry and obtained slip-velocity and temperature-jump conditions. In this case, inlet outlet pressure ratio Π =2.32. *Kn* at the outlet of the channel is equal to 0.018 and working fluid is nitrogen. As in the straight micro channel problem, pressure is prescribed at the outlet of the micro step duct geometry. Temperature value is prescribed as 330°K at the inlet where, vertical component of the velocity is set as zero. The wall temperature is equal to 300°K. At the outlet, boundary term (traction) on the right-hand side of the auxiliary momentum equation is calculated from the results obtained.

Velocity vectors at different locations along the geometry are given in Figure 7.29 for this flow case. In the same figure, temperature and local *Kn* number contours are also plotted. It can be seen from this figure that the fluid particles which have constant velocity and temperature at the entrance of the domain, start to decelerate as they reach the channel entry. This is natural result of wall shear stress. It is expected that the sudden increase in the wall shear stress at the entry of channel causes an increase in static pressure also. It is known that pressure and local *Kn* values are inversely proportional. So, the variation of local *Kn* number near the entrance due to this increase can be seen in the Figure 7.29. From the entrance to the step expansion, fluid particles continue to accelerate and temperatures decrease, due to this acceleration. The particles reach maximum velocity near the step expansion where the compressibility effect can not be neglected anymore. Near this region, the particles have minimum temperature and cross flow component of the velocity start to increase. Adverse pressure gradient is occurred due to the sudden expansion of the geometry. As a result of this adverse pressure gradient, the flow at the bottom wall

separates and then reattaches to the wall. In this separation region, due to the change in pressure, local *Kn* number reaches maximum value. After this point, fluid particles start to accelerate again due to the decreasing pressure along the channel. Near the channel exit, velocity profile takes the parabolic form again and local *Kn* distribution is symmetric. Temperature distribution is also symmetric at the channel outlet. The particles have minimum temperature value in the centerline of the channel due to the parabolic structure of the velocity profile.

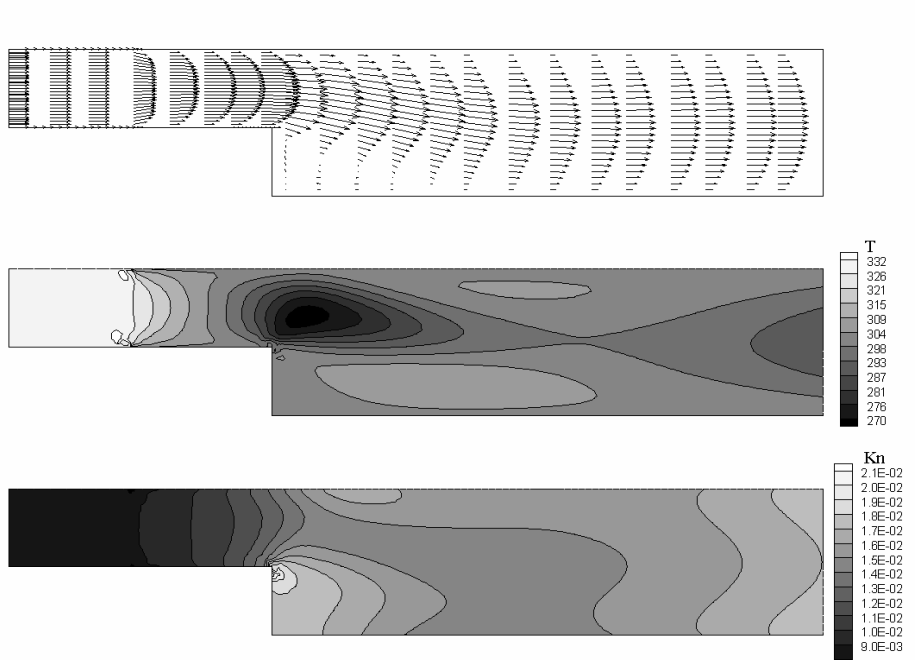

Figure 7.29 : Velocity vectors, temperature and local *Kn* variation through the micro step duct, Kn_{out}=0.018, Π=2.32

Variation of the normalized (with local speed of sound) streamwise velocity at five normal locations are plotted and compared with the results of Baysal&Aslan [55] in Figure 7.30. As seen in the figure, the velocity distribution obtained using CBS solver with Beskok's second order slip-velocity and temperature-jump conditions are in good agreement with the one given in the reference. The slip-velocity distribution at the top and bottom wall (y/h=0.9901 and 0.01456) are nearly the same towards the channel exit. The maximum values of these two distributions are at different locations due to the expansion in geometry which results in adverse pressure gradient and recirculation region. While the slip-velocity along the top wall is always positive, along the bottom wall it is negative in the recirculation region.

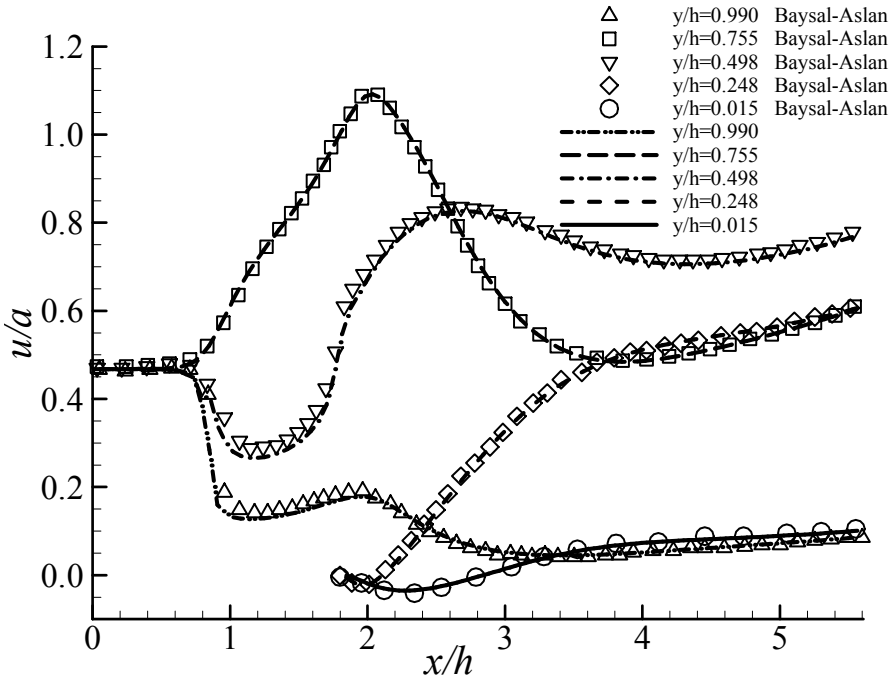

Figure 7.30 : Comparison of normalized streamwise velocity with Baysal&Aslan[55], Kn_{out}=0.018, Π=2.32

Pressure is normalized using dynamic head ($q_{in} = 0.5\rho_{in}u_{in}^2$) at the inlet and compared to the results of Reference [54] and [55] in Figure 7.31. *Kn* distribution along the centerline of the micro step duct given in Figure 7.32. As shown in these figures, results presented for this test case are in good agreement with reference studies.

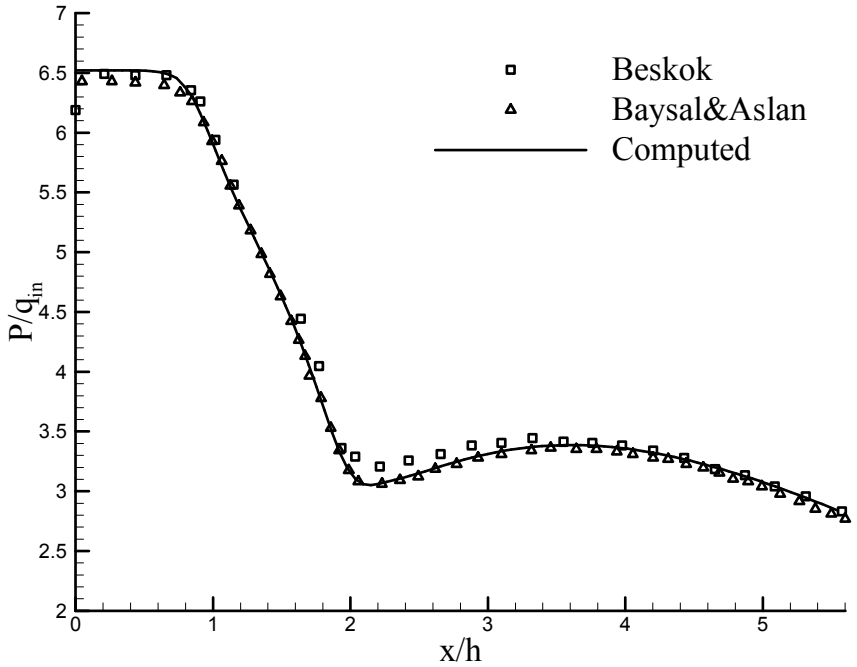

Figure 7.31 : Pressure variation along the channel, Kn_{out}=0.018, Π=2.32

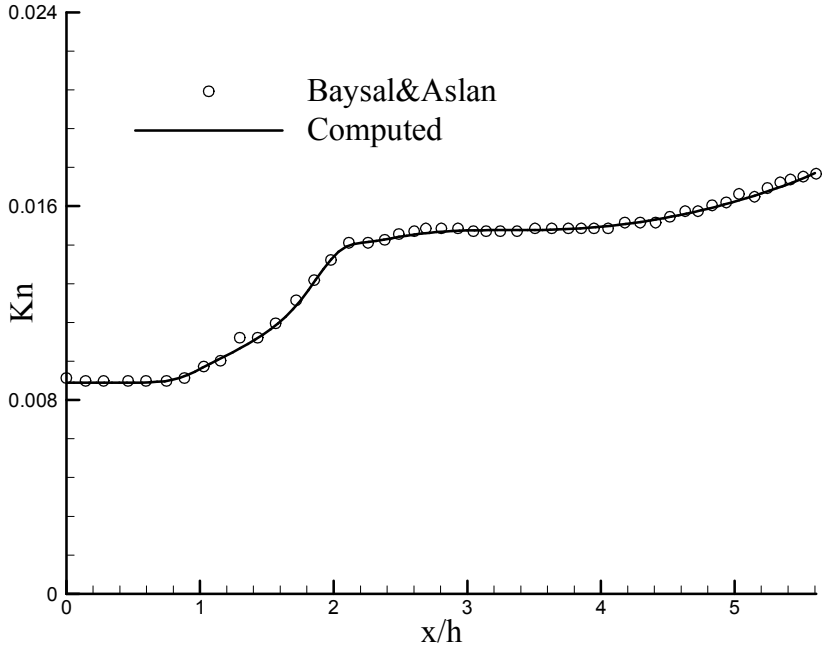

Figure 7.32 : Local *Kn* variation along the centerline of the step duct geometry, Kn_{out}=0.018, Π=2.32

It is obvious that, for the micro flow in slip regime, increasing *Kn* number results in significant raise in slip-velocity and temperature-jump values on the wall due to the increasing rarefaction effect. Macroscopic flow properties such as reattachment length, inlet Mach number or inlet outlet pressure ratio are also varied as *Kn* increases. In this study, the relationship between macroscopic flow properties and slip-velocity/temperature-jump boundary conditions are numerically investigated. To do this, flows in a step-duct were analyzed for various channel sizes with the same inlet-outlet pressure values. Selected channel heights result in a *Kn* range covering most of the slip-flow regime. Additionally, analyses are performed for both no-slip (NS) and slip-velocity (WS) boundary conditions for all cases. As the Knudsen number increases, mass flow rate difference between the results obtained using no-slip ($\dot{m}_{NS}$) and slip-velocity ($\dot{m}_{WS}$) boundary condition increases as shown in Figure 7.33. The change in inflow Mach number (M_{in}) with duct size is plotted in Figure 7.34 for both no-slip and slip model assumptions. As expected, M_{in} decreases with increasing Kn. Inflow Mach number is always higher for slip model compared to the no-slip case.

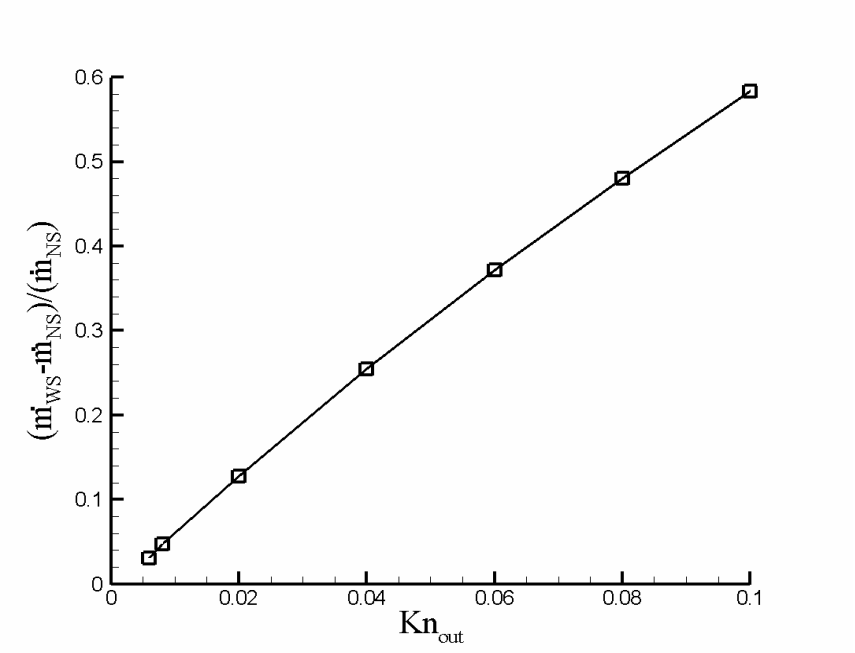

Figure 7.33 : Variation of mass flow rate difference between the results obtained using no-slip and slip-velocity boundary conditions, with Knudsen Number.

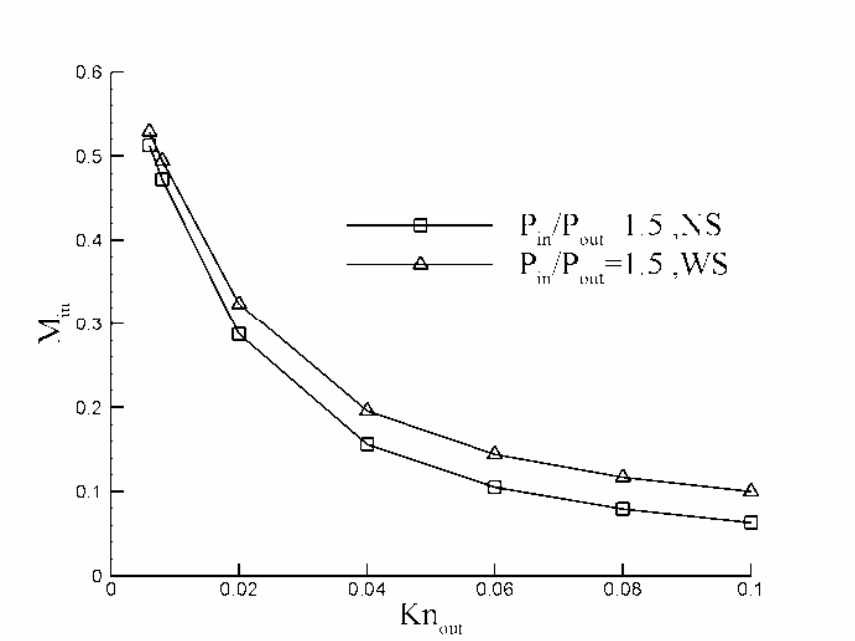

Figure 7.34 : Variation of inlet Mach number with Knudsen Number for the same inlet/outlet pressures

Another set of analyses was constructed by changing the channel height while keeping inflow Mach and outlet pressure values constant. Hence, it was possible to observe the dependence of driving pressure difference to the Knudsen number. In

Figure 7.35, variation of inlet to outlet pressure ratios with Knudsen number is plotted for two different inlet Mach numbers. Results obtained with no-slip and slip-velocity BC's are plotted together for comparison. As expected, increased inlet Mach number requires increased driving pressure difference. Similarly, the difference between slip and no-slip solutions increases with increasing Mach number as well as increasing Knudsen number. The variation of the mass flow rate difference between the slip and no-slip cases with Knudsen number is plotted in Figure 7.36. It is shown that the difference is limited for high inlet Mach number. Another important feature of the flow is the reattachment length. In this study, the reattachment length, X, is used in normalized form with the channel height. In Figure 7.37, variation of the relative difference of the reattachment length between slip and no-slip cases are plotted against Knudsen number. Its behavior is similar to the behavior of the mass flow rate. For low Mach numbers, the difference increases almost monotonously. For high Mach numbers however, the difference presents an asymptotic behavior.

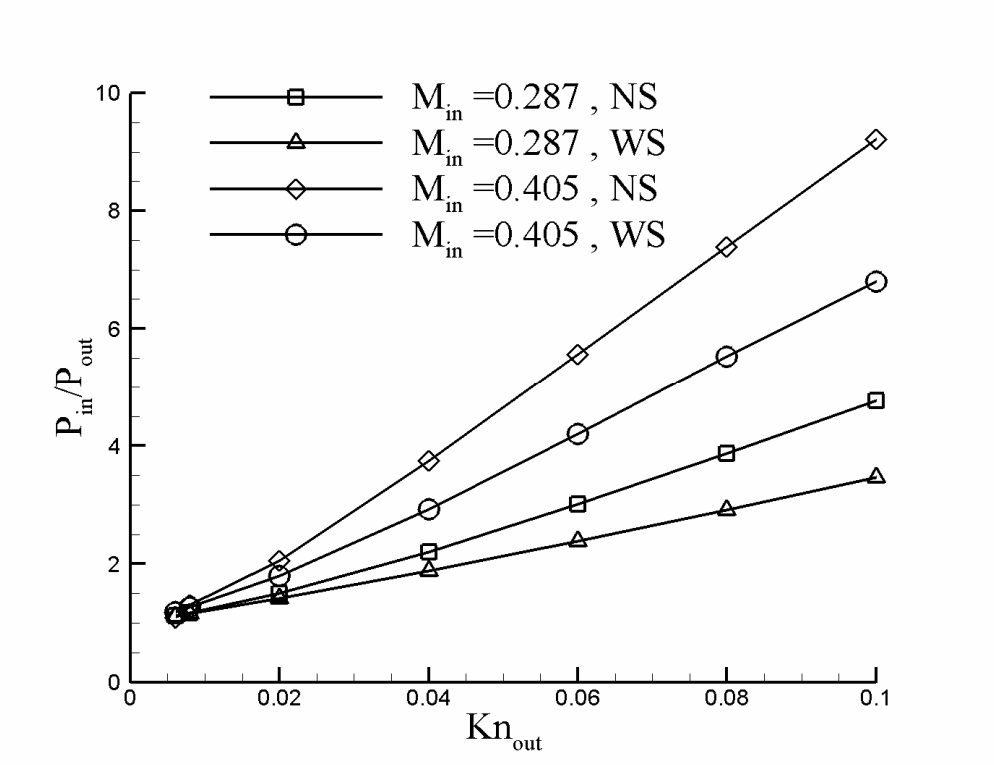

Figure 7.35 : Inlet to outlet pressure ratios vs. Knudsen number.

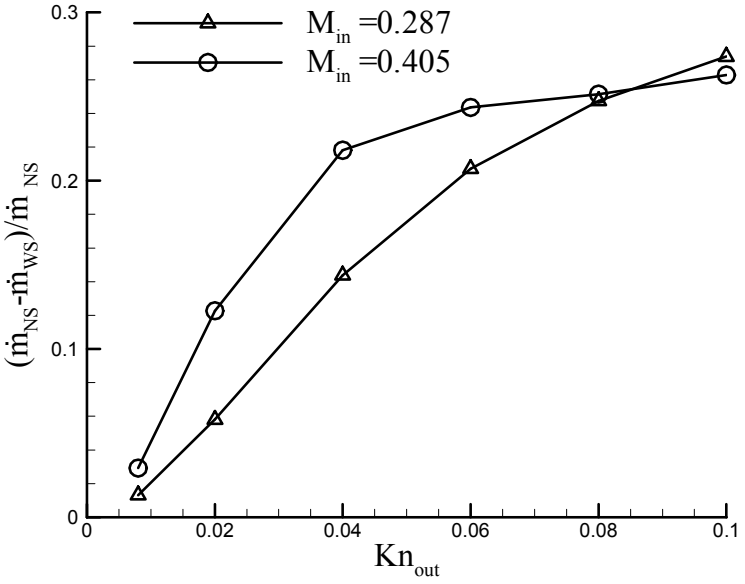

Figure 7.36 : Relative mass flow rate difference between the results with no-slip and slip-velocity boundary conditions

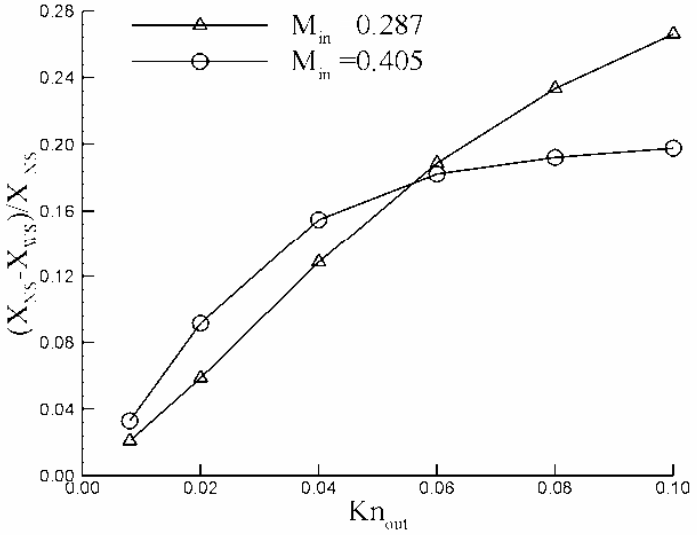

Figure 7.37 : Relative reattachment length difference between the results with no-slip and slip-velocity boundary conditions

The variation of non-dimensional temperature-jump, $\theta = (T - T_{wall})/(T_{inlet} - T_{wall})$, along the lower wall is presented in Figure 7.38. In this expression, T denotes the temperature of the fluid at the wall. As seen in the figure, temperature-jump value increases towards the channel exit for higher exit Kn value. For the smaller exit Kn value, temperature-jump is negligible. As Kn_{out} increases, inlet/outlet pressure ratio

also increases for constant inlet Mach number (see Figure 7.35). It is obvious that for smaller inlet/outlet pressure values more linear velocity profile occurs at the channel outlet. Hence smaller temperature-jump values are considered at this region since lower temperature gradient exist normal to the wall. For greater inlet/outlet pressure ratio, flow accelerates through the channel exit in the development region after reattaching to the wall and high temperature gradient is considered through the centerline of the channel [58].

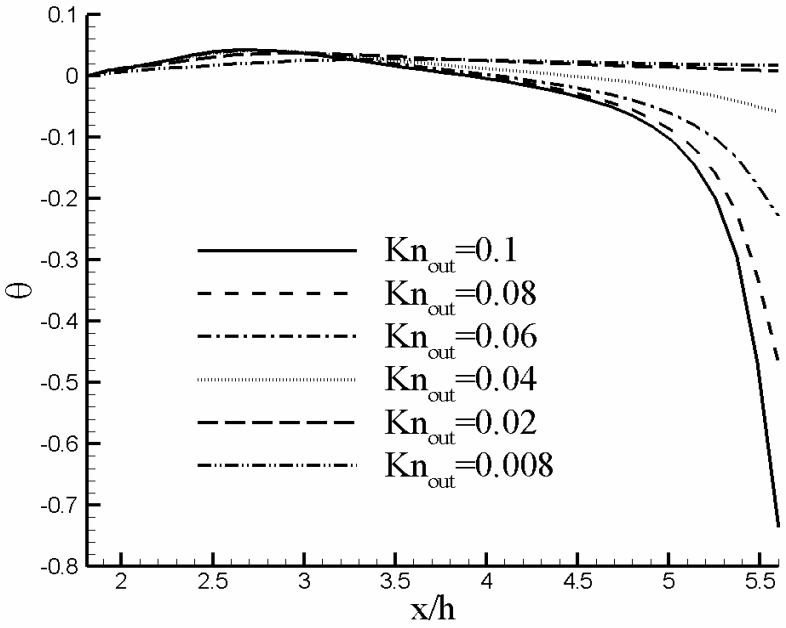

Figure 7.38 : Temperature-jump along the lower wall for cases with M_{in}=0.405

Similarly, the variation of the slip-velocity, u_s, normalized with the inlet velocity, u_{in}, along the lower wall is plotted in Figure 7.39 for different Knudsen numbers and selected inlet Mach number of 0.405. Acceleration of fluid through the channel exit due to increasing rarefaction effect results in high slip-velocity along the lower wall.

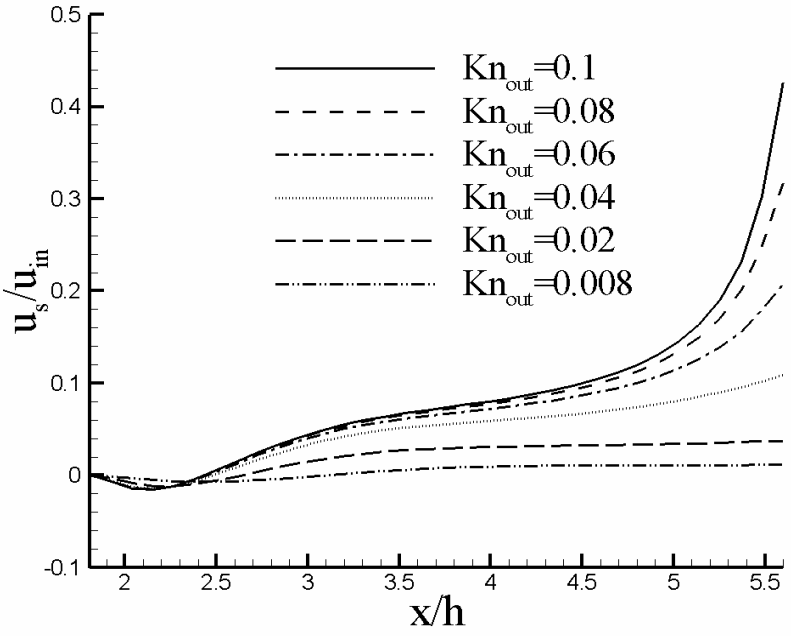

Figure 7.39 : Slip-velocity along the lower wall for cases with M_{in}=0.405

8. CONCLUSION

Governing equations of viscous compressible flow in conservative form are split into two parts using main aspect of Characteristic Based Split (CBS) procedure. Since the first part of the equations is a simple scalar-convection–diffusion type equation, characteristic-Galerkin procedure is applied to it and then it is discretized along the characteristics. Second part of the equation is self-adjoint. Hence, resulting equations are discretized in space using standard-Galerkin approach which is optimal. At the end, CBS FEM algorithm is obtained. In this study CBS FEM algorithm is combined with pseudo-second order velocity interpolation, ALE description and slip-velocity/temperature-jump boundary conditions for micro-flows and used to solve various fluid flow problems.

Laminar viscous flow through backward facing step geometry is one of these problems. In addition to obtaining solution for this flow problem, this result is compared with other results obtained using alternative incompressible fractional step FEM algorithms (Galerkin and Petrov-Galerkin). Since all schemes used in these computations are semi implicit, the problems are solved using pP2P1 types elements besides P1P1. It is observed that the results obtained using CBS algorithm is as good as the results obtained using Petrov-Galerkin scheme in terms of accuracy and computational costs. Using pP2P1 type elements within the computation reduce to computational time up to %59.

Laminar viscous fluid flow past a NACA0012 airfoil at Mach number of 0.5 is another problem solved using CBS algorithm. pP2P1 type elements are also used in this computation. The results obtained using CBS algorithm with barotropic assumption are also in good agreement with the reference values.

Implementation of second order slip-velocity/temperature-jump boundary condition encountered in micro flow within the CBS FEM algorithm which can be used for solution of compressible and incompressible viscous flow problem is presented in this study. With this implementation, applicability of the CBS algorithms is extended

to cover fluid flow in slip-regime. To reduce the size of the implicit part of the CBS algorithm, pP2P1 type elements are used within the computations. Using Arbitrary Lagrangian-Eulerian formulation and modifying the CBS FEM algorithm, the solver becomes an effective tool which can be used for analysis of fluid flow problems with moving boundaries. The applications and implementations mentioned here are the first attempts for utilization of the CBS FEM algorithm for micro-flows.

Another benchmark problem in slip regime which has been solved by many others is pressure driven straight micro channel flow. This problem is also solved using CBS algorithm with pP2P1 type elements. Obtained results are compared with the available analytical and numerical results [40,54-56].

Micro synthetic jet flow is numerically investigated during the thesis study. Since moving deforming mesh concept and slip-velocity boundary condition implementation is essential for numerical simulation of this problem, it is a good case to test the solver and to modify the algorithm. Obtained results are compared with the available results in literature. The results are in good agreement also for this test case. An analysis is done to understand effect of micro synthetic jet cavity geometry on vortex dynamics. Obtained results are very interesting in terms of showing the capability of the CBS algorithm even in the slip regime. This study is one of the first comprehensive micro synthetic jet analysis performed using a compressible solver. Obtained results shows that compressible flow analysis is required, since for some cases jet exit velocity reaches 140 m/s.

Fluid flow through micro backward facing step geometry is one of the complex fluid flow problems numerically investigated in this study. Since there are recirculation region and high pressure and temperature gradient in the flow field, CBS solver with ideal gas assumption is used for the solution of this problem. In this case, the energy equation is coupled with momentum equation; computed slip-velocity and temperature-jump values are also included to this iterative procedure. To see the effect of slip-velocity and temperature-jump to the flow, results which are obtained using both no-slip/temperature-wall and slip velocity/temperature jump conditions are compared in terms of mass flow rate, reattachment length and pressure drop values.

Obtained results show that use of CBS algorithm with pP2P1 type elements is promising for fluid flow problem in both continuum and slip regime. Complex fluid flow problems such as μSJA flow or rarefied gas flow in backward step duct geometry can be solved using the CBS algorithm coupled with ALE approach and slip-velocity/temperature-jump boundary conditions. To overcome the undesirable time step size criteria considered in *semi-implicit* version of the CBS algorithm, *quasi- (nearly) implicit* version of the algorithm may be used in certain cases such as high-viscosity flows and low Mach number flows.

REFERENCES

[1] **Jameson, A.,** 1995. The present status, challenges, and future development in Computational Fluid Dynamics, *77th Fluid Dynamics Panel Symposium* (AGARD-CP-578), Seville, Spain, 2-5 October, 1.1-1.38.

[2] **Venkatakrishnan, V., Salas, M.D. and Chakravarthy R.,** 1998. Barriers and challenges in Computational Fluid Dynamics, Kluver Academic Publishers, Netherlands.

[3] **Ferziger, J.H. and Peric, M.,** 1996. Computational Methods for Fluid Dynamics, Springer, Berlin.

[4] **Anderson, J.D.,** 1985**.** Fundamentals of Aerodynamics, McGraw-Hill, New York.

[5] **White, F.M.,** 1991. Viscous Fluid Flow, McGraw-Hill, New York.

[6] **Gallager, R.H., Oden, J.T., Taylor, C. and Zienkiewicz, O.C.,** 1981. The Finite Elements in Fluids–Volume 1, McGraw-Hill, New York.

[7] **Idelshon, S.R., and Onate, E.,** 1994. Finite Volumes and Finite Elements: two good friends, *Int. J. Numerical Methods in Engineering*, **37**, 3323-3341.

[8] **Nakajima, K., and Kallinderis Y.,** 1993. Comparison of Finite Element and Finite Volume methods for incompressible viscous flow, *AIAA*, **32(8)**, 1090-1093.

[9] **Zienkiewicz, O.C. and Taylor, R.L.,** 1991. The Finite Element Method–Volume 1, McGraw-Hill, New York.

[10] **Zienkiewicz, O.C. and Taylor, R.L.,** 1991. The Finite Element Method–Volume 2, McGraw-Hill, New York.

[11] **Stasa, F.L,** 1985. Applied finite element analysis for engineers, Holt-Rinehart and Winston series in mechanical engineering, New York.

[12] **Donea, J.A.,** 1984. Taylor-Galerkin method for convection transport problems, *Int. J. Numerical Methods in Fluids*, **4**, 1043-1063.

[13] **Zienkiewicz, O.C., Löhner, R., Morgan, K. and Nakazawa, S.,** 1984. A decade of progress, in *Finite Elements in fluid mechanics-Vol 5,* pp. 1.1-1.26, Eds. Gallagher, R.H., et al., J. Wiley & Sons, Chichestar.

[14] **Lax, P.D. and Wendroff, B.,** 1960. Systems of conservative laws. *Comm. Pure. Appl. Math*., **13**, 217-237.

[15] **Löhner, R., Morgan, K., and Zienkiewicz. O.C.,** 1984. The solution of non-linear hyperbolic equation systems by the finite element method, *Int. J. Numerical Methhods in Fluids*, **4**, 1043-1063.

[16] **Löhner, R., Morgan K. and Zienkiewicz, O.C.,** 1985. An adaptive finite element procedure for compressible high speed flows. *Comp. Meth. Appl. Mech. Eng.*, **51**, 441-465.

[17] **Zienkiewicz, O.C., Löhner. R., Morgan, K. and Peraire, J.,** 1986. High speed compressible flow and other advection dominated problems of fluid mechanics, in *Finite element in fluids-Vol.6*, pp. 2.41-2.88, Eds. Gallagher, R.H., et al., J. Wiley & Sons, Chichestar.

[18] **Zienkiewicz, O.C., and Codina**, **R.**, 1995. A general algorithm for compressible and incompressible flows-Part I: The split, characteristic-based scheme, *Int. J. Numerical Methods in Fluids,* **20**, 869-885.

[19] **Zienkiewicz, O.C and Taylor, R.L.,** 2000. Finite Element Method-Fluid Dynamics Vol. 3, McGraw- Hill.

[20] **Chorin, A.,** 1967. A numerical method for solving incompressible viscous problems, *J. Computational. Physics*, **2**, 12-26.

[21] **Chorin, A.,** 1969. On the convergence of discrete approximation to the Navier-Stokes equations, *Math. Comput*., **23**, 341-353.

[22] **Zienkiewicz, O.C., Morgan K., Satya Sai B.V.K., Codina, R. and Vasquez, M.,** 1995. A General algorithm for compressible incompressible flows-Part II: Tests on the explicit form, *Int. J. Numerical Methods in Fluids.*, **20**, 887-913.

[23] **Codina, R., Vasquez, M. and Zienkiewicz, O.C.,** 1998. A General algorithm for compressible incompressible flows-Part III: semi implicit form, *Int. J. Numerical Methods in Fluids*, **27**, 13-32.

[24] **Zienkiewicz, O.C., Nithiarasu, P., Vasquez, M., Codina R. and Ortiz P.,** 1999. The characteristic–based-split procedure: An efficient algorithm for fluid problems, *Int. J. Numerical Methods in Fluids,* **31**, 359-392.

[25] **Edis, F.O.**, 1998. Efficient finite element computation of incompressible viscous flows using pseudo-second-order velocity interpolation, *Ph.D. Thesis*, Istanbul Technical University, Institute of Science and Technology, Istanbul.

[26] **Edis, F.O., Aslan, R.A. and Çelik B**., 2001. Implementation of pseudo-second order velocity interpolation within the characteristic-based-split procedure, *European Congress on Computational Methods in Applied Sciences and Engineering-ECCOMAS Computational Fluid Dynamics Conference,* Swansea, Wales, UK, 4-7 September.

[27] **Edis, F.O., Aslan, R.A.**, 1998. Efficient incompressible flow calculations using pQ2Q1 Elements, *Communications in Numerical Methods in Engineering*, **14**, 161-178.

[28] **Gad-el-Hak, M.,** 2001. Flow physics in MEMS, *Mech. Ind.,* **2**, 313-341.

[29] **Gad-el-Hak, M.,** 2002. *MEMS Handbook*, CRC Press, New York.

[30] **Kiddy, J., Chen, P., Niemczuk, J., DeVoe, D. and Kiger, K**., 2000. Active flow control using MEMS, *Proceedings of 41st AIAA/ASME/ASCE/AHS/ASC Structures, Structural Dynamics and*

Materials Conference and Exhibit, Atlanta, USA, April 2000, AIAA 2000-1561.

[31] **Mittal, R., Rampunggoon, P.,** 2001. Interaction of a Synthetic Jet with a Flat Plate Boundary Layer, *31st AIAA Fluid Dynamics Conference*, Anaheim California, USA, 11-14 June, AIAA 2001-2773.

[32] **Smith, B.L. and Glezer, A.**, 1997. Vectoring and small-scale motions affected in free shear flows using synthetic jet actuators, 35th *Aerospace Sciences Meeting and exhibit*, Reno, Nevada, January 6-10, AIAA 97-0213.

[33] **Glezer, A. and Amitay, M.**, 2002. Synthetic Jets, *Ann. Rev. Fluid Mech*., **34**, 503-529.

[34] **Çelik, B., Edis, F.O. and Mısırlıoğlu, A.,** 2003. Analysis of micro synthetic jets using CBS finite element method on moving deforming grids, *International symposium on Transient convective heat and mass transfer in single and two-phase flows*, 17-22 August, Çesme, Turkey, 417-426.

[35] **Bird, G.A.**, 1994. Molecular gas dynamics and the direct simulation of gas flows, Clarendon Press, Oxford.

[36] **Özışık, M.N.,** 1985. Heat Taransfer, McGraw-Hill, New York.

[37] **Donnea, J., Giuliani, S. and Halleux, J.P.,** 1982. An arbitrary Lagrangian-Eulerian finite element method for transient dynamic fluid-structure interactions, *Computer Methods in Applied Mechanics in Engineering*, **33**, 689-723.

[38] **Gülçat, U., Mısırlıoğlu, A. and Aslan, A.R**., 1997. 3-D Navier-Stokes solutions with moving deforming finite elements, *Communications in Numerical Methods in Engineering*, **13**, 273-284.

[39] **Gülçat, U., Mısırlıoğlu, A. and Aslan, A.R**., 2000. 3-D viscous flow solution about the bodies in relative motion, *Int. J. Computational Fluid Dynamics*, **14**, 1-19.

[40] **Agarwal, R. and Yun, K.**, 2002. Burnett Simulations of Flow in microdevices, in *MEMS Handbook*, pp. 7.1.-7.36, Eds. Gad-el-Hak, M., CRC Press, New York.

[41] **Arkilic, E.B., Schmidt, M.A. and Bruer, K.S.,** 1997. Gaseous slip flow in long microchannels, *Journals of MEMS*, **6(2)**, 167-178.

[42] **Beskok, A**., 1994. Simulation of heat and momentum transfer in complex micro-geometries, *M. Sc. Thesis*, Princeton University, Princeton.

[43] **Beskok, A.,** 1996. Simulations and models of gas flows in micro geometries, *Ph. D. Thesis*, Princeton University, Princeton.

[44] **Beskok, A. and Karniadakis, G.E.,** 1994. Simulation of heat and momentum transfer in complex micro-geometries, *J. Thermo-phys. Heat Transfer*, **8,** 355-370.

[45] **Beskok, A. and Karniadakis, G.E.,** 1999. A model for flows in channels, pipes and ducts at micro and nano scales, Microscale *Thermophysical Eng.*, **3**, 43-77.

[46] **Aslan, R. A., Baysal, O., and Edis, F.O**., 2002. Computing micro synthetic jet in slip regime with moving membrane**,** *Proceedings of 2002 ASME International Mechanical Engineering Congress and Exposition*, New Orleans, USA, November 17-22, IMECE 2002-33770.

[47] **Menon. S., and Wang, H.,** 2001. Fuel-Air mixing enhancement using synthetic micro jets, AIAA Journal, **39,** 12.

[48] **Mallinson, S.G., Kwok, C.Y., Reizes, J.A.,** 2003. Numerical simulation of micro-fabricated zero mass flux jet actuators, *Sensors and Actuators*, **A 105**, 229-236.

[49] **Yuan, S., Zhou, Z., Wang, Liu, C.**, 2003. MEMS-based piezoelectric array microjet, *Microelectronic Engineering*, **66**, 767-772.

[50] **Utturkar, Y., Holman, R., Mittal, R., Carroll, B., Sheplak, M. and Cattafesta, L**., 2003. A Jet formation criterion for synthetic jet actuators, *41st Aerospace Sciences Meeting and exhibit*, Reno, Nevada, 6-9 January, AIAA 2003-636.

[51] **Denham, M.K. and Patrick, M.A.**, 1974. Laminar flow over a downstream facing step in two dimensional flow channel, *Trans. Int. Eng.*, **52(4)**, 361-367.

[52] **Zienkiewicz, O.C., Satya Sai B.V.K., Morgan, K. and Codina R**., 1996. Split characteristic based semi implicit algorithm for laminar/turbulent incompressible flows, *Int. J. Numerical Methods in Fluids.*, **23**, 787-809.

[53] **Vinckier, A., Jacobsen, J., Wagner, S.,** 1995. A flux filter scheme applied to the Euler Navier Stokes equations, *77th Fluid Dynamics Panel Symposium (AGARD-CP-578),* Seville, Spain, 2-5 October, 16.1-16.17.

[54] **Beskok, A.**, 2002. Molecular based microfluidic simulation models, in *MEMS Handbook*, pp. 8.1-8.28, Eds. Gad-el-Hak, M., CRC Press, New York.

[55] **Baysal, O. and Aslan A.R.,** 2002. Computing separated flows in MEMS devices. *ASME Fluids Engineering Division Summer Meeting*, Montreal, Quebec, Canada, July 14-18.

[56] **Beskok, A., Karniadakis, G.E., and Trimmer, W.**, 1996. Rarefaction and compressibility effects in gas microflows, *Journal of Fluids Engineering*, **118**, 448-456.

[57] **Çelik, B., Edis, F.O. and Mısırlıoğlu, A.,** 2003. Şekil değiştiren bir ağ üzerinde CBS sonlu elemanlar metodu kullanılarak sentetik mikro jet akışı analizi, *XIII. Ulusal Mekanik Kongresi*, Gaziantep, 8-12 Eylül*,* 311-319.

[58] **Çelik, B. and Edis, F.O.,** 2006**.** Analysis of Fluid Flow through micro-fluidic devices using characteristic-based-split procedure. Accepted 18 January 2006 to appear in *Int. J. Numerical Methods in Fluids*.

APPENDIX A. CHARACTERISTIC GALERKIN PROCESS

Convection-diffusion equation for a scalar ϕ function in conservative form is as follows:

$$\frac{\partial \phi}{\partial t} + \frac{\partial F_i}{\partial x_i} + \frac{\partial G_i}{\partial x_i} + Q = 0 \tag{A.1}$$

In he equation above, x_i is the i th component of the Cartesian co-ordinate (i=1, 2, 3). Convected flux, diffusion flux and source term can be written explicitly in the following forms:

$$F_j = u_j \phi \tag{A.2}$$

$$G_i = -k \frac{\partial \phi}{\partial x_i} \tag{A.3}$$

$$Q = Q(x,t) \tag{A.4}$$

Velocity components u_i placed in the convected flux term given above is assumed to be known. Equation (A.1) can be written alternatively by defining a new term $a = \partial u_i / \partial x_i$ in the following form:

$$\frac{\partial \phi}{\partial t} + u_i \frac{\partial \phi}{\partial x_i} - \frac{\partial}{\partial x_i}\left(k \frac{\partial \phi}{\partial x_i} \right) + a\phi + Q = 0 \tag{A.5}$$

The trajectory of the fluid located at the x_{ref} at time t_{ref} is denoted by $\tilde{x}(x_{ref}, t_{ref}; t)$. Following equations can be written using definition of trajectory:

$$\frac{d}{dt}\tilde{x}(t) = u(\tilde{x}(t), t) \tag{A.6}$$

$$\tilde{x}(t_{ref}) = x_{ref} \tag{A.7}$$

Using the short-hand notation $\tilde{x}(t)$ instead of $\tilde{x}(x_{ref}, t_{ref}; t)$, following equation can be written;

$$\frac{d}{dt}\phi(\tilde{x}(t), t)\Big|_{t=t_{ref}} = \left(\frac{\partial \phi}{\partial t} + u_i \frac{\partial \phi}{\partial x_i} \right)\Bigg|_{X=X_{ref}, t=t_{ref}} \tag{A.8}$$

Then, Equation (A.5) can be written as follows.

$$\frac{d}{dt}\phi(\tilde{x}(t),t)-\frac{\partial}{\partial x_i}\left(k\frac{\partial\phi}{\partial x_i}\right)+a\phi+Q=0 \tag{A.9}$$

All the terms in the equation given above are assumed to be evaluated at $x=\tilde{x}(t)$. Using finite difference scheme for discretization of derivative d/dt in Equation (A.9) means discretization of total derivative in Equation (A.5) along the characteristics. Assuming that values of scalar ϕ function at time t_n is known and the values at time t_{n+1} are needed. If t_{ref} is chosen in $[t_n, t_{n+1}]$ interval, the Equation (A.9) can be written in following form after discretization:

$$\begin{aligned}&\frac{1}{\Delta t}\left[\phi(\tilde{x}(t_{n+1}),t_{n+1})-\phi(\tilde{x}(t_n),t_n)\right]\\&-\theta\frac{\partial}{\partial x_i}\left(k\frac{\partial\phi}{\partial x_i}\right)(\tilde{x}(t_{n+1}),t_{n+1})-(1-\theta)\frac{\partial}{\partial x_i}\left(k\frac{\partial\phi}{\partial x_i}\right)(\tilde{x}(t_n),t_n)\\&+\theta a\phi(\tilde{x}(t_{n+1}),t_{n+1})+(1-\theta)a\phi(\tilde{x}(t_n),t_n)\\&+\theta Q(\tilde{x}(t_{n+1}),t_{n+1})+(1-\theta)aQ(\tilde{x}(t_n),t_n)=0\end{aligned} \tag{A.10}$$

If t_{n+1} is chosen as the reference time ($\tilde{x}(t_{n+1})=x_{ref}$), location of the particle at time t_n can be written using second order approximation as follows:

$$\begin{aligned}\tilde{x}(t_n)&=\tilde{x}(t_{n+1})-\Delta t u(\tilde{x}(t_{n+1}),t_n)+O(\Delta t^2)\\&=x-\Delta t u^n+O(\Delta t^2)\end{aligned} \tag{A.11}$$

In the equation above x is used instead of x_{ref}. So, following equation can be written.

$$\begin{aligned}u(\tilde{x}(t_n),t_n)&=u(x-\Delta t u^n+O(\Delta t^2),t_n)\\&=u^n-\Delta t u_i^n\frac{\partial u^n}{\partial x_i}+O(\Delta t^2)\end{aligned} \tag{A.12}$$

Third-order approximation for trajectory $\tilde{x}$ can be written using the equation above as follows:

$$\begin{aligned}\tilde{x}(t_n)&=\tilde{x}(t_{n+1})-\frac{\Delta t}{2}\left[u(\tilde{x}(t_{n+1}),t_{n+1})+u(\tilde{x}(t_n),t_n)\right]+O(\Delta t^3)\\&=x-\Delta t u^{n+1/2}\frac{\Delta t^2}{2}u_i^n\frac{\partial u^n}{\partial x_i}+O(\Delta t^3)\end{aligned} \tag{A.13}$$

In the equation above, $u^{n+1/2}=\left[u^{n+1}+u^n\right]/2$. Using the approximation given above, a third order approximation is obtained for the scalar function in the following form:

$$\begin{aligned}\phi(\tilde{x}(t_n),t_n) &= \phi\left(x - \Delta t u^{n+1/2} + \frac{\Delta t^2}{2} u_i^n \frac{\partial u^n}{\partial x_i} + O(\Delta t^3), t_n \right) \\ &= \phi^n - \Delta t u_j^{n+1/2} \frac{\partial \phi^n}{\partial x_j} + \frac{\Delta t^2}{2} u_i^n \frac{\partial u_j^n}{\partial x_i} \frac{\partial \phi^n}{\partial x_j} \\ &+ \frac{\Delta t^2}{2} u_i^{n+1/2} u_j^{n+1/2} \frac{\partial}{\partial x_i} \frac{\partial \phi^n}{\partial x_j} + O(\Delta t^3)\end{aligned} \tag{A.14}$$

Using $u^{n+1/2} = u^n + O(\Delta t)$ approximation, Equation (A.14) can be expressed as follows:

$$\phi(\tilde{x}(t_n),t_n) = \phi^n - \Delta t u_j^{n+1/2} \frac{\partial \phi^n}{\partial x_j} + \frac{\Delta t^2}{2} u_i^n \frac{\partial}{\partial x_i}\left(u_j^n \frac{\partial \phi^n}{\partial x_j} \right) + O(\Delta t^3) \tag{A.15}$$

For any scalar function ϕ simplified version of the equation above is as following:

$$\phi(\tilde{x}(t_n),t_n) = \phi^n - \Delta t u_j^n \frac{\partial \phi^n}{\partial x_j} + O(\Delta t^2) \tag{A.16}$$

Temporal derivatives in Equation (A.10) (with $\theta = 1/2$) can be discretized using Equation (A.15) and all the terms in the equation evaluated at $x = \tilde{x}(t_n)$ and $t = t_n$ can be approximated using Equation (A.16). Finally, following equation is obtained:

$$\begin{aligned}&\frac{1}{\Delta t}\left(\phi^{n+1} - \phi^n\right) + u_j^{n+1/2} \frac{\partial \phi^n}{\partial x_j} - \frac{\partial}{\partial x_i}\left(k \frac{\partial \phi^{n+1/2}}{\partial x_i} \right) + a\phi^{n+1/2} + Q^{n+1/2} \\ &- \frac{\Delta t}{2} u_k^n \frac{\partial}{\partial x_k}\left[u_i \frac{\partial \phi^n}{\partial x_i} - \frac{\partial}{\partial x_i}\left(k \frac{\partial \phi^n}{\partial x_i} \right) + a\phi^n + Q^n \right] = 0\end{aligned} \tag{A.17}$$

Fully explicit scheme is obtained approximate values at time level $n+1/2$ by n.

$$\begin{aligned}&\frac{1}{\Delta t}\left(\phi^{n+1} - \phi^n\right) + u_j^n \frac{\partial \phi^n}{\partial x_j} - \frac{\partial}{\partial x_i}\left(k \frac{\partial \phi^n}{\partial x_i} \right) + a\phi^n + Q^n \\ &- \frac{\Delta t}{2} u_k^n \frac{\partial}{\partial x_k}\left[u_i \frac{\partial \phi^n}{\partial x_i} + a\phi^n + Q^n \right] = 0\end{aligned} \tag{A.18}$$

In the equation above, the diffusion term in the last bracketed in Equation (A.17) is canceled if linear elements are used for the space discretization. And the equation of characteristic Galerkin method is obtained and it can be written alternatively in the following form:

$$\Delta\phi = \Delta t\left[-\frac{\partial}{\partial x_j}\left(u_j \phi\right) + \frac{\partial}{\partial x_j}\left(k \frac{\partial \phi}{\partial x_j} \right) - Q \right]^n + \frac{\Delta t^2}{2}\left[u_i^n \frac{\partial}{\partial x_i}\left(\frac{\partial}{\partial x_j}\left(u_j \phi\right) \right) + Q \right]^n \tag{A.19}$$

In the equation above, $\Delta\phi = \phi^{n+1} - \phi^n$. Spatial discretization by Galerkin method is optimal for the equation given above, since this equation is derived from self adjoint problem in space.

APPENDIX B. GREEN'S THEOREM

A domain integral expression can be integrated by parts using the following formula

$$\int_{\Omega} \Phi \frac{\partial \Psi}{\partial x_i} d\Omega = \oint_{\Gamma} \Phi \Psi n_i d\Gamma - \int_{\Omega} \frac{\partial \Phi}{\partial x_i} \Psi d\Omega \tag{B.1}$$

Where Γ is the boundary of domain Ω, n_i is the i th component of the outward unit normal vector.

APPENDIX C. FIRST AND SECOND DERIVATIVES OF SHAPE FUNCTIONS OF pP2P1 ELEMENTS

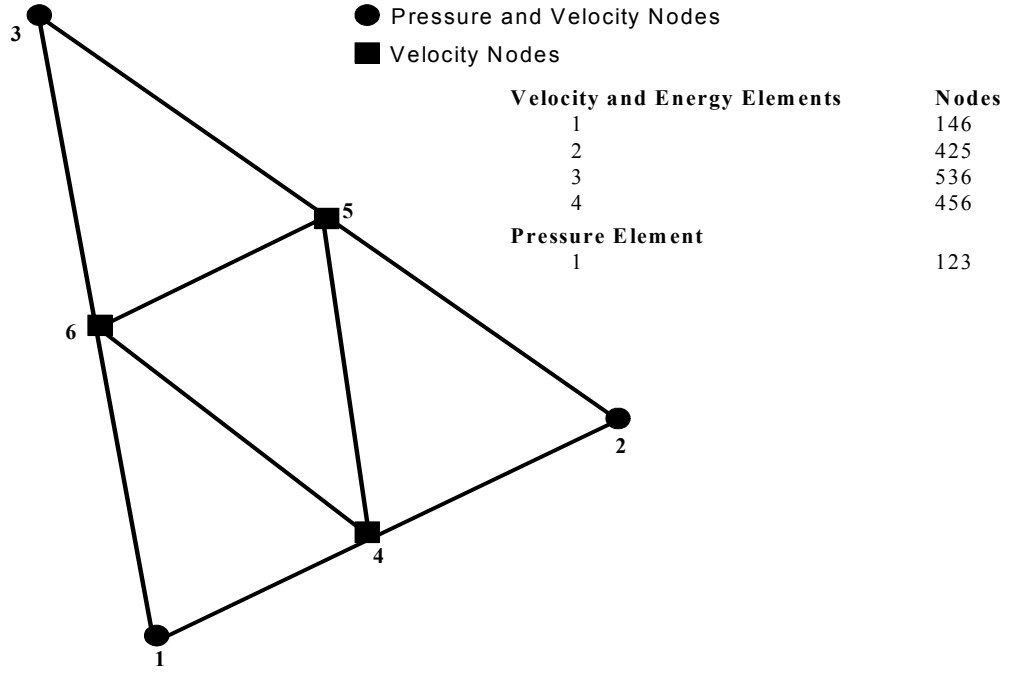

Figure C.1 : Pseudo-quadratic velocity/linear pressure interpolation elements in 2-D

The shape function of quadratic triangle element (triangle123) can be written as a function of linear triangle elements shape function (Triangle 146, 425, 653 and 456) as follows:

$$N_1 = L_1(2L_1 - 1)$$

$$N_2 = L_2(2L_2 - 1)$$

$$N_3 = L_3(2L_3 - 1) \qquad \text{(C.1)}$$

$$N_4 = 4L_1L_2$$

$$N_5 = 4L_2L_3$$

$$N_6 = 4L_1L_3$$

Remembering the definition of shape function of linear triangle element

$$L_1 = m_{11} + m_{21}x + m_{31}y$$

$$L_2 = m_{12} + m_{22}x + m_{32}y \qquad \text{(C.2)}$$

$$L_3 = m_{13} + m_{23}x + m_{33}y$$

,where the term seen in the equation above can be written explicitly as follows:

$$m_{11} = (x_2y_3 - x_3y_2)/2A \qquad m_{12} = (x_3y_1 - x_1y_3)/2A \qquad m_{13} = (x_1y_2 - x_2y_1)/2A$$

$$m_{21} = (y_2 - y_3)/2A \qquad m_{22} = (y_3 - y_1)/2A \qquad m_{23} = (y_1 - y_2)/2A$$

$$m_{31} = (x_3 - x_2)/2A \qquad m_{32} = (x_1 - x_3)/2A \qquad m_{33} = (x_2 - x_1)/2A$$

The first derivatives of this shape functions are given below,

$$\frac{\partial N_1}{\partial x} = m_{21}(4L_1 - 1) \qquad \frac{\partial N_1}{\partial y} = m_{31}(4L_1 - 1)$$

$$\frac{\partial N_2}{\partial x} = m_{22}(4L_2 - 1) \qquad \frac{\partial N_2}{\partial y} = m_{32}(4L_2 - 1)$$

$$\frac{\partial N_3}{\partial x} = m_{23}(4L_3 - 1) \qquad \frac{\partial N_3}{\partial y} = m_{33}(4L_3 - 1)$$

$$\frac{\partial N_4}{\partial x} = 4(m_{21}L_2 + m_{22}L_1) \qquad \frac{\partial N_4}{\partial y} = 4(m_{31}L_2 + m_{32}L_1)$$

$$\frac{\partial N_5}{\partial x} = 4(m_{22}L_3 + m_{23}L_2) \qquad \frac{\partial N_5}{\partial y} = 4(m_{32}L_3 + m_{33}L_2)$$

$$\frac{\partial N_6}{\partial x} = 4(m_{23}L_1 + m_{21}L_3) \qquad \frac{\partial N_6}{\partial y} = 4(m_{33}L_1 + m_{31}L_3)$$

Finally, second derivatives of shape function can be written as follows

$$\frac{\partial^2 N_1}{\partial x^2} = 4m_{21}^2 \qquad \frac{\partial^2 N_1}{\partial y^2} = 4m_{31}^2$$

$$\frac{\partial^2 N_1}{\partial x \partial y} = 4m_{21}m_{31} \qquad \frac{\partial^2 N_2}{\partial x^2} = 4m_{22}^2$$

$$\frac{\partial^2 N_2}{\partial y^2} = 4m_{32}^2 \qquad \frac{\partial^2 N_2}{\partial x \partial y} = 4m_{22}m_{32}$$

$$\frac{\partial^2 N_3}{\partial x^2} = 4m_{23}^2$$

$$\frac{\partial^2 N_3}{\partial y^2} = 4m_{33}^2$$

$$\frac{\partial^2 N_3}{\partial x \partial y} = 4m_{23}m_{33}$$

$$\frac{\partial^2 N_4}{\partial x^2} = 8m_{22}m_{21}$$

$$\frac{\partial^2 N_4}{\partial y^2} = 8m_{31}m_{32}$$

$$\frac{\partial^2 N_4}{\partial x \partial y} = 4\left(m_{31}m_{22} + m_{32}m_{21}\right)$$

$$\frac{\partial^2 N_5}{\partial x^2} = 8m_{22}m_{23}$$

$$\frac{\partial^2 N_5}{\partial y^2} = 8m_{33}m_{32}$$

$$\frac{\partial^2 N_4}{\partial x \partial y} = 4\left(m_{32}m_{23} + m_{33}m_{22}\right)$$

$$\frac{\partial^2 N_6}{\partial x^2} = 8m_{23}m_{21}$$

$$\frac{\partial^2 N_6}{\partial y^2} = 8m_{33}m_{31}$$

$$\frac{\partial^2 N_6}{\partial x \partial y} = 4\left(m_{33}m_{21} + m_{31}m_{23}\right)$$

CURRICULUM VITAE

Bayram Çelik was born in Istanbul on September 6th, 1971. In 1989, he started his undergraduate education in Istanbul Technical University, Department of Aeronautics and Astronautics. He obtained his B.Sc. degree in 1993 in Aerospace Engineering. He attended English preparatory course at İTÜ before starting his M. Sc. study at Space Science and Technology department. He completed his M.Sc. studies in 1997 and started his Ph.D. education in same year at same department. He has been working as a Research Assistant at the Faculty of Aeronautics and Astronautics of Istanbul Technical University since September 2000.